

4

AD-A228 713

CHEMICAL
RESEARCH,
- DEVELOPMENT &
ENGINEERING
CENTER

DTIC FILE COPY

CRDEC-TR-221

HOT FILM
VELOCITY MEASUREMENTS DOWNSTREAM
OF A SWEEP BACKWARD-FACING STEP

Daniel J. Weber
RESEARCH DIRECTORATE

August 1990

DTIC
ELECTE
OCT 09 1990

Co E

D

U.S. ARMY
ARMAMENT
MUNITIONS
CHEMICAL COMMAND



Aberdeen Proving Ground, Maryland 21010-5423

DISTRIBUTION STATEMENT A

Approved for public release;
Distribution Unlimited

90 10 05 074

Disclaimer

The findings in this report are not to be construed as an official Department of the Army position unless so designated by other authorizing documents.

Distribution Statement

Approved for public release; distribution is unlimited.

REPORT DOCUMENTATION PAGE

Form Approved
OMB No. 0704-0188

Public reporting burden for this collection of information is estimated to average 1 hour per response, including the time for reviewing instructions, searching existing data sources, gathering and maintaining the data needed, and completing and reviewing the collection of information. Send comments regarding this burden estimate or any other aspect of this collection of information, including suggestions for reducing this burden, to Washington Headquarters Services, Directorate for Information Operations and Reports, 1215 Jefferson Davis Highway, Suite 1204, Arlington, VA 22202-4302, and to the Office of Management and Budget, Paperwork Reduction Project (0704-0188), Washington, DC 20503.

1. AGENCY USE ONLY (Leave blank)		2. REPORT DATE 1990 August	3. REPORT TYPE AND DATES COVERED Final, 87 Jul - 89 Jul	
4. TITLE AND SUBTITLE Hot Film Velocity Measurements Downstream of a Swept Backward-Facing Step			5. FUNDING NUMBERS PR-1C161102A71A	
6. AUTHOR(S) Weber, Daniel J.				
7. PERFORMING ORGANIZATION NAME(S) AND ADDRESS(ES) CDR, CRDEC, ATTN: SMCCR-RSP-A, APG, MD 21010-5423			8. PERFORMING ORGANIZATION REPORT NUMBER CRDEC-TR-221	
9. SPONSORING/MONITORING AGENCY NAME(S) AND ADDRESS(ES)			10. SPONSORING/MONITORING AGENCY REPORT NUMBER	
11. SUPPLEMENTARY NOTES				
12a. DISTRIBUTION/AVAILABILITY STATEMENT Approved for public release; distribution is unlimited.			12b. DISTRIBUTION CODE	
13. ABSTRACT (Maximum 200 words) The purpose of this study was to determine the effects of sweep angle on the velocity field around a swept backward-facing step. Three step sweep angles were investigated: 0, 15 and 30 degrees. Velocity measurements were made using a single component hot film anemometer. Results from this study indicate the following: the flow in the recirculation region is almost perpendicular to the step, flow reattachment length decreases with increasing sweep angle, and in the reattachment region the velocity component parallel to the step face retains a finite magnitude. Coles' law of the wall and wake was used to correlate the data from this study. The results indicate that upstream of the step, weak pressure gradients act on the flowfields, and downstream of reattachment of the flow recovers more rapidly as the sweep angle increases. A Baldwin-Lomax analysis on the separated profiles in the recirculation region suggest that all length scales must take into account the displacement of the shear layer from the wall. The correlation of the separated, normal and parallel, velocity profiles with the Baldwin-Lomax variables was fair.				
14. SUBJECT TERMS Backward-facing step Rearward-facing step			15. NUMBER OF PAGES 140	
			16. PRICE CODE	
17. SECURITY CLASSIFICATION OF REPORT UNCLASSIFIED	18. SECURITY CLASSIFICATION OF THIS PAGE UNCLASSIFIED	19. SECURITY CLASSIFICATION OF ABSTRACT UNCLASSIFIED	20. LIMITATION OF ABSTRACT UL	

Blank

PREFACE

The work described in this report was authorized under Project No. 1C161102A71A. This work was started in July 1987 and completed in July 1989.


The use of trade names or manufacturers' names in this report does not constitute an official endorsement of any commercial products. This report may not be cited for purposes of advertisement.

Reproduction of this document in whole or in part is prohibited except with permission of the Commander, U.S. Army Chemical Research, Development and Engineering Center, ATTN: SMCCR-SPS-T, Aberdeen Proving Ground, Maryland 21010-5423. However, the Defense Technical Information Center and the National Technical Information Service are authorized to reproduce the document for U.S. Government purposes.

This report has been approved for release to the public.

Acknowledgments

I would like to thank Dr. James Danberg, of Ballistic Research Laboratory, for his assistance and guidance with this project. I would also like to thank Miles Miller, John Molnar, and Daniel Wise for their support during the testing and data reduction. Finally, I would like to thank Carol Hansen for her help with typing and editing of this report.

Accession For	
NTIS GRA&I	<input checked="checked" type="checkbox"/>
DTIC TAB	<input type="checkbox"/>
Unannounced	<input type="checkbox"/>
Justification	
By	
Distribution/	
Availability Codes	
Dist	Avail and/or Special
A-1	

Blank

CONTENTS

Chapter	page
1 INTRODUCTION	1
Overview	1
Research Objectives	1
Description of Flowfield	2
Literature on Swept and Unswept Backward-Facing Steps	4
Experimental Technique and Procedure	4
Experimental Results	6
Computational and Theoretical Literature	7
2 EXPERIMENTAL FACILITIES, HARDWARE AND MODEL ..	9
Overview	9
Description of Wind Tunnel	9
Description of Traversing Mechanism	9
Description of Wind Tunnel Model	12
Description of Hot Film Anemometer	18
Description of Data Acquisition Equipment	20
3 EXPERIMENTAL PROCEDURE	22
Overview	22
Oil Flow Visualization Procedure	22
Hot Film Calibration Procedure	23
Hot Film Probe Alignment	23

Velocity Calibration	23
Yaw Calibration	24
Velocity Profile Test Procedure	24
Flow Reversal Ambiguity	26
4 DATA REDUCTION PROCEDURE	27
Overview	27
Calibration Data Reduction Procedure	27
Velocity Calibration Reduction Procedure	27
Fourth Order Polynomial Curve Fit	27
Linear Curve Fit	27
Comparison of Polynomial and Linear Curve Fits	29
Yaw Calibration	29
Effect of Probe Yaw on Velocity Measurement .	29
Velocity Profile Data Reduction	29
Overview of Data Reduction Procedure	32
Example of Data Reduction Procedure	33
Data Reduction Procedure	34
Flow Reversal Determination	34
Edge u Velocity Component	38
Approximate Boundary-Layer Thickness	38
Format for Presentation of Results	38
Tabulated Results	38
Plotted Results	43
Measurement Uncertainty	43
Calibration Data	43
Probe Positioning	48
Data Reduction - Total Velocity and Flow Direction ...	48
5 DISCUSSION OF RESULTS	49
Overview	49
Oil Flow Results	49
0 Degree Step	49
15 Degree Step	49
30 Degree Step	51

Velocity Profile Results	51
Overview	51
0 Degree Swept Step	54
Overview of Velocity Profiles	54
Recirculation Region Velocity Profiles	54
Comparison With Other Investigators' Results	54
15 Degree Swept Step	61
Selected Velocity Profiles	61
Recirculation Region Velocity Profiles	61
30 Degree Swept Step	72
Selected Velocity Profiles	72
Recirculation Region Velocity Profiles	72
Comparison of Results	79
Estimation of Stagnation Line Within the Recirculation Region	82
Correlation of Results to Computational Turbulence Models ..	86
Overview	86
Coles' Law	86
Description of Coles' Law	86
Results From Coles' Law	87
Baldwin-Lomax Method	94
General Baldwin-Lomax Method	94
Qualification to the Baldwin-Lomax Model	101
Comparing Ccp and Cwk	106
Correlation of Profiles With Baldwin-Lomax Variables	108
6 SUMMARY, CONCLUSIONS AND RECOMMENDATIONS	115
Summary	115
Conclusions	115
Recommendations	118
REFERENCES	119
LIST OF SYMBOLS	123

LIST OF FIGURES

Figure 1.1	Parts of the Flowfield Over a Backward-Facing Step	3
Figure 1.2	Terminology Used to Describe the Flow Over a Backward-Facing Step	5
Figure 2.1	Subsonic Wind Tunnel Test Facility	10
Figure 2.2	Side View of Traversing Mechanism Installed in Wind Tunnel	11
Figure 2.3	Top View of Traversing Mechanism Installed in Wind Tunnel	13
Figure 2.4	Position of Model Relative to Subsonic Wind Tunnel Test Section	14
Figure 2.5	Model Base Hardware (top) 0.25 Inch Aluminum Plate, (bottom) 0.5 Inch Plexiglass Base	15
Figure 2.6	Three 0.5 Inch High Steps, (left) 0 Degree Step, (center) 15 Degree Step, (right) 30 Degree Step	16
Figure 2.7	Wind Tunnel Model With the 0 Degree Step Installed in the Subsonic Wind Tunnel	17
Figure 2.8	Thermal System Incorporated (TSI) Hot Wire/Film Anemometer System	19
Figure 4.1	Raw Hot Film Calibration Data and Fourth Degree Polynomial Curve Fit	28
Figure 4.2	King's Law Applied to Hot Film Calibration Data and Compared to Linear Curve Fit	28

Figure 4.3	Effect of Yaw Angle on Hot Film Probe Output and Compared to a Second Order Polynomial Curve Fit	31
Figure 4.4	Probe Yaw Angle Versus $F(\alpha)$ and $G(\alpha)$	35
Figure 4.5	Total Velocity Profile, $\Lambda = 0$ Degree and $x/h = 2.0$	36
Figure 4.6	Total Velocity Profile With Flow Reversal, $\Lambda = 0$ Degree and $x/h = 2.0$	37
Figure 4.7	u Component of Velocity With Edge Velocity Represented by the Dashed Line	39
Figure 4.8	Estimating Boundary-Layer Thickness From Intersection of Constant u_e Line and Linear Fit of Remaining Data	40
Figure 4.9	Refining Estimate of Boundary-Layer Thickness Using Fewer Points in the Linear Fit	41
Figure 4.10	Total Flow Angle (α) Versus y/h for $\Lambda = 15$ Degrees and $x/h = 2.0$	44
Figure 4.11	y/h Versus U/U_e for $\Lambda = 15$ Degrees and $x/h = 2.0$	44
Figure 4.12	y/h Versus u/u_e for $\Lambda = 15$ Degrees and $x/h = 2.0$	45
Figure 4.13	y/h Versus w/u_e for $\Lambda = 15$ Degrees and $x/h = 2.0$	45
Figure 4.14	y/δ Versus u/u_e for $\Lambda = 15$ Degrees and $x/h = 2.0$	46
Figure 4.15	y/δ Versus w/u_e for $\Lambda = 15$ Degrees and $x/h = 2.0$	46
Figure 4.16	$\ln(y)$ Versus $\ln(u)$ for $\Lambda = 15$ Degrees and $x/h = 2.0$	47
Figure 5.1	Oil Flow Visualization Downstream of the 0 Degree Step, $U_\infty = 73$ fps	50
Figure 5.2	Oil Flow Visualization Downstream of the 30 Degree Step, $U_\infty = 73$ fps, (15 seconds after flow began)	52

Figure 5.3	Oil Flow Visualization Downstream of the 30 Degree Step, $U_{\infty} = 73$ fps, (final results)	53
Figure 5.4	Carpet Plot of the U/U_e Profiles for $\Lambda = 0$ Degree, $x/h = -5.5$ to 15	55
Figure 5.5	Carpet Plot of the α Profiles for $\Lambda = 0$ Degree, $x/h = -5.5$ to 15	56
Figure 5.6	Carpet Plot of the u/u_e Profiles for $\Lambda = 0$ Degree, $x/h = -5.5$ to 15	57
Figure 5.7	Carpet Plot of the w/u_e Profiles for $\Lambda = 0$ Degree, $x/h = -5.5$ to 15	58
Figure 5.8	Carpet Plot of the U/U_e Profiles in the Recirculation Region for $\Lambda = 0$ Degree, $x/h = .2$ to 8.0	59
Figure 5.9	Carpet Plot of the α Profiles in the Recirculation Region for $\Lambda = 0$ Degree, $x/h = .2$ to 8.0	60
Figure 5.10	Comparison of Results at Reattachment to the Results of This Study Near Reattachment	62
Figure 5.11	Comparison of Results Downstream of Reattachment	62
Figure 5.12	Carpet Plot of the U/U_e Profiles for $\Lambda = 15$ Degrees, $x/h = -5.1$ to 15	63
Figure 5.13	Carpet Plot of the α Profiles for $\Lambda = 15$ Degrees, $x/h = -5.1$ to 15	64
Figure 5.14	Carpet Plot of the u/u_e Profiles for $\Lambda = 15$ Degrees, $x/h = -5.1$ to 15	65
Figure 5.15	Carpet Plot of the w/u_e Profiles for $\Lambda = 15$ Degrees, $x/h = -5.1$ to 15	66
Figure 5.16	Carpet Plot of the U/U_e Profiles in the Recirculation Region for $\Lambda = 15$ Degrees, $x/h = .3$ to 8.0	67
Figure 5.17	Carpet Plot of the α Profiles in the Recirculation Region for $\Lambda = 15$ Degrees, $x/h = .3$ to 8.0	69

Figure 5.18	Carpet Plot of the u/u_e Profiles in the Recirculation Region for $\Lambda = 15$ Degrees, $x/h = .3$ to 8.0	70
Figure 5.19	Carpet Plot of the w/u_e Profiles in the Recirculation Region for $\Lambda = 15$ Degrees, $x/h = .3$ to 8.0	71
Figure 5.20	Carpet Plot of the U/U_e Profiles for $\Lambda = 30$ Degrees, $x/h = -5$ to 15	73
Figure 5.21	Carpet Plot of the α Profiles for $\Lambda = 30$ Degrees, $x/h = -5$ to 15	74
Figure 5.22	Carpet Plot of the u/u_e Profiles for $\Lambda = 30$ Degrees, $x/h = -5$ to 15	75
Figure 5.23	Carpet Plot of the w/u_e Profiles for $\Lambda = 30$ Degrees, $x/h = -5$ to 15	76
Figure 5.24	Carpet Plot of the U/U_e Profiles in the Recirculation Region for $\Lambda = 30$ Degrees, $x/h = .3$ to 8.0	77
Figure 5.25	Carpet Plot of the α Profiles in the Recirculation Region for $\Lambda = 30$ Degrees, $x/h = .3$ to 8.0	78
Figure 5.26	Carpet Plot of the u/u_e Profiles in the Recirculation Region for $\Lambda = 30$ Degrees, $x/h = .3$ to 8.0	80
Figure 5.27	Carpet Plot of the w/u_e Profiles in the Recirculation Region for $\Lambda = 30$ Degrees, $x/h = .3$ to 8.0	81
Figure 5.28	Boundary-Layer Thickness as a Function of x'/h for the Three Step Sweep Angles	83
Figure 5.29	Location of the u/u_e Stagnation Line Within the Recirculation Region for the Three Swept Step Configurations	84
Figure 5.30	Location of the w/u_e Stagnation Line Downstream of the Step for the 15 and 30 Degree Step Configurations	85
Figure 5.31	Skin Friction Coefficient as a Function of x'/h for the Three Step Sweep Angles	88

Figure 5.32	The Law of the Wall Intercept, C , as a Function of x'/h for the Three Step Sweep Angles	89
Figure 5.33	Coles' Wake Parameter as a Function of x'/h for the Three Step Sweep Angles	91
Figure 5.34	Coles' Wake Parameter Upstream of the Step, Plotted on an Expanded Scale	92
Figure 5.35	Comparison of Coles' Law Boundary-Layer Thickness and Those Determined Directly From the Experimental Results	93
Figure 5.36	Law of the Wall Semi-Logarithmic Wake Profiles at $x'/h = 0.0$ for the Three Step Sweep Angles (symbols are experimental data)	95
Figure 5.37	Law of the Wall Semi-Logarithmic Wake Profiles After Reattachment for $\Lambda = 30$ Degrees (symbols are experimental data)	96
Figure 5.38	Typical Coles' Law Velocity Profiles Ahead of Separation for $\Lambda = 15$ Degrees (symbols are experimental data)	97
Figure 5.39	Coles' Law Velocity Profiles After Reattachment for $\Lambda = 0$ Degree (symbols are experimental data)	98
Figure 5.40	Coles' Law Velocity Profiles After Reattachment for $\Lambda = 15$ Degrees (symbols are experimental data)	99
Figure 5.41	Coles' Law Velocity Profile After Reattachment for $\Lambda = 30$ Degrees (symbols are experimental data)	100
Figure 5.42	Typical Separated Profile Illustrating Terms Important to Modification to the Baldwin-Lomax Model	102
Figure 5.43	Typical Polynomial Fit for the Separated Profiles, $\Lambda = 15$ Degrees	105
Figure 5.44	Baldwin-Lomax Constant for the Attached and Separated Profiles	107
Figure 5.45	Correlation of the u Component Separated Profiles With the Baldwin-Lomax Variable for $\Lambda = 0$ Degree	109

Figure 5.46	Correlation of the u Component Separated Profiles With the Baldwin-Lomax Variable for $\Lambda = 15$ Degrees	110
Figure 5.47	Correlation of the u Component Separated Profiles With the Baldwin-Lomax Variable for $\Lambda = 30$ Degrees	111
Figure 5.48	Correlation of the w Component Separated Profiles With the Baldwin-Lomax Variable for $\Lambda = 15$ Degrees	112
Figure 5.49	Correlation of the w Component Separated Profiles With the Baldwin-Lomax Variable for $\Lambda = 30$ Degrees	113

LIST OF TABLES

Table 4.1	Typical Hot Wire Calibration Results	30
Table 4.2	Typical Yaw Calibration Results	30
Table 4.3	Typical Velocity Profile Results	42

HOT FILM VELOCITY MEASUREMENTS DOWNSTREAM OF A SWEEP BACKWARD-FACING STEP

Chapter 1 INTRODUCTION

Overview

Over the past 25 years many investigators have been interested in the flow over an unswept backward-facing step. Through their experimental and computational efforts, a modest attempt has been made at understanding the resulting flowfield. Because of the large number of parameters required to accurately define the flowfield and reattachment point downstream of a backward-facing step, the work has progressed slowly. Even today, all the parameters still have not been identified. Recently, some interest has developed in the more general flowfield over a swept backward-facing step, of which the unswept step is a special case. Very little experimental data and theoretical analysis exist for the swept backward-facing step.

The purpose of this study is to provide preliminary measurements of the mean velocity profiles at various survey locations up- and downstream of a backward-facing step with sweep angles of 0, 15, and 30 degrees. It is felt that the results from this study can be applied, at least indirectly, to many of the problems involving this type of flow. Several examples of where the flow over a swept backward-facing step could be applied are: the flow around buildings, cliffs and mountains; the flow through diffusers and combustion chambers; and the flow over seams of an airplane wing or over the rotating band of a nutating artillery projectile. One very important use for the results from a study of the flow over a swept backward-facing step is in the development and verification of computational turbulence models, both two- and three-dimensional.

In order to understand the flow over a swept backward-facing step several aspects of the flowfield must be defined, such as: the initial conditions at the point of flow separation, the flow in the recirculation region, the flow reattachment region and the recovery region downstream of reattachment. Eaton and Johnston (1981), in their review of the research to date of the flow over unswept backward-facing steps, listed several reasons why this geometry is the best choice for investigating turbulent flowfields. First, although the flowfield itself is extremely complex, the flow downstream of a backward-facing step is one of the simplest two-dimensional reattaching flows known. The flow separates along a straight line represented by the edge of the step. At flow separation, the streamlines are nearly parallel to the wall. Finally, the flow within the recirculation region is highly turbulent and the boundary-layer is separated. The same reasons can also be applied to the three-dimensional flow over a swept backward-facing step.

Research Objectives

In this study, three 0.5 inch high, backward-facing step configurations with sweep angles of 0, 15 and 30 degrees, respectively, were tested in a subsonic wind tunnel. A step height of 0.5 inches was selected in order to allow comparisons to be made with Selby's (1982) work. Selby performed numerous flow observations over a 0.5 inch swept backward-facing step. Oil

flow observations were performed in order to determine if the flowfields were similar to those obtained by other investigators. A hot film anemometer system was used to measure the components of the total velocity parallel and perpendicular to the step face. The intent of this study was to provide preliminary data on how the mean velocity was affected by step sweep angle, so that a more detailed survey of the flowfield could be accomplished during future testing. Velocity profile surveys were conducted at locations up- and downstream of the step. Probe positioning was a manual operation with data acquisition, storage and reduction being computer controlled. From the hot film measurements, the total velocity and flow angle were determined. Knowing this information, the velocity components parallel and perpendicular to the step face, as well as an estimate of the boundary-layer thickness at each survey location were calculated. The results from this study were also applied to two computational turbulence models. The first method examined was Coles' law of the wall and wake for approximating attached turbulent boundary-layers. The second method was a modified Baldwin-Lomax algebraic model for attached and separated turbulent flows over a backward-facing step.

Description of Flowfield

The flow over a backward-facing swept or unswept step represents a relatively simple reattaching flow but the flowfield itself is extremely complex. For the unswept step, the flow is basically perpendicular to the face of the step. It is believed that the flow over a swept backward-facing step is similar to the flow over a yawed cylinder as described by Schlichting (1979). By using this comparison the flowfield can be greatly simplified. The flowfield is no longer truly 3-dimensional. The flow over an infinite swept step is then composed of two components, one parallel and the other perpendicular to the face of the step. The perpendicular component is independent (uncoupled) from the other, with the perpendicular flow being analogous to the flow over an unswept step and the parallel flow being that part of the flow caused by the sweep angle of the step.

A diagram of the different regions of the flowfield over a swept or unswept backward-facing step is illustrated in Figure 1.1. Above the surface of the step ($y > \delta$), within the freestream, the flowfield is inviscid. Ordinary boundary-layer growth is experienced upstream of the step, with this part of the flow having little effect on the flow downstream of the step. The upstream flow is used to determine the fluid properties at separation. The edge of the shear layer separates the inviscid flow of the freestream from the boundary-layer flow where viscous and turbulent stresses dominate. Just downstream of the step is the recirculation region. The dividing streamline separates the recirculation region from the rest of the shear layer. The dividing streamline begins at the edge of the step and continues downstream nearly parallel to the surface of the wall. Then, as the reattachment region is approached the dividing streamline curves sharply down to the surface. The recirculation region is below the dividing streamline. Within the recirculation region there are several areas of interest. There is believed to

Free Stream or Inviscid Flow Region

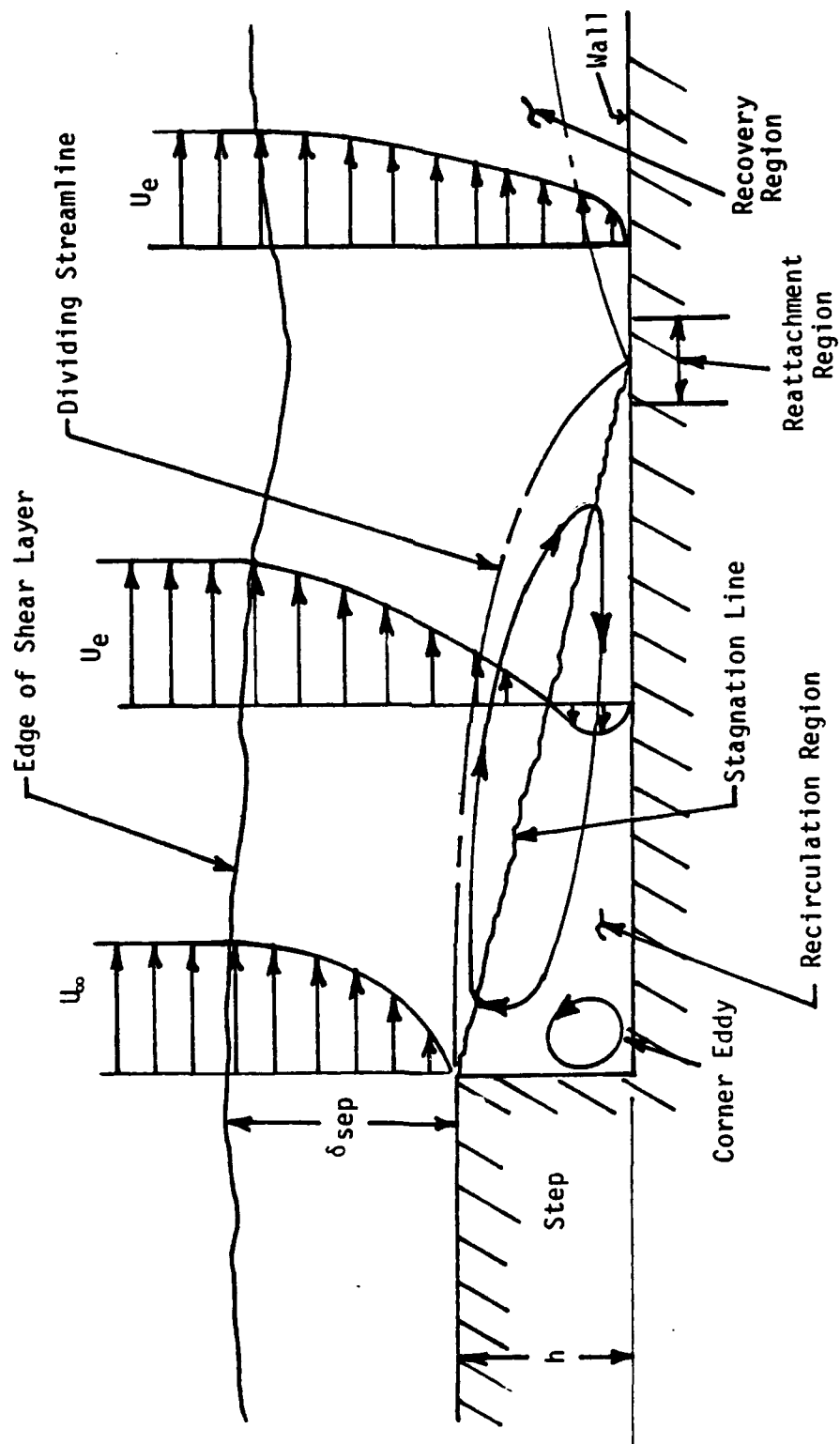


Figure 1.1 Parts of the Flowfield Over a Backward-Facing Step

be a corner eddy in the area where the step face meets the lower plate surface. The major area of interest is the recirculation region. This area is split roughly in half by a stagnation line. Above this line the fluid in the recirculation region is in the direction of the freestream but below the line the flow direction is reversed. Within the recirculation region the boundary-layers are separated from the wall. The reattachment region is located at the downstream edge of the recirculation region. Downstream of the reattachment region is the recovery region where the flow is realigning itself in the direction of the freestream. Another part of the flowfield not indicated in Figure 1.1 is the crossflow which is that part of the flowfield parallel to the step face. Note that with parallel flow along the swept step, the perpendicular flow stagnation line is not necessarily a line of zero velocity.

The terminology and variables used to describe the flow over a backward-facing step are shown in Figure 1.2. The x axis is along the wind tunnel centerline in the direction of the free stream. The y axis is perpendicular to the wind tunnel floor and the z axis is in the direction of the tunnel side wall with the positive sense to the left when looking downstream. The x' and z' directions are perpendicular and parallel to the step face, respectively. The y' axis is in the same direction as the y axis. The u and w velocity components are along the x' and z' axes, respectively, with the positive sense indicated. The step angle is denoted by Δ . The total velocity, U and flow direction, α are shown with their positive sense indicated.

Literature on Swept and Unswept Backward-Facing Steps

The amount of literature available on the flow over backward-facing steps is extensive. Since several investigators [Eaton and Johnston (1981), Selby (1982), and Hartman (1988)], have provided detailed historical reviews of work performed on this type of flowfield, one will not be provided here. Instead, a brief discussion will be presented of those references used extensively in this study as well as recent published works on the subject. A complete list of cited and uncited references is contained in the Bibliography.

Experimental Technique and Procedure

Several texts and reports describing hot wire/film techniques, data acquisition and reduction were used to establish the test and data reduction procedure used in this study.

Lomas's (1986) text on hot wire anemometry was an invaluable source of theoretical and practical information on the use of hot wire/film to measure air velocities and flow directions. This text describes the effects on the probe's output as a function of the probe's yaw and pitch angle to the flow. Also, effects of humidity, temperature differences, heat conduction to probe supports, measurements close to a wall and many other experimental concerns are discussed.

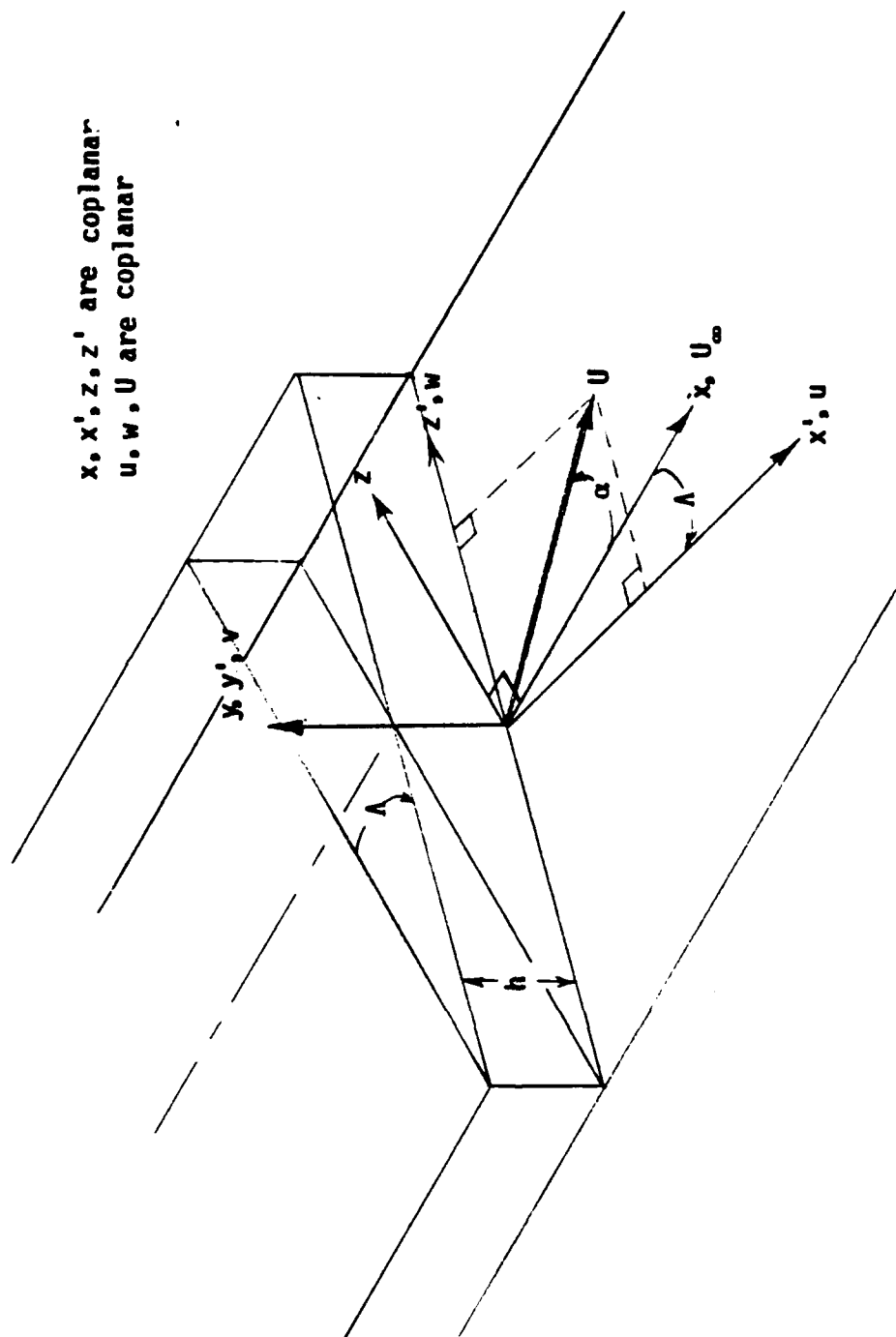


Figure 1.2 Terminology Used to Describe the Flow Over a Backward-Facing Step

Several Thermal Systems Incorporated (TSI) technical bulletins were used in this study (Thermal Systems Incorporated TB5, TB16 and TB18). Technical Bulletins 16 and 18 describe several techniques that could be used to compensate hot film measurements for differences in temperature between the calibration results and the test data. Technical Bulletin 5 provides general information on the use of hot wire/film anemometers for velocity measurements.

The data reduction procedure used to determine the flow velocity and direction from a single component hot film anemometer is described by Olivari (1978). For a specific data point, this procedure requires that readings be taken at two or three yaw angles. Then, using the velocity and yaw calibration results, the total velocity and flow direction can be determined. Another technique, described by Al-Beirutty, Arterberry and Gessner (1988), uses a single component, slanted hot wire to measure the three velocity components as well as the six Reynolds Stress terms. This procedure could prove extremely useful in future velocity and turbulence measurements in the flowfield around swept backward-facing steps.

Experimental Results

The results from Selby's (1982) phenomenological study of the subsonic flow over a swept backward-facing step proved very helpful with the experimental setup for this study. Selby performed numerous oil drop, smoke wire and surface-mounted tufts flow visualization tests, which were useful in establishing the degree of similarity between the flowfields of this study and his. He measured the mean velocity using a hot wire anemometer and also measured the static pressure along the surface of the model. From his observations and measurements he was able to determine the flow reattachment location. He examined what effect step height, sweep angle, base geometry and end condition had on the flowfield and the flow reattachment location. Two important findings came from his work. First, for sweep angles less than 38 degrees, the w velocity component, that part of the flow parallel to the step, could be uncoupled from the two-dimensional flow normal to the step. Second, the u velocity component, the flow normal to the step, behaved like the flow over a unswept backward-facing step. This is similar to the flow over a yawed cylinder described by Schlichting (1979).

The experimental work performed by Bradshaw and Wong (1972) provided data for comparison with the mean velocity flow over the unswept backward-facing step near reattachment.

A good source of experimental data and an excellent historical review of research on the flow over a backward-facing step was presented by Eaton and Johnston (1981). Eaton and Johnston discussed some of the parameters that affect the flowfield. These parameters include: the initial boundary-layer state, initial boundary-layer thickness, freestream turbulence, pressure

gradients and the ratio of step height to channel width (aspect ratio, AR).

A recent study performed by Ellzey and Berbee (1988) investigated the effects of Reynolds number and aspect ratio on the flow behind a backward-facing step. They found that there is little effect on the mean velocity profiles down to an $AR=4$, which is considerably lower than the value of 10 recommended by deBroderode and Bradshaw (1972).

Computational and Theoretical Literature

Compared to experimental studies there are far fewer computational and theoretical investigations and most of these have been limited to the flow over the unswept backward-facing step.

A recent investigation by Avva, Kline and Ferziger (1988) for the flow over an unswept backward-facing step employed a zonal approach in determining the turbulent flowfield. Their method used a second-order accurate, differencing scheme applied to the different zones of the flow behind the backward-facing step. Their technique yielded a better prediction of the turbulence terms than could be obtained from the standard $k-\epsilon$ method.

A finite element analysis was conducted by Thomas, Morgan and Taylor (1980) for the flow over a unswept backward-facing step. Their procedure was applied to both laminar and turbulent flows and achieved acceptable agreement with experimental results.

Hu, Wang, Danberg and Seidel (1984) developed a finite element method for calculating an incompressible, laminar flow over a swept backward-facing step. Their procedure separated the flow into two parts, the first being along the step face and the second perpendicular to the step face. The two flows were then solved independent of each other. They indicated that their results looked promising, but for their method to be useful it should be expanded to cover turbulent flows.

Work performed by Hartman (1988) and Hartman, Seidel and Danberg (1989) included the development of a finite-difference computer code to investigate the flow behind a swept backward-facing step. A two-layer eddy viscosity model was used within the computer code which provided for the presence of a vertical wall and flow reattachment. The computations indicated that reattachment length decreased with sweep angle and step height and these findings agreed reasonably well with experimental results.

Several investigations which proved helpful with the theoretical analysis of this study included the work performed by Danberg (1971). In this work Danberg describes a procedure that uses a least squares method to determine the coefficients of an equation based on Coles' law of the wall and wake. This procedure can then be used to approximate the velocity profiles

of an attached flowfield.

Danberg and Patel (1989) applied the Baldwin-Lomax algebraic turbulence model to the flow over a rotating band of an artillery projectile. The geometry of this application is similar to a forward and rearward facing step. A detailed discussion of the Baldwin-Lomax model was provided along with the modifications necessary to apply it to the flow over a swept backward-facing step.

The experimental, computational and theoretical studies cited above are not intended to be a comprehensive listing of all work on the subject of the flow over swept and unswept backward-facing steps. Instead, the intent is to highlight some of the recent developments as well as present those investigations which pertained directly to this study.

Chapter 2 EXPERIMENTAL FACILITIES, HARDWARE AND MODEL

Overview

This study was conducted at the U.S. Army Chemical Research Development and Engineering Center (CRDEC), Aberdeen Proving Ground, Maryland. CRDEC facilities used during this study included the Aerodynamic Research Concepts and Assistance Branch (ARCA Br) and the Experimental Design and Fabrication Branch (EDF Br). The ARCA Br provided the subsonic wind tunnel, data acquisition and computer systems; while the EDF Br built the wind tunnel model.

Description of Wind Tunnel

The continuous flow, open circuit, subsonic wind tunnel used for this test is shown in Figure 2.1, and is described by Miller (1983). Air flow in the tunnel is created by a 125 horsepower electric motor driving a squirrel cage fan located downstream of the test section. The air is drawn from the outside of the building into the tunnel settling chamber through a section of honeycomb and two fine mesh screens. The air moves from the settling chamber through a 6:1 area contraction into the test section. Dimensions of the tunnel test section are 28 inches high by 40 inches wide by 88 inches long. Downstream of the test section, the air flows through a diffuser, passes the fan and then is exhausted through the roof of the laboratory. Tunnel velocity is controlled by adjusting a series of vanes in front of the fan. The velocity range for the tunnel is approximately 10 fps to 220 fps, (0.009 to 0.2 Mach Number). The test section velocity is indicated on an inclined manometer attached to the tunnel. The tunnel is capable of continuous operation. One minor problem that developed during testing was the influence of ambient wind gusts on the test section velocity. Wind gusts in the direction of the inlet could cause the test section velocity to fluctuate as much as 2 fps during a test. To avoid this problem the outside wind conditions were continually monitored.

Description of Traversing Mechanism

After several iterations, a final design for a probe traversing mechanism was settled on. Figure 2.2 shows the traversing mechanism installed in the roof of the subsonic wind tunnel. In order to insure accurate vertical positioning of the probe, relative to the surface of the model, a commercially available 24 inch height gauge was acquired. The height gauge scribe was replaced with a specially designed adapter which allowed the rotation of the hot film probe holder about the longitudinal axis while, not allowing the probe to move vertically towards or away from the plate. The adapter incorporated a yaw angle indicator, calibrated in one degree increments (0 to 360 degrees), to determine probe yaw angle or flow direction. A thumb screw was used to lock the probe at the desired yaw angle. The hot film probe holder ran through a thin walled steel tube which acted as a wind shield and both were secured to the adapter. The wind shield stopped approximately 6 inches above the probe tip so that it would



Figure 2.1 Subsonic Wind Tunnel Test Facility

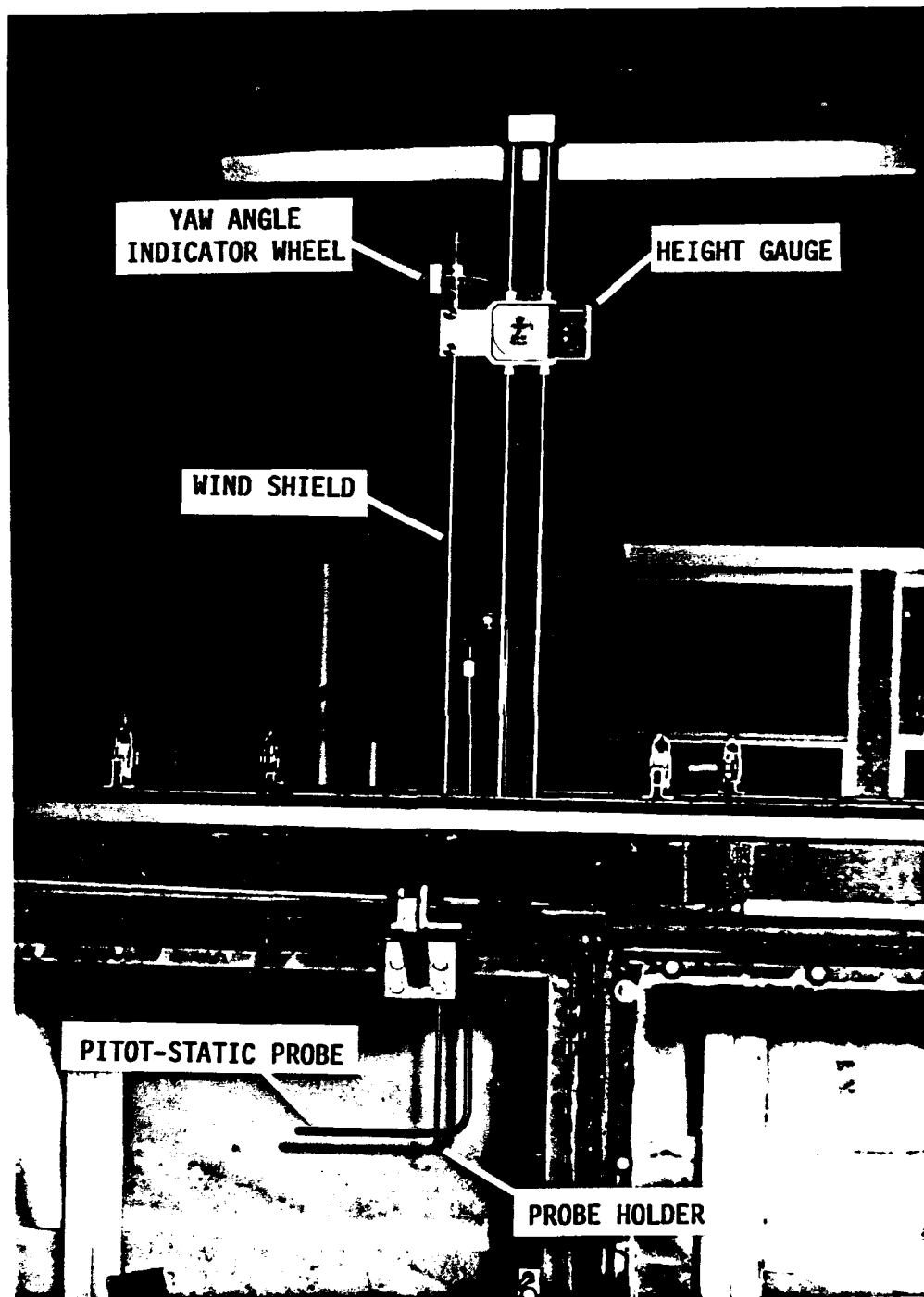


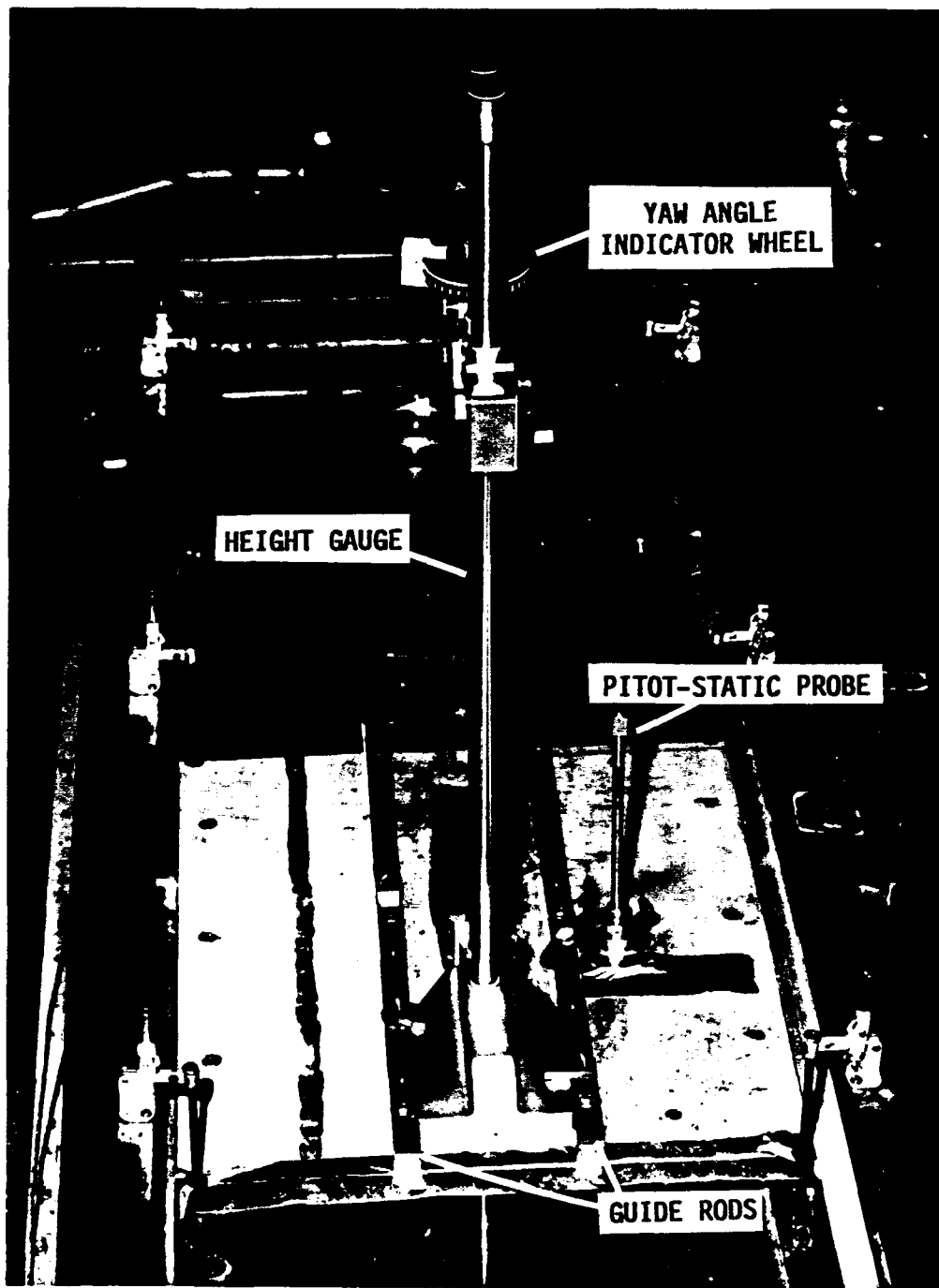
Figure 2.2 Side View of Traversing Mechanism
Installed in Wind Tunnel

not adversely affect the measurements. A slot, milled into the roof and along the centerline of the tunnel, shown in Figure 2.3, allowed the traversing mechanism to be positioned over the range of approximately 2.75 inches upstream to 7.5 inches downstream of the step. Two guide rods were positioned an equal distance along both sides to keep the traversing mechanism aligned with the slot. The positioning of the probe, both vertically and longitudinally, was a manual operation. For future testing, it would be advantageous to automate the probe positioning operation to reduce errors, fatigue and test time.

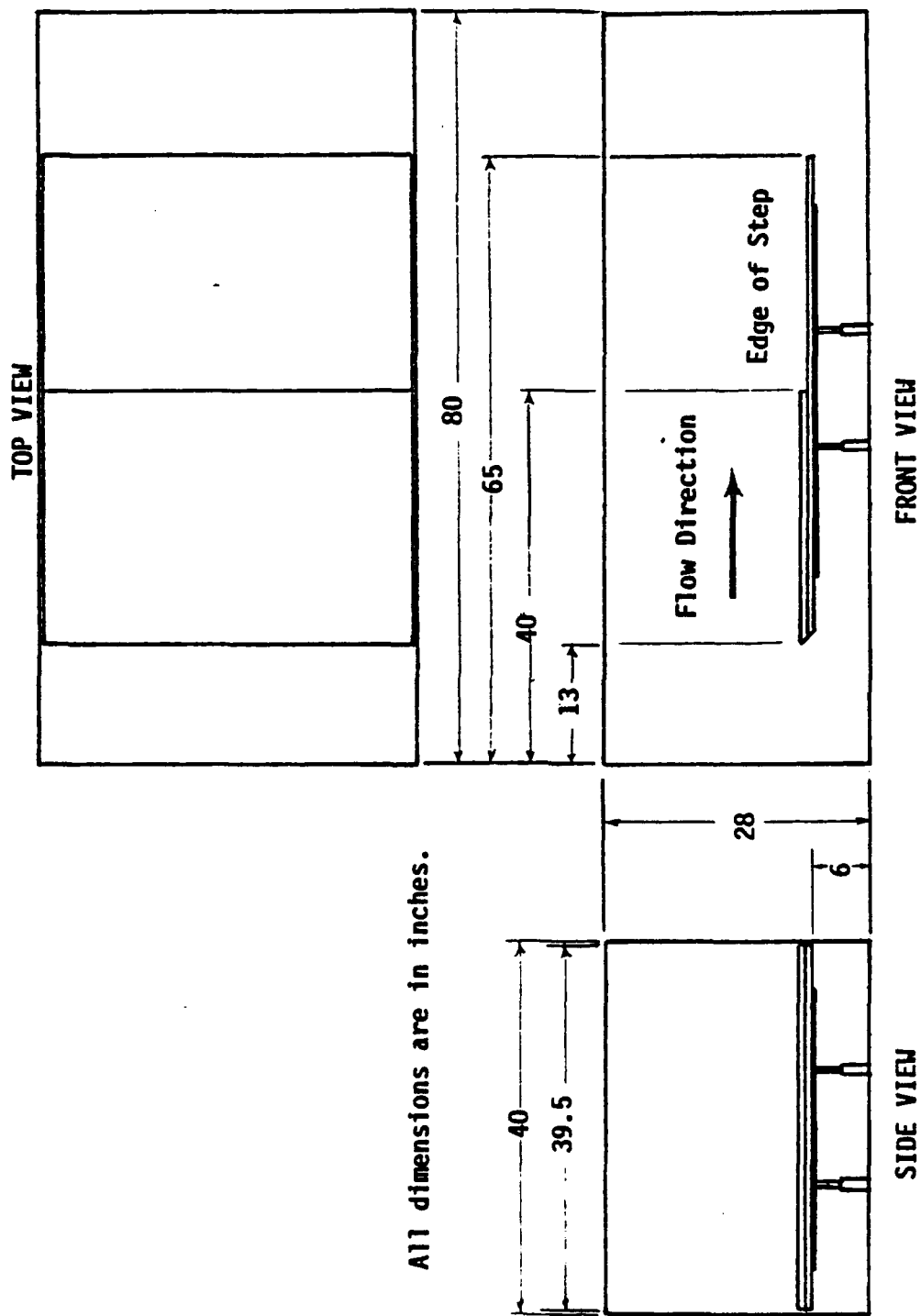
Description of Wind Tunnel Model

The wind tunnel model was fabricated from half inch plexiglass, thus providing a half inch step height. Figures 2.4 through 2.6 give the overall dimensions and layout for the backward-facing step wind tunnel model. A 0.25 inch aluminum plate was used to support the base of the model and provide for a solid connection to the floor of the wind tunnel. Connection of the support plate to the tunnel was made by four 0.5 inch threaded rods located near the support plate center and four 0.25 inch turnbuckles located at the corners of the support plate. The use of threaded rods and turnbuckles allowed for setting the plate at an angle-of-attack to the flow in the wind tunnel. The base of the model was fabricated from 0.5 inch plexiglass and was designed to span the width of the test section; thus, the side walls of the test section acted as end plates for the model. In order to improve the flow around the leading edge, the base plate was beveled to a 40 degree wedge. The overall dimensions of the base plate were 39.5 by 59.6 inches. The final components of the model were the three interchangeable swept backward-facing steps. The first step was unswept or had a 0 degree sweep angle, the other two had a 15 and 30 degree sweep angle, respectively. All three steps had a centerline distance of 27 inches measured from the leading edge to the step edge. It is important to note that the upstream portion of each step was constructed as one piece so that there would be no joints between the leading edge and the step. While this approach eliminated all upstream joints it presented a problem in that there were different leading edges for each step. Thus, the upstream flowfields may not have been identical for each configuration.

Initially, the leading edge of the three step configurations were machined to continue the 40 degree wedge from the base plate to a knife edge along the upper surface of the step plates. As will be explained in the next chapter, the leading edge of each step plate was radiused in order to improve the flow over the upper surface. All model hardware were secured together with screws from the underside so that the upper surface remained as smooth as possible. Figure 2.7 shows the 0 degree step installed in the subsonic wind tunnel.

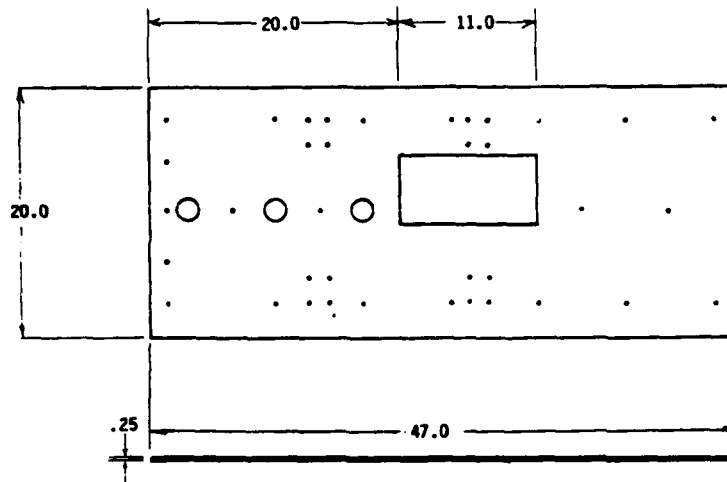


**Figure 2.3 Top View of Traversing Mechanism
Installed in Wind Tunnel**



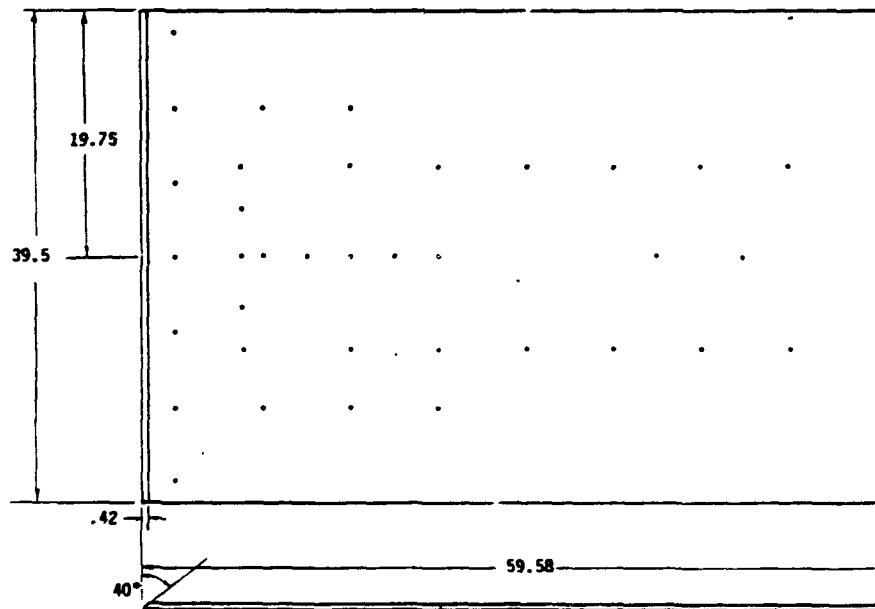
All dimensions are in inches.

Figure 2.4 Position of Model Relative to Subsonic Wind Tunnel Test Section



All dimensions are in inches.

NOTE: Small circles are mounting holes.



All dimensions are in inches.

Figure 2.5 Model Base Hardware (top) 0.25 Inch Aluminum Plate, (bottom) 0.5 Inch Plexiglass Base

Note: Small circles are mounting holes.

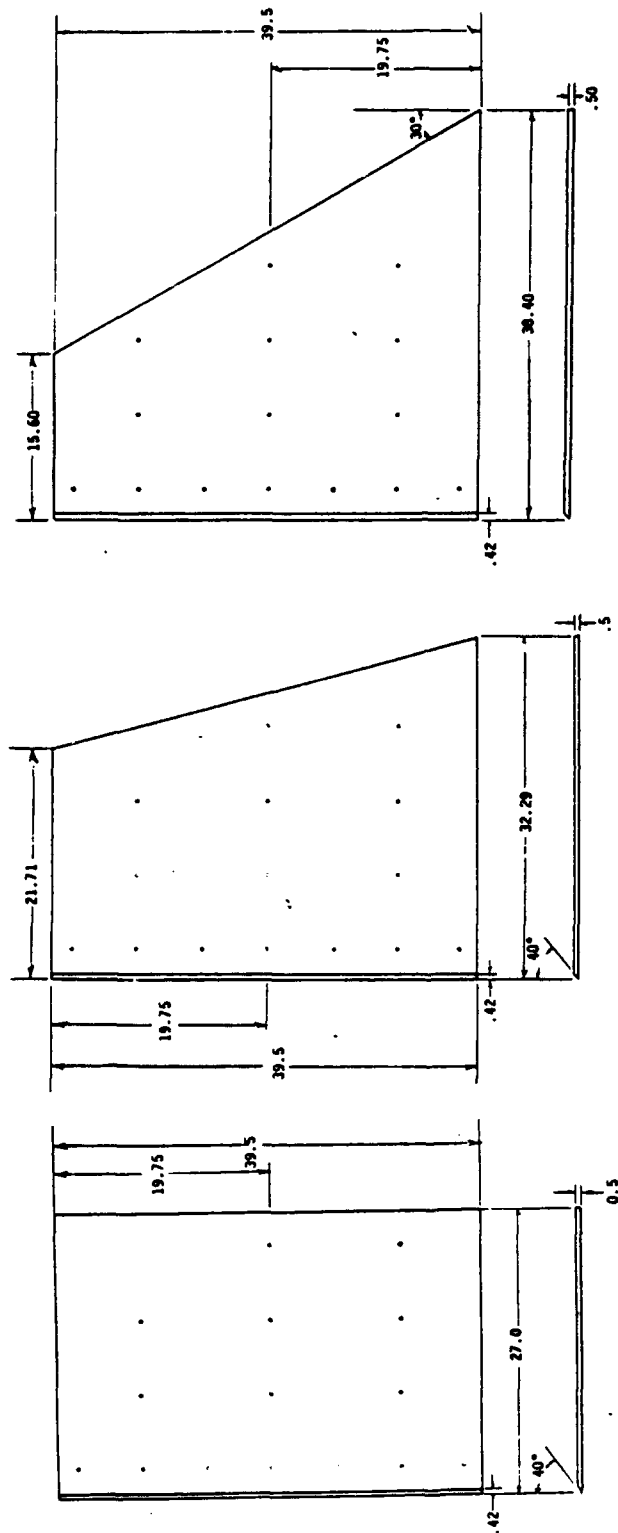


Figure 2.6 Three 0.5 Inch High Steps, (left) 0 Degree Step, (center) 15 Degree Step, (right) 30 Degree Step



Figure 2.7 Wind Tunnel Model With the 0 Degree Step
Installed in the Subsonic Wind Tunnel

Two physical parameters commonly used to describe the experimental apparatus and setup for measuring the flow over a backward-facing step are the test apparatus aspect ratio, AR, and expansion ratio. Both of these parameters affect the flowfield and are dependent on the physical dimensions of the wind tunnel and model. The AR of the test apparatus is defined as the width of the wind tunnel divided by the step height. For this wind tunnel facility and model, the $AR = 80$. If the AR is too small it is possible that the side walls of the test section could adversely effect the flow over the step. de Brederode and Bradshaw (1972) found that the lower limit for ignoring the effects due to AR was 10, but Ellzey and Berbee (1988) found little or no effect down to values as low as 4. The second parameter, the expansion ratio, is defined as the ratio, relative to the step, of the downstream to upstream cross sectional areas. The backward facing step model was installed in the wind tunnel so that the upper surface of the model was approximately 6.25 inches above the test section floor. The location of the model at this position yielded an expansion ratio of 1.03. The expansion ratio effects the flowfield by producing a streamwise pressure gradient. Kuehn (1980), showed that as the expansion ratio increased so did the reattachment length. Selby (1982) investigated the coupling between the wind tunnel model and the test section. He concluded that the streamwise expansion ratio is the major cause of the streamwise pressure gradient within the separated flow region of swept backward-facing step mounted in a typical wind tunnel test section. A compensating roof step is the easiest and best method of eliminating any pressure gradient due to the expansion ratio. Since the expansion ratio for this study was very close to unity, and any streamwise pressure gradient was assumed negligible, compensating roof steps were not used.

Description of Hot Film Anemometer

The velocity profile measurements were made using a Thermo-Systems Inc. (TSI) constant temperature hot wire/film anemometer system. A photograph of the TSI system is shown in Figure 2.8. The system consisted of a 1051-6 power supply and analog meter, three 1050 Constant Temperature Anemometers (CTA), and three 1052 Linearizers. For these tests, the 1052 Linearizers were not used. Typical CTA settings were as follows: Bridge Selection, setting 1 under 5:1; Probe Resistance Decades, set to manufacture recommended value; High Frequency Filter, set to 100 kHz; and Reference Voltage, set to 5 volts, which is recommended for hot film probes. A 36 inch probe holder provided the needed capability of traversing from the ceiling to the floor of the wind tunnel test section. A TSI 1210-20 Hot Film single component probe was used to measure the velocity profiles throughout the experiments. The 1210-20 Hot Film probe has a sensor diameter of 0.002 inches and a length of approximately 0.040 inches. These probes also have a recommended minimum and maximum velocity range of 0.5 to 1000 fps, respectively.

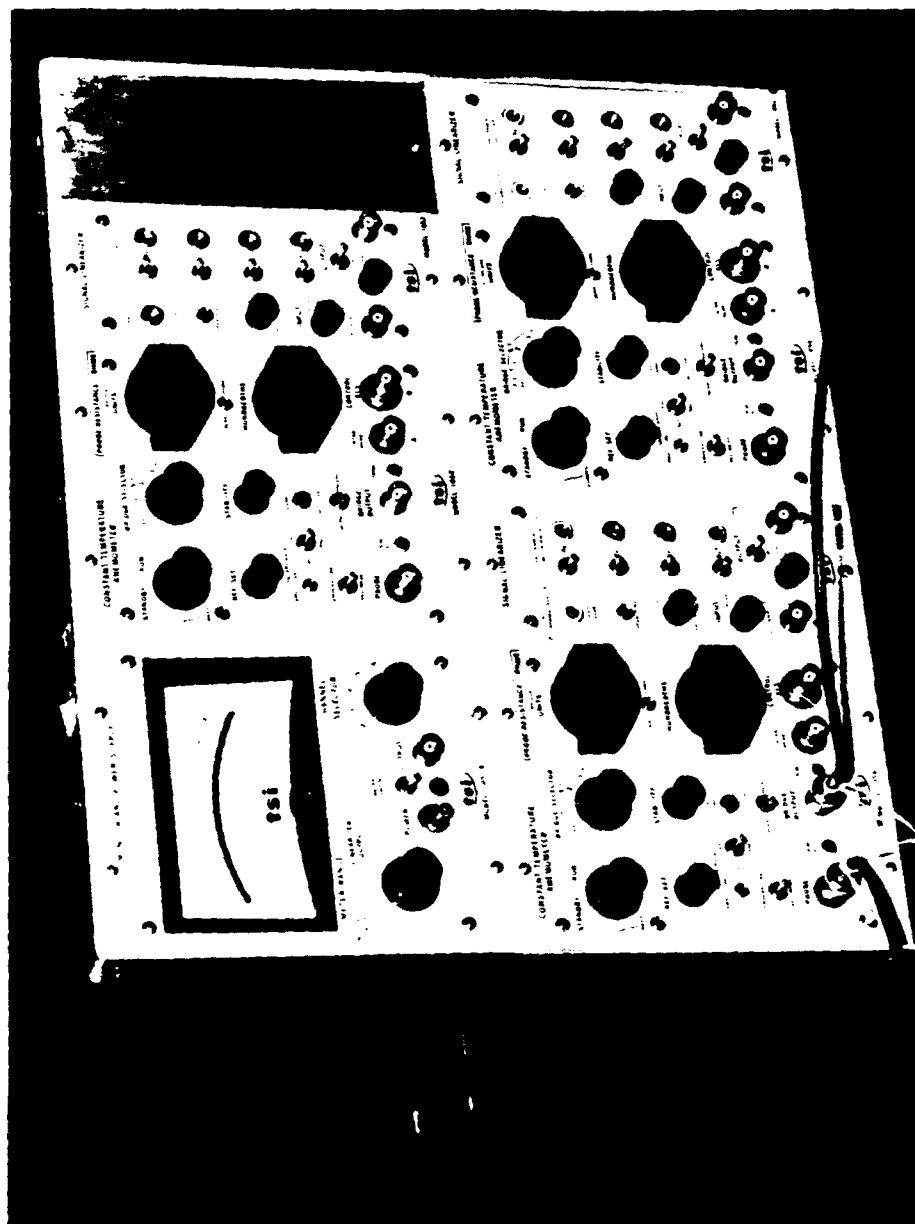


Figure 2.8 Thermal System Incorporated (TSI) Hot Wire/Film Anemometer System

The capability to measure flow angles in at least one plane and availability of hot film probes were the main reasons for the selection of a hot film anemometer to measure the velocity profiles in the flowfield around a swept backward-facing step. Although other instrumentation such as a Laser Doppler Velocimeter (LDV), pulse wire anemometer, or split film anemometer may have been better suited to resolve the reverse flow ambiguity in the recirculation region behind a swept backward-facing step, it was felt that a hot wire or film anemometer was capable of providing meaningful data within the scope of this study. Multi-component probes were not used for several reasons: first, none were available and they were not as easy to use as a single component probe; second, interference between multiple probes being spaced too close together could cause measurement problems; third, it was desirable for the measurement to be spatially as small as possible (i.e., point) and since the size of many multiple component probes were considerably larger, the single component probe best met this requirement; and fourth, the flow was assumed to be basically two dimensional (v component being small), thus, within this assumption, a single probe could easily make the necessary measurements. Because of these reasons and the added advantages of ruggedness, abundant supply and relative ease of use, the 1210-20 Hot Film single component probe was chosen. Also, since the intent of this study was to be a preliminary attempt at determining the mean flowfield behind a backward-facing swept step, the disadvantages of using a hot film probe, rather than a hot wire, were deemed acceptable. The drawback of using a hot film anemometer is a lower frequency response but since only mean velocities were measured this was not a major concern.

Several assumptions were made pertaining to the use of a hot film anemometer. According to TSI (TSI Bulletin TB18), the effects of heat transfer from the probe to the substrate and/or probe supports was assumed to be negligible. As described by Lomas (1986), changes in humidity and near wall effects could be neglected. The closest measurement taken to the wall was 0.020 inches and wall effects normally do not become appreciable until a distance of 0.010 inches from the wall. Thus, these effects were neglected. Ambient temperature changes were corrected using a simple ratio of temperature and output voltages as is suggested by Spring (1987) and TSI TB5, TB16 and TB18. This correction factor will be presented when the data reduction procedure is discussed in chapter 4.

Description of Data Acquisition Equipment

A Hewlett-Packard data acquisition system was used to acquire the calibration and velocity profile data for this study. This system consists of the following hardware: HP 3497A Controller, which switches the various data channels into the HP3456A Digital Integrating Voltmeter (it in turn, converts the hot film anemometer bridge output voltages from analog to digital); and a HP9826 Technical Computer system, which controls the data acquisition system. The HP9826 is programmed in HP BASIC and contains 1.5 mbytes of RAM.

Other equipment used during the wind tunnel tests included a 0.25 inch diameter pitot static tube, which was used to measure the freestream velocity for calibrating the hot film anemometer. The pitot static tube was connected to a set of three Magnehelic Pressure Gauges, with a range of 0.0 to 0.25, 0.0 to 1.0 and 0.0 to 10.0 inches of water, respectively. The ambient test conditions were determined, using a digital thermocouple to measure the test section air temperature and a barometer to measure atmospheric pressure. The ambient temperature and pressure were required to calculate the air density in the test section.

Chapter 3 EXPERIMENTAL PROCEDURE

Overview

The measurement of the flowfield in the vicinity of a backward-facing step was conducted in two parts. The first part consisted of experimental flow observations and velocity measurements, and the second part was the data reduction of these observations and measurements. The testing and the data acquisition procedure are presented in this chapter. Data reduction will be discussed in Chapter 4.

The experimental portion of this study was also accomplished in two parts, the first part being a qualitative analysis, using oil flow visualization, of the flowfield behind the three backward-facing step configurations. The second part of the test used a single component hot film anemometer to provide quantitative measurements of the velocity profiles at different longitudinal centerline distances both upstream and downstream of the step.

Two Reynolds numbers definitions usually associated with the measurements of the flowfield over a backward-facing step. The first Reynolds number, is referenced to the step height, Re_h , and the other to the separation location, Re_{sep} . For this study, a 0.5 inch step height yields a value for $Re_h = 2 \times 10^5$ and with a distance from the leading edge to the step of 27.0 inches the Reynolds number based on L_{sep} is $Re_{sep} = 1 \times 10^6$. These two quantities are useful when comparing results from different studies.

Oil Flow Visualization Procedure

The oil flow experiments were conducted to determine if the flow downstream of the backward-facing step was approximately the same as presented by Selby (1982). The oil mixture used for these tests was produced by combining 80.0 ml of 100 centistoke silicone fluid with 2.0 ml of titanium dioxide. The titanium dioxide does not dissolve in the silicone fluid but remains suspended. The mixture was poured onto the plate several inches downstream of the step. The tunnel was turned on and the movement of the fluid observed. The results from the oil flows downstream of the step are presented in Chapter 5.

Oil flow observations were also made along each of the three leading edges of the three swept step configurations. Initially, the flow over the leading edge of each step was separated and the downstream velocity profiles were thus affected. In order to improve the flow, each step configuration leading edge was blunted to a 0.25 inch radius and hand sanded to smooth the transition from the lower plate wedge, around the radius, and then onto the upper surface. This improved the flow slightly but not to an acceptable level. Finally, the model was placed at a slight negative angle-of-attack, approximately 2.0 degrees nose down. This greatly improved the flow over the leading edge of the plate. By placing the plate at an angle-of-attack a small favorable pressure gradient was generated. After examining the free stream velocities at several positions along the tunnel centerline little effect

due to the pressure gradient on the flow could be detected. A grit strip, of #60 grit, 1.0 inch wide, was placed 2.0 inches downstream of each leading edge in order to assure transition to turbulent flow as far upstream of the step as possible.

Hot Film Calibration Procedure

Calibration of the probe at a specific ambient temperature took approximately twenty minutes to complete. The procedure required some manual operations such as probe alignment and positioning, and tunnel velocity adjustments, but the data were acquired and stored automatically. To calibrate the hot film anemometer, the probe was positioned half way between the model and the tunnel ceiling, approximately 10.0 inches above the wind tunnel model surface. The tunnel was then turned on and set at 70 mph (or 103 fps). The same traversing mechanism used for the velocity profile tests was also used to calibrate the probe.

Hot Film Probe Alignment

Alignment of the probe was accomplished first by sight positioning the film sensor as close to parallel to the freestream as possible. Then the minimum output voltage was found by monitoring the bridge output voltage on the digital voltmeter while making fine rotational adjustments about the longitudinal axis of the probe. The minimum output voltage corresponded to the film sensor being aligned parallel to the flow. When the minimum was found, the yaw angle indicator on the traversing adapter was set to 90 degrees. As a check, the probe was then rotated plus and minus 10 degrees about 90 degrees and the bridge output compared. If the probe was properly aligned the two readings would be identical, if not the probe alignment process was repeated. With the alignment completed, the probe was then rotated so that the yaw angle indicator read 0 degrees and the film sensor was perpendicular to the flow. The next step was to record the effect of velocity on the bridge output voltage of the hot film probe.

Velocity Calibration

The velocity calibration began with the input of initial conditions into the data acquisition program. These inputs included: test and run numbers, date of the test, comment about the test, probe serial number, test section temperature, ambient pressure, calibration velocity range, bridge reference voltage, and number of readings per sample. The calibration velocity range was 70 mph (103 fps) to 7 mph (10 fps). The wind tunnel manometer board was used only as a reference to set the approximate test section velocity. The actual velocity was determined by manually reading the appropriate Magnehelic water gauge which was connected to the pitot tube installed in the test section. Starting at 70 mph, the data acquisition system read the bridge output voltage and stored the average value of 50 readings. The voltmeter was set for a reading rate of 50 readings per second; thus, it took approximately 1.0 second to complete one sample. The test section velocity

was decreased by 5 mph and the process repeated until, a velocity of approximately 5 mph was reached.

Yaw Calibration

The yaw calibration of the probe was the next step in the calibration process. The probe was yawed by rotating the probe about its longitudinal axis. In order for a single component probe to resolve the direction of the total velocity vector, the effects of yaw angle on the probe output must be known. The reason for this yaw effect is that as the yaw angle increases, the component of the velocity perpendicular to the film sensor decreases. Thus, the effective cooling of the sensor and the bridge output voltage decreases. Generally the yaw effect on a hot film or wire follows a cosine law, defined as follows:

$$U_{\text{eff}} = U \cos(\alpha) \quad (3.1)$$

but according to Lomas (1986) this is only an approximation if the probe's aspect ratio is less than 600. The probe aspect ratio is defined as the ratio of the length to diameter of the film sensor. For this study the hot film probe had an aspect ratio of about 20. Since the aspect ratio was so low, probe support interference could also affect the accuracy of the cosine law. Thus, the yaw calibration of the hot film probe was necessary for these tests.

The yaw calibration was conducted at a velocity of 50 mph (73.3 fps), which was also the freestream velocity used for all the velocity profile surveys. It should be noted that the effect of yaw on the non-dimensional probe output is independent of the freestream velocity, as stated by Olivari (1978), and was experimentally verified during this study. The yaw calibration was performed with the probe positioned at the same height above the step as was used for the velocity calibration. The probe was rotated to a -60 degree yaw angle and the average of 50 readings of the bridge output was recorded and stored. The yaw angle was incremented 10 degrees and the process repeated until a +60 degree yaw angle was achieved.

All calibration data were stored on a flexible disc for later reduction and analysis. Whenever the test section temperature for a velocity profile test was more than three degrees Fahrenheit from any of the calibration temperatures, a new calibration was performed. The calibration results and data reduction technique are discussed in the Chapter 4.

Velocity Profile Test Procedure

The test procedure for performing the velocity profile survey was similar to the calibration test. First, the initial conditions for the data acquisition program were entered. These included: a test and run number, test section temperature and ambient pressure, sweep angle of the step, position along the model centerline with respect to the step where the profile would be surveyed, and the probe rotation or yaw angle, which was arbitrary chosen to be

15 degrees. The traversing mechanism was positioned and locked into place above the point where a velocity profile was to be measured.

The next step was to establish a reference height between the surface of the plate and the tip of the hot film probe. It was discovered that because of the negative pressure in the test section during tunnel operations, the tunnel ceiling and floor would move relative to each other. This made it difficult to establish a reference height between the probe tip and the surface of the model. It was also discovered that other unknown factors, possibly temperature, affected the amount of displacement. After extensive testing the following procedure was developed to provide the necessary accuracy in the height measurement. This technique established the height of the probe above the surface of the plate to plus or minus 0.002 inches. The technique consisted of replacing the probe in the probe holder with a measurement standard, a modified hot film probe. The exact difference in length between the measurement standard and the hot film probe was determined using an optical comparator. The wind tunnel was turned on and the velocity adjusted to the test speed of 50 mph. After allowing the tunnel to run for several minutes the standard was lowered to the surface of the model and the height indicator on the traversing mechanism was zeroed. The standard was raised and lowered until the height indicator read zero repeatedly. The standard was then offset from the plate a distance equal to the difference in length of the standard to the hot film probe. The height indicator was then reset to zero. This position then indicated the point at which the probe tip would touch the plate. With the height reference set, the tunnel was turned off and the measurement standard replaced with the hot film probe.

Next the probe was positioned 10.000 inches above the surface of the plate. At this position the probe was aligned with the freestream velocity direction using the same alignment procedure as discussed above for the velocity calibration of the probe. It was assumed that at 10.000 inches above the plate the freestream velocity was parallel to the sides of the tunnel. The velocity surveys consisted of three measurements taken at each vertical position above the plate. Only two measurements were necessary to resolve the magnitude and direction of the total velocity, and the third measurement increased the accuracy of this procedure. The first measurement was taken with the yaw angle indicator set at zero degrees. The average of 50 readings was recorded and stored. The probe was then rotated plus and minus 15 degrees about 0 degrees, with the average of the 50 reading being read and stored for each rotation. The same process was repeated for each vertical survey position above the plate. Vertical positioning varied depending on whether the profile was being taken upstream of the step, in the recirculation region, or downstream of the recirculation region. Most profiles began at 10.000 inches and ended at 0.020 inches above the step. The lower limit of 0.020 inches was chosen in order to avoid breaking probes by inadvertently driving them into the plate. The same procedure was then repeated for various longitudinal positions upstream and downstream for each of the three step configurations.

Flow Reversal Ambiguity

For this first attempt at measuring the flowfield in the vicinity of a swept backward-facing step, no provisions were made to experimentally resolve the flow reversal ambiguity within the recirculation region. Instead, the point of flow reversal was determined during the data reduction procedure, the assumption being, that as the stagnation line in the recirculation region was approached from the freestream side, the total velocity would decrease to a minimum. Then, on the model side of the stagnation line, the total velocity would increase slightly before going to zero again at the surface of the model. This approach was only partially successful. Two simple experimental methods may prove useful in future testing for resolving the flow reversal ambiguity. One method would be to use a small rotatable pitot probe to find the direction of maximum pressure and thus the flow direction. The other method described by Naverbury (1969) uses a hot wire/film with a shield around it. The shield causes the probe to be sensitive to the flow in only one direction. Then, similar to the pitot probe, by rotating the hot wire/film probe to find the maximum bridge output voltage, the flow direction can be determined. However, for these preliminary tests these techniques were not attempted.

Chapter 4 DATA REDUCTION PROCEDURE

Overview

This chapter presents a discussion of the procedure used in this study to reduce the velocity profile measurements. The calibration procedure, including the velocity and yaw effects on the hot film probe are discussed first. Next the data reduction procedure to determine the total velocity and flow angle from the three measurements at each survey position is explained. The data analysis procedure for determining the flow reversal point, the u and w velocity components and the u component boundary-layer thickness is reviewed. Typical results from each procedure are presented. Finally, the format for the tabulated and graphical presentation of the results from the above procedures are explained. The intermediate results from the data reduction procedure have not been included for the sake of brevity. The intermediate results can be obtained upon request.

Calibration Data Reduction Procedure

Velocity Calibration Reduction Procedure

The procedure followed to calibrate the hot film probe for the effect of velocity on bridge output was relatively straightforward. The acquisition of the calibration data was described in Chapter 3. With the film sensor aligned perpendicular to the freestream the bridge output from the anemometer was recorded along with the true test section velocity, which was determined from a pitot static probe. The velocity calibration was calculated using two different methods.

Fourth Order Polynomial Curve Fit. The first approach fitted the raw velocity and output voltage data to a fourth degree polynomial, using a least square routine. This approach is similar to the way the 1052 Linearizer component of the TSI Hot Wire Anemometer System functions. The difference is that the Linearizer fits a fourth degree polynomial to the bridge output electronically where this procedure fits the polynomial numerically. A typical plot of the raw calibration data and resulting curve fit is shown in Figure 4.1.

Linear Curve Fit. The second method of determining a relationship between the bridge output and the velocity was by using King's law and a least squares linear fit of the data. King's law describes the heat transfer from a cylinder of infinite length. The law for a hot film anemometer is often written as

$$E^2 = A + B U^n \quad (4.1)$$

where E is the hot wire bridge output voltage, U is the velocity, A and B are constants and n varies between 0.45 and 0.5. For this study, $n = 0.5$ provided the best results. A and B were determined using a linear least squares fit of the calibration data. Figure 4.2 compares the experimental data to linear

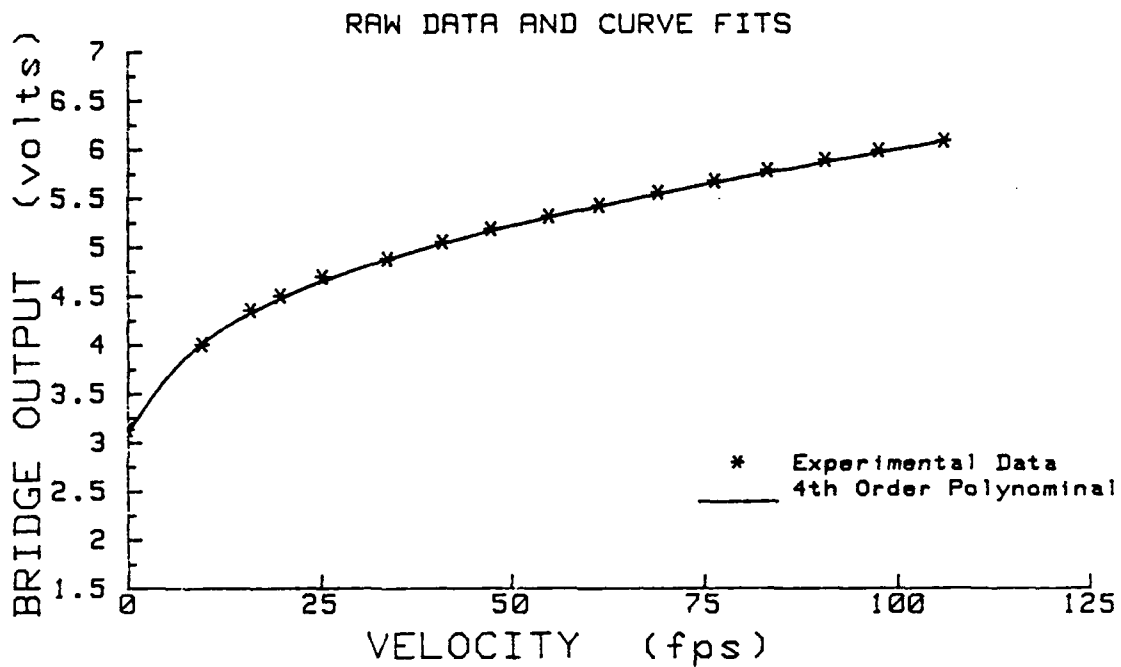


Figure 4.1 Raw Hot Film Calibration Data and Fourth Degree Polynomial Curve Fit

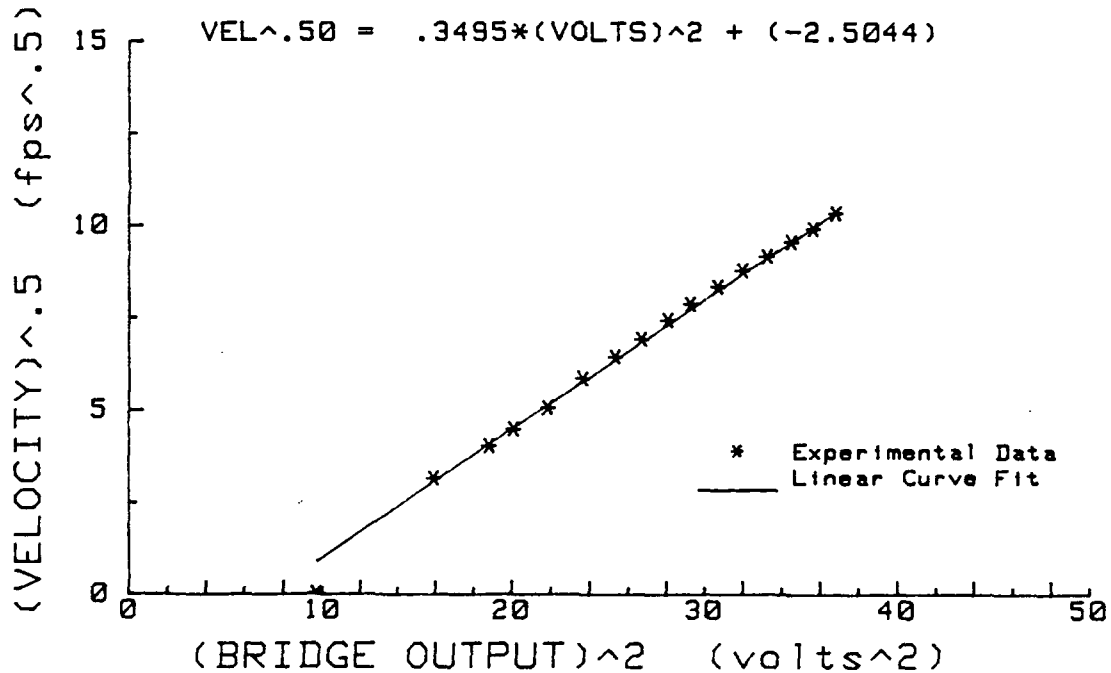


Figure 4.2 King's Law Applied to Hot Film Calibration Data and Compared to Linear Curve Fit

curve fitted data for a typical calibration test. It should be noted that the measurement taken at zero velocity was not used in the least squares calculation because of the potential for buoyancy effects. Better agreement was achieved between the true and calculated velocities over the entire calibration range by neglecting the zero velocity measurement.

Comparison of Polynomial and Linear Curve Fits. Typical calibration data is presented in Table 4.1. The important information in this table is the percent difference between the velocity measured with the pitot static probe, and the velocities calculated by the two curve fitted equations: linear and fourth order polynomial. Overall the agreement was very good, with percent differences generally around 2% or less. At the lower velocities, the percent difference was slightly higher with the highest being 5%, but this was to be expected. The increase in error at the low velocities, below 10 mph, was due to the reduced sensitivity of the water gauges at such low pressures. The uncertainty of the measurements is discussed in the last section of this chapter. All velocities were calculated with the polynomial fit, since it was slightly more accurate than the linear curve fit.

Yaw Calibration

Effect of Probe Yaw on Velocity Measurement. Typical yaw characteristics of a hot film probe are listed in Table 4.2. The first step in determining the effects of yaw angle on the probe's output was to calculate the velocities corresponding to the yawed voltage readings, obtained during calibration, using the fourth order polynomial from the velocity calibration. Next, the yaw data were non-dimensionalized by dividing the velocities by the maximum velocity which occurred at 0 degrees. Then, the yaw angle and the non-dimensional velocity were curve fitted using a second order, least squares technique. Figure 4.3 compares the experimental data with the resulting yaw calibration curve. As can be seen from the plot and the tabulated percent differences the agreement is quite good, 2% error or less. From this curve the total velocity could be determined once the flow direction was known.

Velocity Profile Data Reduction

A procedure for determining the total flow velocity and direction in an unknown, two-dimensional flowfield was described by Olivari (1978). In this study, the two dimensions of interest were the components perpendicular (u) and parallel (w) to the step face. The v component of the velocity vector was assumed to be negligible. An overview of the procedure will be given first, followed by an explanation of how it was used to resolve the total velocity and direction from the velocity profile measurements.

Table 4.1 Typical Hot Wire Calibration Results

HOT WIRE CALIBRATION RESULTS

DATE : 12/20/88

TEST NO.-RUN NO.: 1Z10-2

COMMENT: CALIBRATION RUN

PROBE SERIAL NO.: 85234

CALIBRATION TEMPERATURE: 58 deg F

PRESSURE: 764.4 mm-hg

SAMPLES/READING: 50

TEST FREE STREAM VELOCITY: 50 fps

CALIBRATION VELOCITY RANGE: 5 TO 70 mph

HOTWIRE REFERENCE VOLTAGE: 5.00425 volts

YAW CALIBRATION ANGULAR STEP 10 deg

N	IND VEL	PRESSURE	ACTUAL VELOCITY	BRIDGE	BRIDGE	DELTA	BRIDGE	DELTA
	mph	inch-H2O	fps	volts	VEL LIN	%	VEL POLY	%
1	0.0	0.000	0.00	3.122	.81	0.0	.05	0.0
2	70.0	2.600	106.19	6.073	107.86	1.6	105.47	-1.7
3	65.0	2.200	97.68	5.974	99.33	1.7	98.12	.5
4	60.0	1.900	90.77	5.878	91.61	.9	91.29	.6
5	55.0	1.600	83.30	5.770	83.38	.1	83.76	.6
6	50.0	1.350	76.51	5.662	75.68	-1.1	76.50	-0.0
7	45.0	1.100	69.07	5.546	67.99	-1.6	69.03	-0.0
8	40.0	.870	61.42	5.413	59.86	-2.5	60.93	-.8
9	35.0	.695	54.90	5.303	53.62	-2.3	54.58	-.6
10	30.0	.520	47.49	5.172	46.86	-1.3	47.58	-.2
11	25.0	.390	41.13	5.037	40.50	-1.5	40.93	-.5
12	20.0	.265	33.90	4.865	33.27	-1.9	33.31	-1.7
13	15.0	.148	25.33	4.679	26.49	4.5	26.19	3.4
14	10.0	.091	19.87	4.490	20.61	3.7	20.13	1.3
15	8.0	.059	16.00	4.344	16.73	4.6	16.22	1.4
16	5.0	.022	9.77	3.996	9.46	-3.1	9.28	-5.0

Table 4.2 Typical Yaw Calibration Results

YAW CHARACTERISTICS, based on bridge output

ANGLE	YAW	YAW VEL	UE/U	UE/U	%
deg	volts	fps	actual	poly	
60	5.077	42.82	.558	.556	-.5
50	5.264	52.46	.684	.690	.9
40	5.421	61.40	.800	.800	-.1
30	5.544	68.87	.898	.885	-1.4
20	5.585	71.48	.932	.946	1.6
10	5.648	75.56	.985	.983	-.2
0	5.665	76.72	1.000	.996	-.4
-10	5.651	75.79	.988	.984	-.4
-20	5.585	71.52	.932	.948	1.7
-30	5.535	68.35	.891	.887	-.4
-40	5.447	62.91	.820	.803	-2.1
-50	5.264	52.47	.684	.694	1.4
-60	5.080	42.95	.560	.560	.1

NOTE: YAW_VEL 's are calculated using a polynomial fit

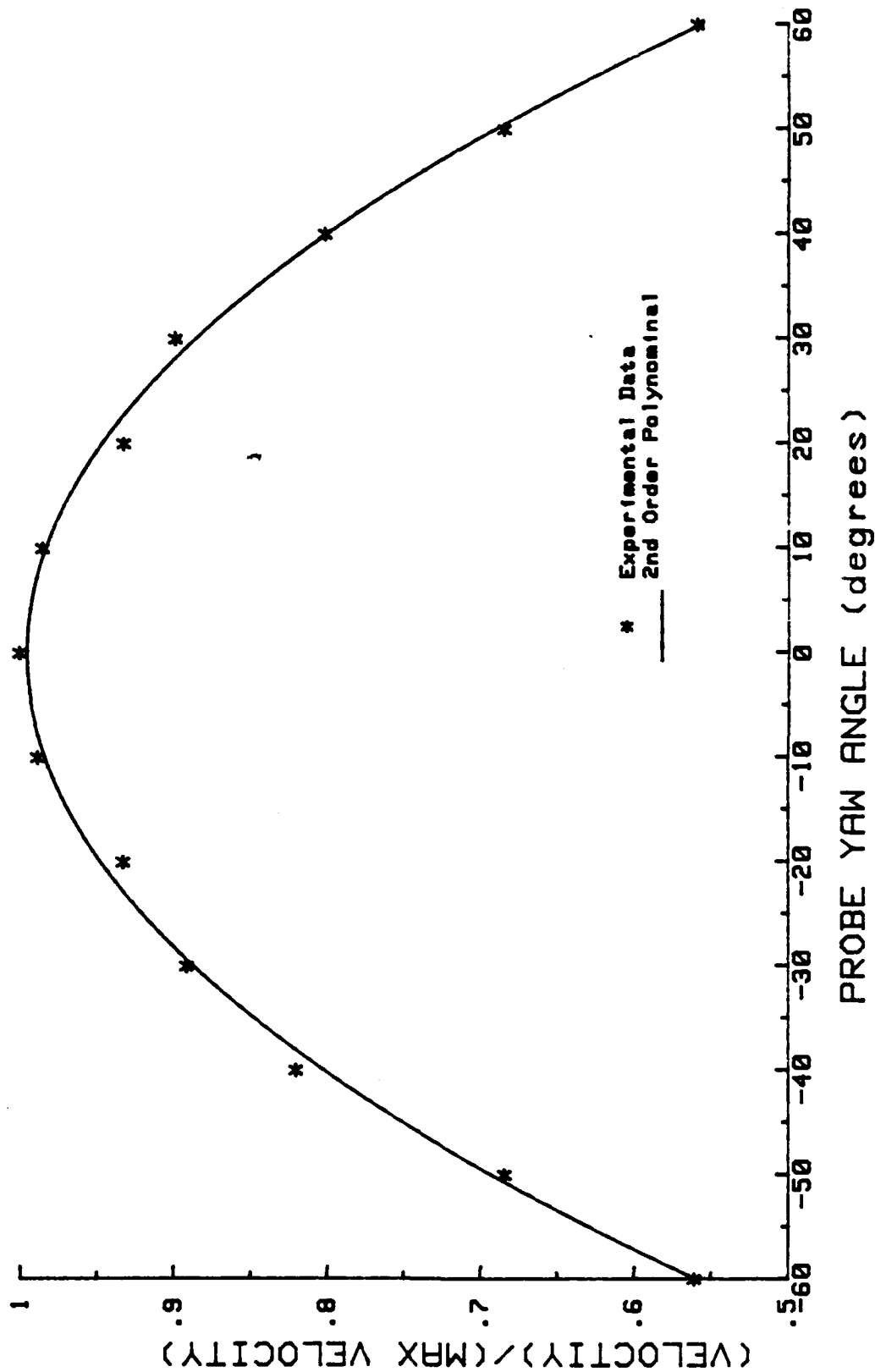


Figure 4.3 Effect of Yaw Angle on Hot Film Probe Output and Compared to a Second Order Polynomial Curve Fit

Overview of Data Reduction Procedure

By using the yaw calibration curve, which represents the angular sensitivity of the hot film probe, the magnitude and direction of the velocity in an unknown two-dimensional flowfield can be found. At each test point in the velocity profiles, three measurements are made, α , $\alpha + \theta$, and $\alpha - \theta$, where α is the unknown flow direction relative to some reference, and θ is an arbitrarily chosen angle. The only requirement for this procedure is that the angles α , $\alpha + \theta$ and $\alpha - \theta$ be less than 60 degrees, because the calibration curve is only valid between -60 and +60 degrees. In this study, the reference was chosen to be the free stream flow direction. The following three equations represent the three measurements:

$$\frac{U_{eff_1}}{U} = f(\alpha) \quad (4.2)$$

$$\frac{U_{eff_2}}{U} = f(\alpha + \theta) \quad (4.3)$$

$$\frac{U_{eff_3}}{U} = f(\alpha - \theta) \quad (4.4)$$

The function f is the yaw calibration curve determined from the reduction of the calibration data. The next step is to ratio equation (4.2) to (4.3) and (4.4) to (4.2). These ratios yield the following:

$$\frac{U_{eff_1}/U}{U_{eff_2}/U} = \frac{f(\alpha)}{f(\alpha + \theta)} = F(\alpha) \quad (4.5)$$

$$\frac{U_{eff_3}/U}{U_{eff_1}/U} = \frac{f(\alpha - \theta)}{f(\alpha)} = G(\alpha) \quad (4.6)$$

Equations (4.5) and (4.6) allowed the flow direction, α , to be determined because the three hot film measurements and θ are known. Actually, two separate α 's are found and averaged to give the final flow direction at that particular point. Knowing the average α , it is then substituted into (4.2) to determine the magnitude of the total velocity. If the requirement for α , $\alpha + \theta$, $\alpha - \theta$ being less than 60 degrees, is not met, then the calculated α is only an estimate, which can be used to reposition the probe to find a more accurate result.

Example of Data Reduction Procedure

The first step in reducing the anemometer voltage measurements, to velocity and flow direction is to compensate for temperature differences between the calibration and velocity profile tests. This compensation is necessary because of the way in which a constant temperature hot film anemometer operates. The film sensor makes up one leg of a Wheatstone Bridge and is typically heated to almost 500 degrees Fahrenheit. As a fluid, such as air, flows over the sensor, the sensor is cooled and the bridge becomes unbalanced. The anemometer balances the bridge to maintain a constant sensor temperature by adjusting the voltage across the sensor, thus the name, constant temperature anemometer. If the sensor is calibrated at one temperature and then tested at another, the anemometer will adjust for the temperature difference by raising or lowering the bridge voltage. Since the bridge voltage and fluid velocity are related by the calibration equation which was determined at a specific calibration temperature, any temperature difference will cause the anemometer to indicate an incorrect fluid velocity.

There are several ways to correct for temperature variations between calibrated and test temperatures when using a hot film anemometer. Most are complicated and require several assumptions, which leave the results questionable. A simple method suggested by Spring (1987) and TSI (TB18), adjusts for the temperature difference by a single correction factor. The correction factor is defined as:

$$\frac{E_{\text{corr}}^2}{E^2} = \frac{T_s - T_{\text{cal}}}{T_s - T} \quad (4.7)$$

where E_{corr} is the corrected bridge output voltage, E is the voltage from the velocity profile measurements, T_s is the sensor temperature supplied by the manufacture (482 degrees Fahrenheit), T_{cal} is the fluid temperature during calibration, and T is the temperature of fluid during the velocity profile tests. This correction factor was used for temperature differences up to 3 degrees Fahrenheit. If the difference was greater, a new calibration was performed at the new temperature.

In order to reduce the velocity profile data, an approximation to the functions $F(\alpha)$, equation (4.5), and $G(\alpha)$, equation (4.6), had to be determined. $F(\alpha)$ was found by generating a locus of data using the yaw calibration curve. Starting with an α equal to -60 degrees and equation (4.2), the velocity ratio corresponding to that particular alpha was calculated. Next, the corresponding velocity ratio for equation (4.3) was found using a θ equal to 15 degrees. Then employing equation (4.5), the value of F was determined for an α of -60 degrees. The process was repeated incrementing α by +5 degrees until an α of +45 degrees was achieved. The upper limit of +45 degrees was required in order that $\theta + \alpha$ did not exceed +60 degrees because the yaw calibration curve was only valid between -60 and +60 degrees. With the locus of points calculated, $F(\alpha)$ was approximated by a fourth order, least squares polynomial. A slight modification to the above procedure was necessary in

order to approximate $G(\alpha)$. The initial and final α was -45 degrees and $+60$ degrees, respectively. θ was still 15 degrees, but instead of equation (4.5), equation (4.6) was used. Figure 4.4 compares the locus of points and the fourth order polynomial curve fits for the function $F(\alpha)$ and $G(\alpha)$. The agreement between the data and curve fits were very good, with a maximum error of less than 1%.

With the approximation of $F(\alpha)$, $G(\alpha)$ and the three survey measurements at α , $\alpha + \theta$ and $\alpha - \theta$, the flow direction (α) was calculated. Knowing α and the effective velocity measured at α , and using the yaw calibration equation (4.2), the magnitude of the total velocity was determined.

Data Reduction Procedure

The data reduction procedure described in this section did not provide satisfactory results in the region of $x/h=0.0$ to 1.0 and from $y/h=0$ to 1.0. This was due to the total velocity being very low and out of range of the calibration data. Also, the flow reversal could not be resolved in this region.

Flow Reversal Determination. Once the magnitude of the total velocity and the flow direction were calculated, other quantities necessary for the analysis of the flowfield in the vicinity of the backward-facing swept step were determined. These quantities included the u and w velocity components and the boundary-layer thickness. Although the velocity profiles were measured to a height of 10.000 inches (20 step heights) above the surface of the model, only data between 2.000 inches (4 step heights) and the surface were used in the analysis. The reason for this is that the upstream and downstream boundary-layers are much smaller than 2.0 inches and the boundary-layer and separated flow region are the primary focus of this work.

After modifying the data acquisition program to assist with the data analysis part of the study, the first step was to place the upper limit of the profile at 2.000 inches. Next, the total velocity profile was displayed on the computer CRT to determine if a flow reversal was present. As explained in chapter 3, the flow reversal was identified by examining the total velocity profile and looking for a minimum followed by a slight increase in the total magnitude of the velocity. Figure 4.5 shows the total velocity for the 0 degree swept step, $x=1$ inch downstream of the step. The flow reversal occurs approximately 0.25 inches above the surface. If a particular profile was not in the recirculation region or a clear flow reversal was not evident, the total velocity profile was accepted as displayed and the data analysis continued. If a flow reversal was present, as is shown in Figure 4.5, all data points below the stagnation line were modified. This modification included reversing the sign of both the total velocity and the flow direction. Generally, at the point of flow reversal, the total velocities were close to or below the lower calibration limit of the hot film probe, so that the accuracy of these results were questionable. In some cases, it was necessary to drop one or two data points around the flow reversal point because of the lack of reliability of the calibration curve at low velocities. Figure 4.6 is the profile of Figure 4.5 modified for flow reversal and

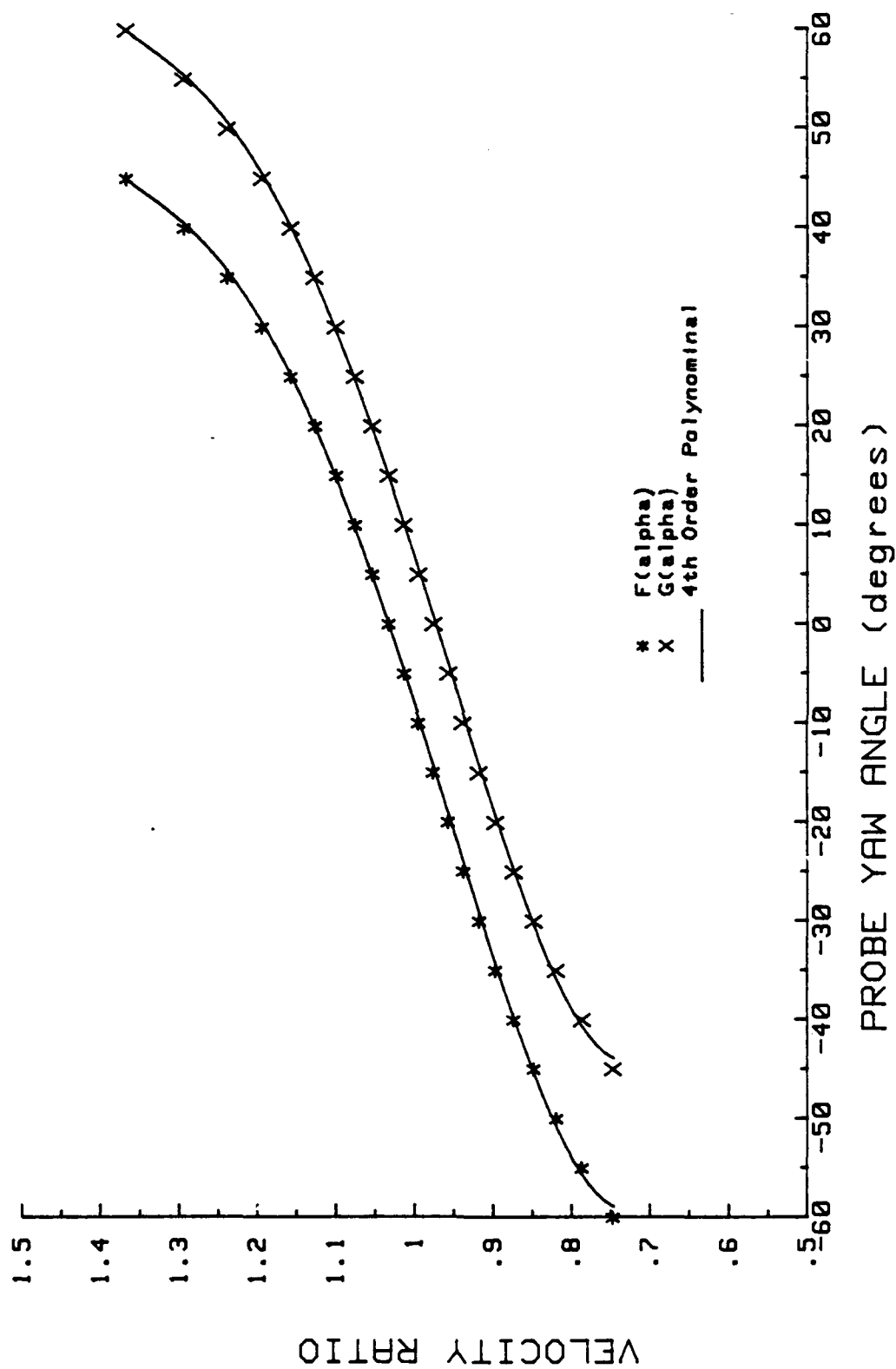


Figure 4.4 Probe Yaw Angle Versus $F(\alpha)$ and $G(\alpha)$

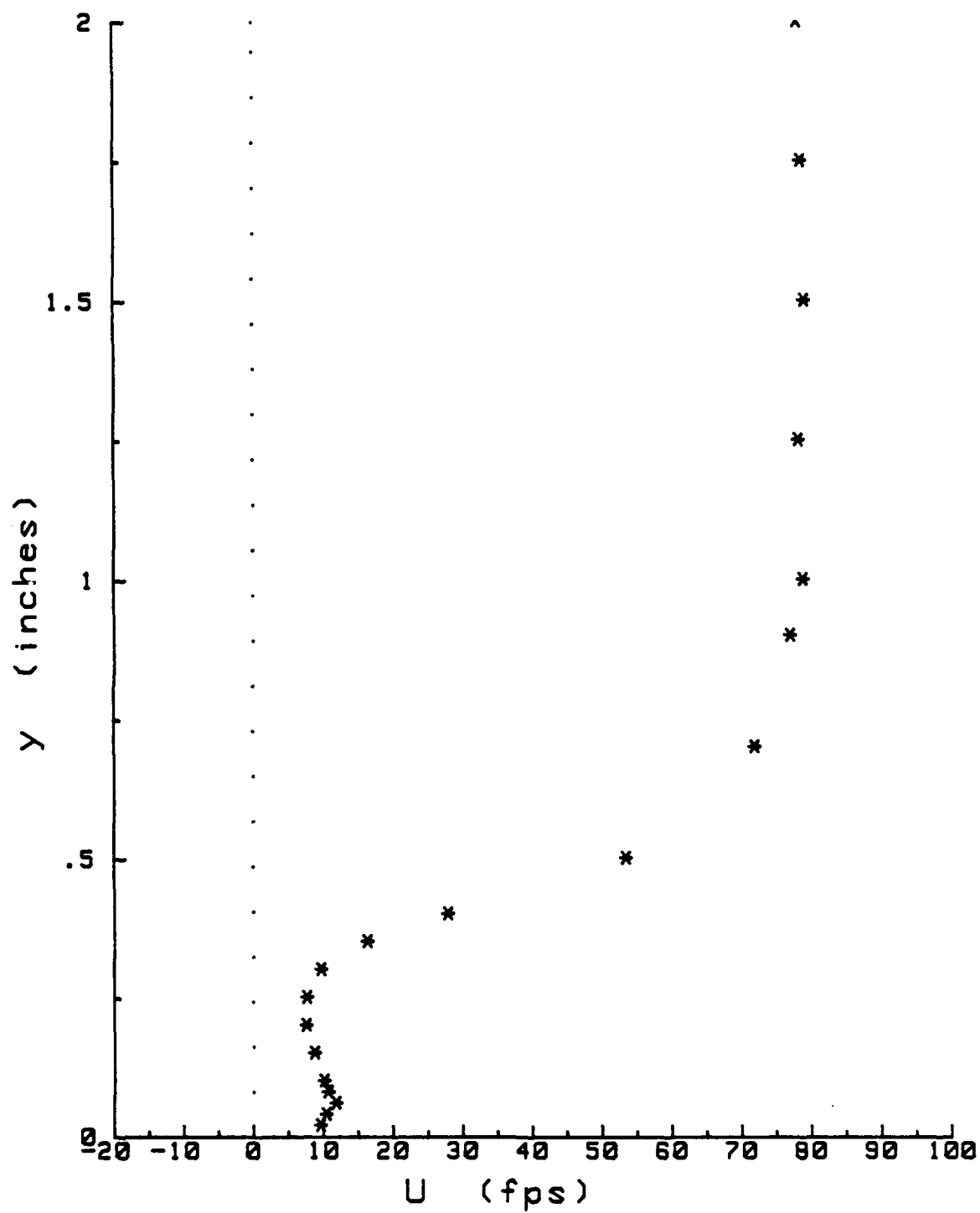


Figure 4.5 Total Velocity Profile, $\Lambda = 0$ Degrees
and $x/h = 2.0$

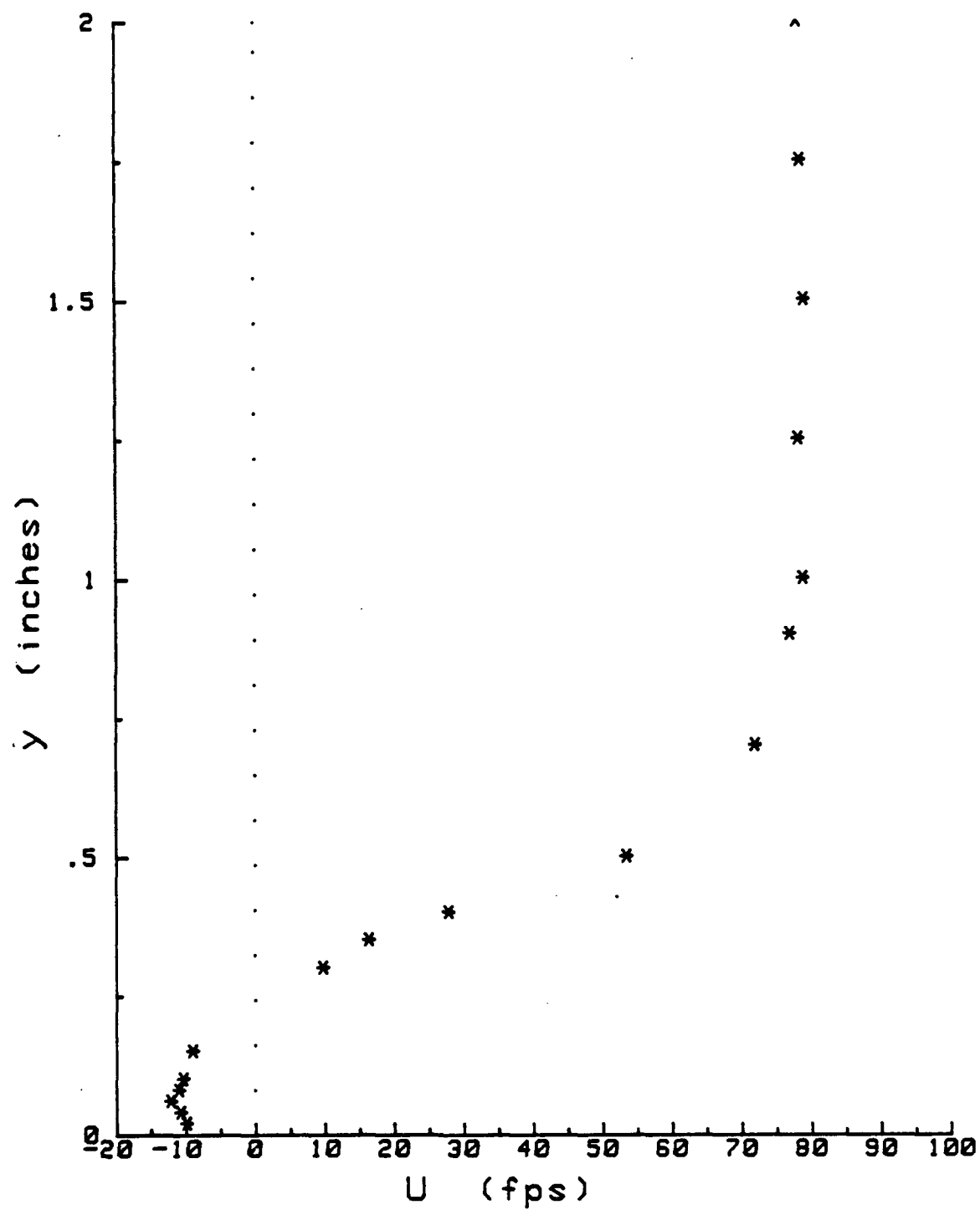


Figure 4.6 Total Velocity Profile With Flow Reversal, $\Lambda = 0$ Degrees and $x/h = 2.0$

two data points, corresponding to probe heights of 0.25 and 0.20 inches, being deleted from the plot. It should be noted that all data points are listed in the tabulated data with the points that are not used in the analysis indicated at the bottom of the table.

Edge u Velocity Component. With the flow reversal determined, a graph of the u velocity component was displayed. This was necessary for determining the edge free stream u velocity component. The edge velocity was determined by averaging the velocities of all data points between $y=2.0$ inches and below to the first data point that appeared to be in the boundary-layer. A typical plot of the u velocity component versus probe height is shown in Figure 4.7 with the edge u component, u_e , indicated by the dashed line. The edge u velocity component was needed for several reasons: first, the u and w components were both non-dimensionalized by u_e ; secondly, the cut-off for determining u_e was also used to calculate an edge total velocity, U_e , for the purpose of non-dimensionalizing the total velocity results; and finally, u_e was needed to approximate the boundary-layer thickness.

Approximate Boundary-Layer Thickness. The final quantity determined was an approximate boundary-layer thickness for the u component velocity profile. By employing a power law and using a $\ln\text{-}\ln$ plot an estimate of the boundary-layer thickness was made. The computer displayed a plot of $\ln(u)$ versus $\ln(y)$, this is shown in Figure 4.8. The edge velocity is indicated by a horizontal line through the data points that were used to determine the average. All remaining velocity data, below the last data point used to determine u_e and above the data point where a possible flow reversal took place, were used in a linear least squares fit. The linear fit is also indicated on the \ln plot. Two criteria used for selecting the best linear fit were: first, how well did the curve fit the available data and second, where did the linear fit cross the horizontal line representing the edge velocity. If the fit was unsatisfactory or it did not intersect the constant $\ln(u_e)$ line properly, the number of data points in the linear fit was adjusted. The criterion for the proper intersection of the two lines was that the linear curve fit had to intersect the horizontal u_e line near the last data point used to determine u_e . Once the graph of the two lines was acceptable, the intersection of the two lines determined the value of the $\ln(\delta)$. Figure 4.9 shows an example of the final results from this procedure. With this final piece of information, the results were tabulated and plotted.

Format for Presentation of Results

Tabulated Results. The results from the velocity profile measurements are presented in both tabulated and graphical formats. Typical tabulated results are listed in Table 4.3 for a step sweep angle of 15 degrees at a distance of $x=1$ inch downstream of the step. At the top of each table, the test conditions are listed, along with the edge or average total velocity, the edge or average u component of the total velocity and the boundary layer thickness of the u component. All results were temperature compensated in order to account for any temperature difference between the calibration test and the velocity

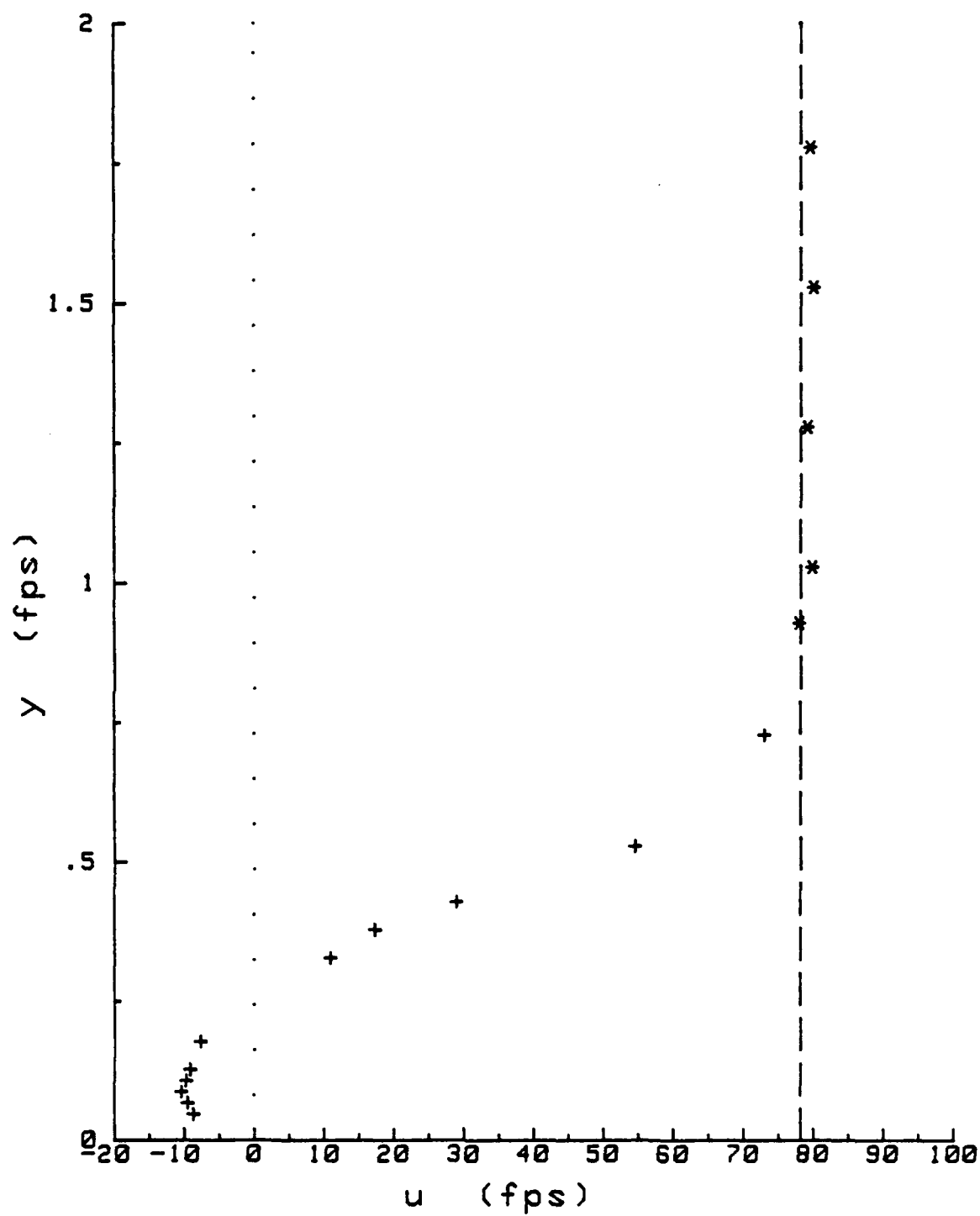


Figure 4.7 u Component of Velocity With Edge
Velocity Represented by the Dashed Line

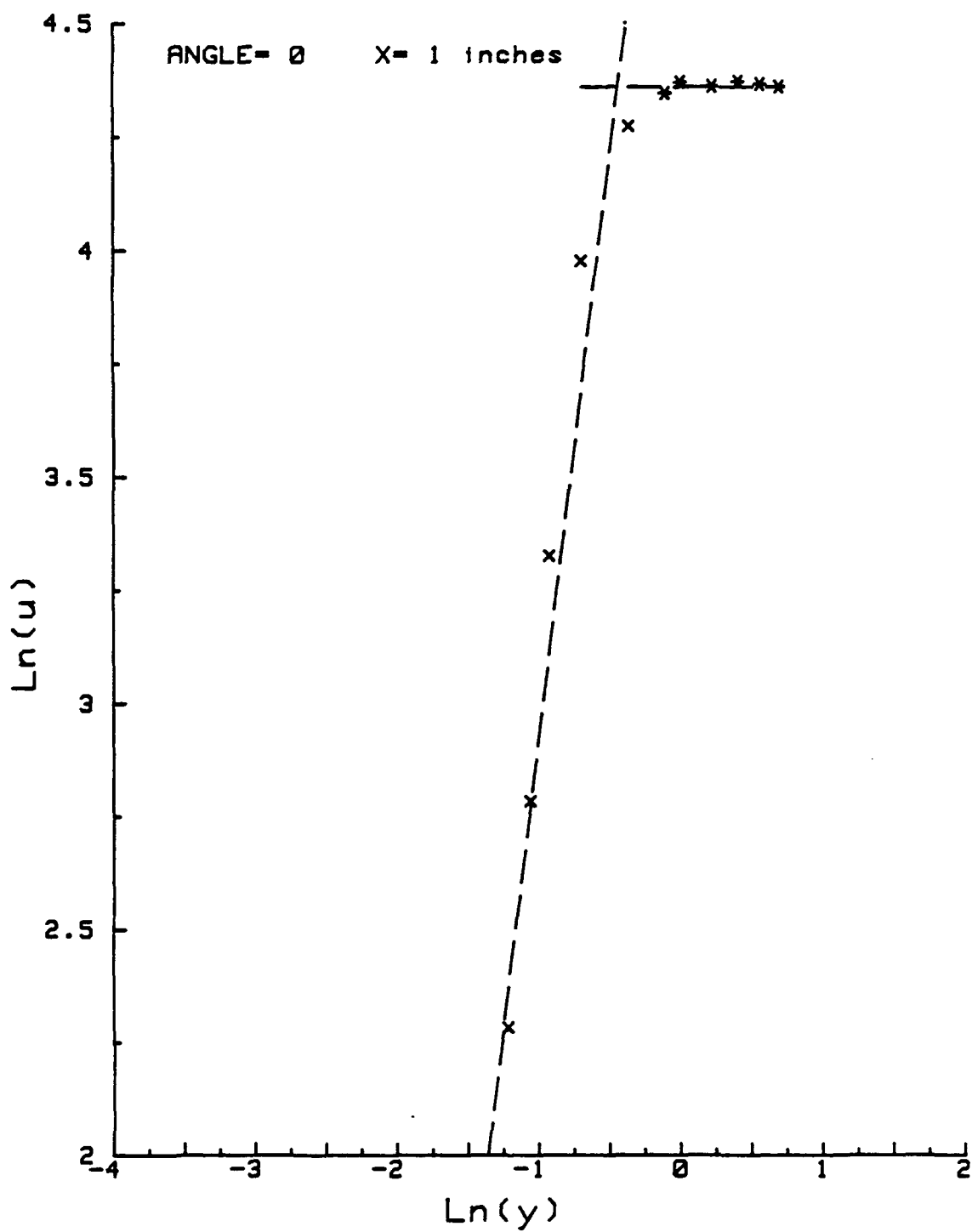


Figure 4.8 Estimating Boundary-Layer Thickness
From Intersection of Constant u_e Line
and Linear Fit of Remaining Data

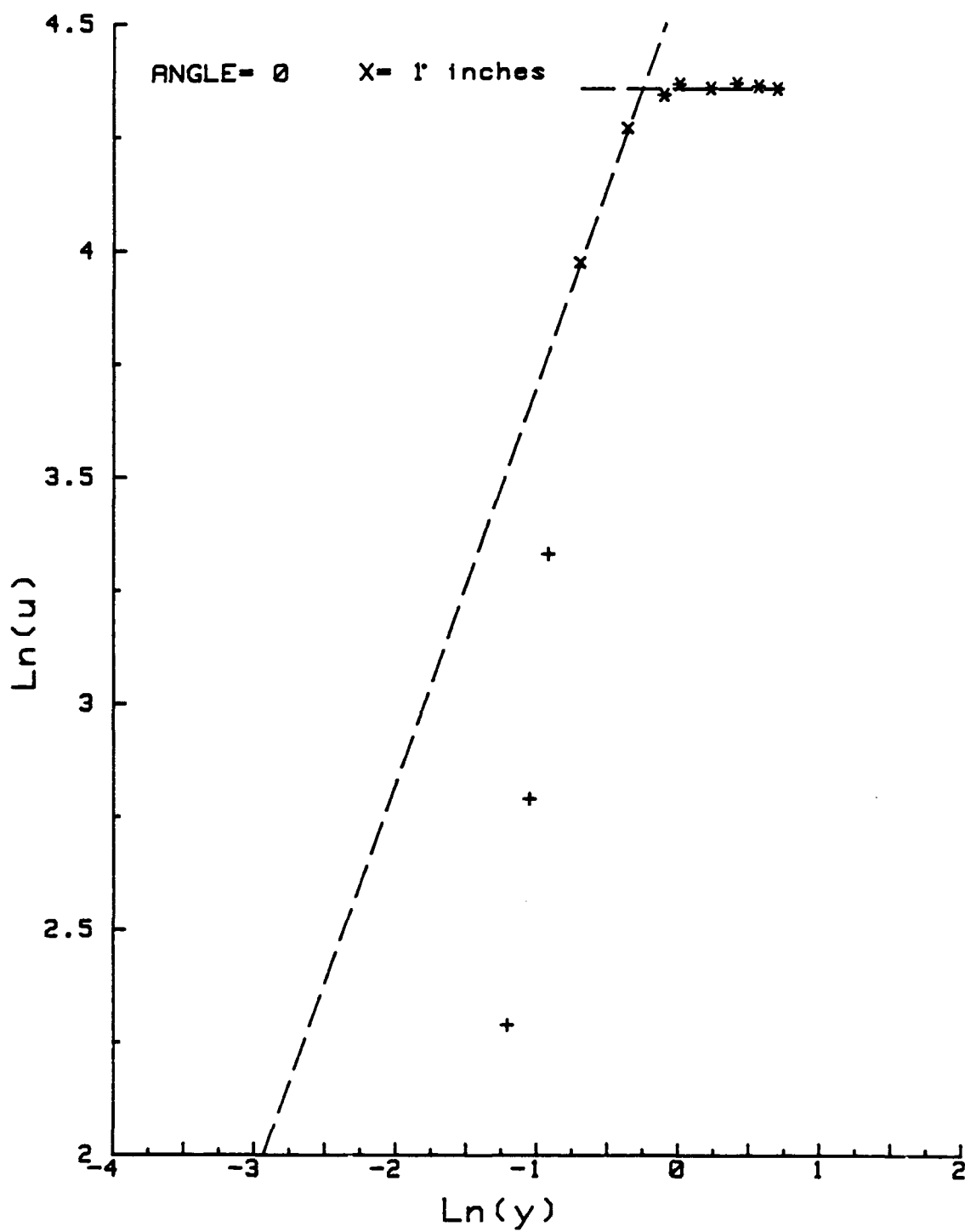


Figure 4.9 Refining Estimate of Boundary-Layer Thickness Using Fewer Points in the Linear Fit

Table 4.3 Typical Velocity Profile Results

VELOCITY PROFILE RESULTS
 DATE : 12/14/88
 TEST NO.-RUN NO.: 1209-9
 COMMENT: VELOCITY PROFILE ALPHA=1 DEG 56 MIN
 TUNNEL VELOCITY FROM PITOT PROBE: 76.75 fps
 STEP ANGLE: 15 degrees
 DISTANCE FROM STEP: 1 inches
 CALIBRATION TEST AND RUN NO.: CAL12092
 CALIBRATION TEMPERATURE: 44 deg F
 TEST TEMPERATURE: 45 deg F
 TEST PRESSURE: 766.6 mm-Hg
 TEST DATA TAKEN AT + AND - VALUES OF 15
 EDGE TOTAL VELOCITY: 79.692 fps
 EDGE u COMPONENT OF VELOCITY: 74.684 fps
 BOUNDARY LAYER THICKNESS: .862 inches

DATA TEMPERATURE COMPENSATED

N	y (in)	U/Ue	alpha (deg)	alpha + LAMBDA (deg)	u/ue	w/ue
1	10.00	.980	-.04	14.96	1.010	.270
2	8.00	.979	.71	15.71	1.005	.283
3	6.00	.979	-1.78	14.22	1.012	.257
4	4.00	.983	-1.36	13.64	1.020	.247
5	2.00	.991	3.89	18.89	1.001	.342
6	1.50	1.005	5.78	20.78	1.003	.380
7	1.25	1.006	4.41	19.41	1.013	.357
8	1.00	1.001	6.08	21.08	.997	.384
9	.90	.997	6.81	21.81	.987	.395
10	.80	.984	6.44	21.44	.958	.376
11	.70	.931	4.94	19.94	.934	.339
12	.60	.852	4.10	19.10	.859	.298
13	.50	.669	2.51	17.51	.681	.215
14	.40	.316	-10.04	4.96	.336	.029
15	.30	.151	-28.04	-13.04	.157	-.036
16	.20	.105	3.97	18.97	.106	.037
17	.10	-.119	-27.11	-42.11	-.094	.085
18	.08	-.125	-30.72	-45.72	-.095	.086
19	.06	-.125	-32.04	-47.04	-.091	.088
20	.04	-.126	-33.32	-48.32	-.090	.101
21	.02	-.114	-30.75	-45.75	-.085	.087

VELOCITIES CALCULATED USING A 4th ORDER POLYNOMIAL CURVE FIT

NUMBER OF POINTS NOT USED: 1
 THESE POINTS ABOVE ARE NOT PLOTTED: 16

profile test. The tabulated results include the following: y , distance from the probe tip to the model surface in inches; U/U_e , total velocity non-dimensionalized by the edge total velocity; α , flow direction with respect to the freestream; $\alpha + \Delta$, positive sense in the clockwise direction; u/u_e , the component of the total velocity normal to the step face non-dimensionalized by the u component edge velocity, positive sense is in freestream direction; w/u_e , the component of the total velocity parallel to the step face non-dimensionalized by the u component edge velocity, positive sense is right to left when looking downstream. The total velocity was determined from the fourth order polynomial which was more accurate than the linear fit of King's law.

Plotted Results. The data reduction and analysis program plotted the results on seven different graphs. An example of these plots for the 15 degree swept step, at $x=1$ inch downstream of the step, is shown in Figure 4.10 to 4.16. Figure 4.10 is a plot of α versus y/h . The zero flow angle is indicated by a dashed line to make it easier to identify positive and negative flow angles. Figures 4.11, 4.12 and 4.13 are of the non-dimensional total velocity and non-dimensional u and w velocity components versus y/h . The zero velocity is indicated by a dashed line. Figures 4.14 and 4.15 are the two velocity components, u and w , versus the ratio of probe height to the u velocity component boundary-layer thickness. Again, the zero velocity is indicated by a dashed line. The final plot, Figure 4.16, is the natural log plot used to determine the u velocity component boundary-layer thickness. The constant u component edge velocity and the linear curve fit is shown as a dashed line. The intersection of these two lines indicate the boundary-layer thickness.

Measurement Uncertainty

Calibration Data

The Magnehelic pressure gauges used to calibrate the hot film anemometer had an uncertainty of $\pm 2\%$ full scale, according to manufacturer's data. At the lower limit of each gauge this uncertainty translates to a 50% error in determining flow velocity. The lowest velocities read from each gauge were as follows: for the 0 to 10 inch water gauge, 68 fps; for the 0 to 1 inch water gauge, 34 fps, and for the 0 to 0.25 inch water gauge, 9 fps. It was felt, based on the extremely good linear fit of the calibration data to King's law, that the actual error in calculating the velocity was considerably smaller. Repeatability of the calibration data was within ± 0.5 fps which corresponds to a maximum of 5% difference between readings. As stated previously, the calibration velocity measured from the pitot tube and the velocity calculated from the fourth degree polynomial yielded a maximum of $\pm 5\%$ difference. From information described in TSI Bulletin TB5, the error due to a fluid temperature difference of 4 degrees Fahrenheit between the calibration and velocity profile tests is considered to be less than 1%.

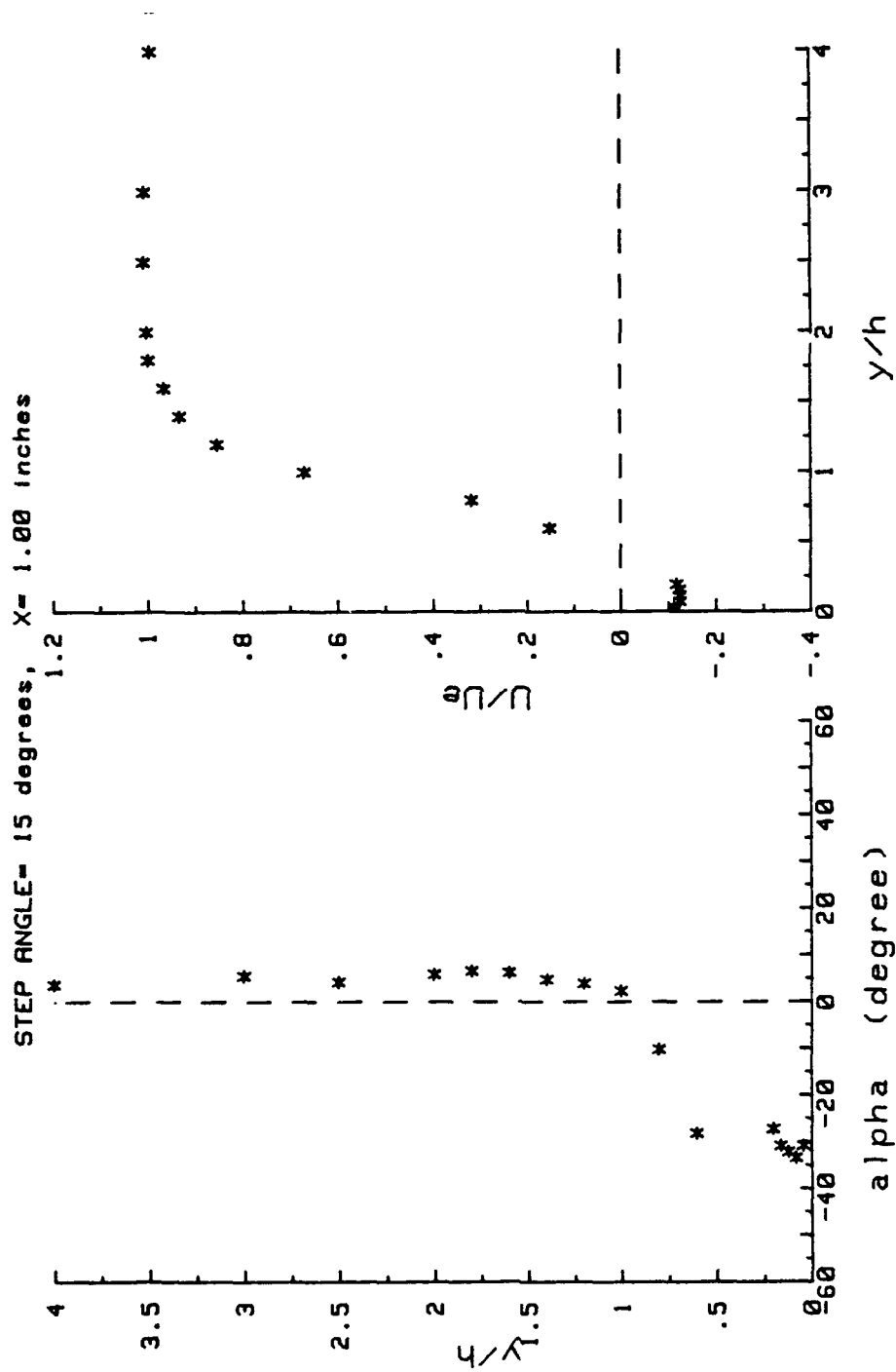


Figure 4.10 Total Flow Angle (α) Versus y/h for $\Lambda = 15$ Degrees and $x/h = 2.0$

Figure 4.11 y/h Versus U/U_e for $\Lambda = 15$ Degrees and $x/h = 2.0$

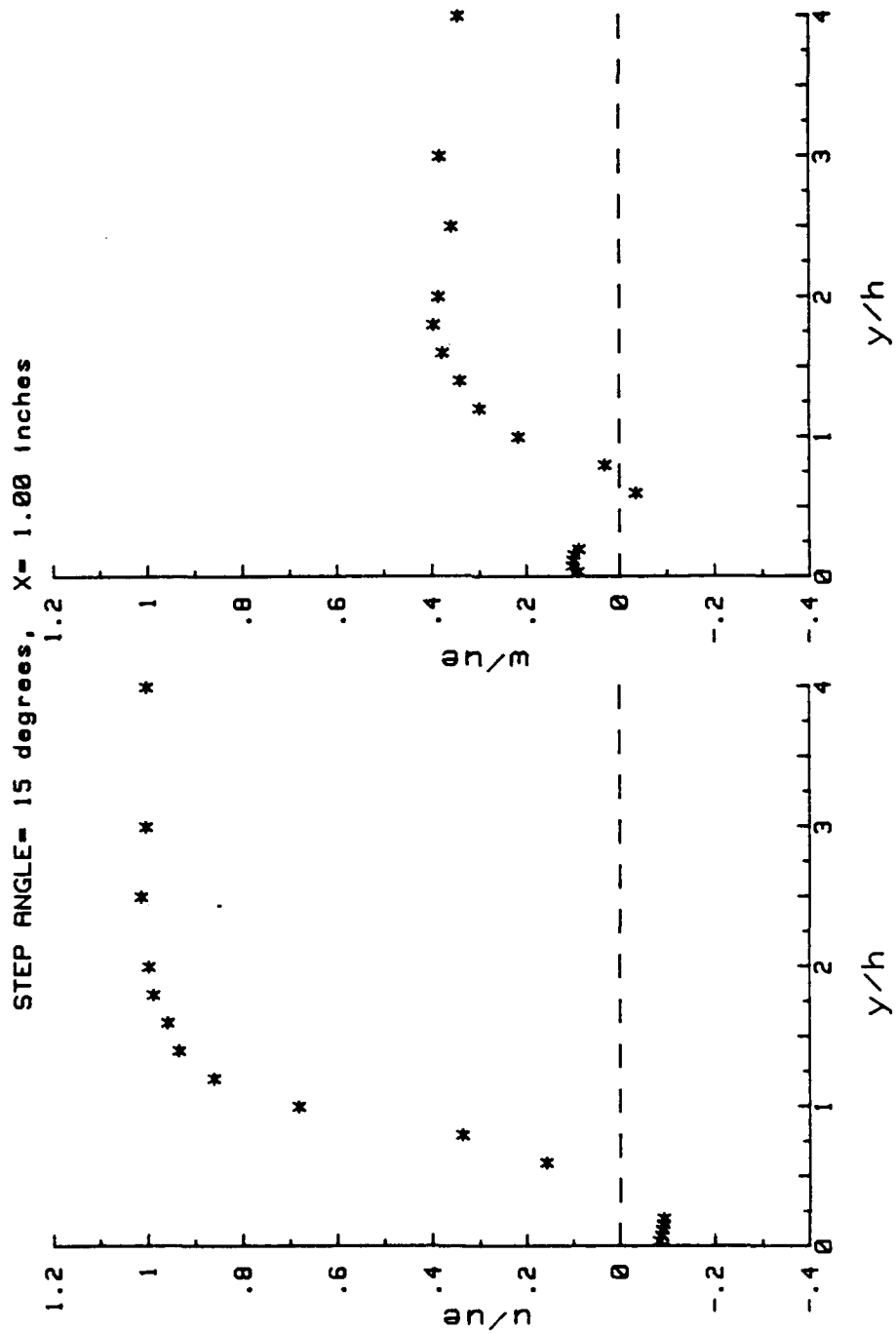


Figure 4.12 y/h Versus u/u_e for
 $\Lambda = 15$ Degrees and
 $x/h = 2.0$

Figure 4.13 y/h Versus w/u_e for
 $\Lambda = 15$ Degrees and
 $x/h = 2.0$

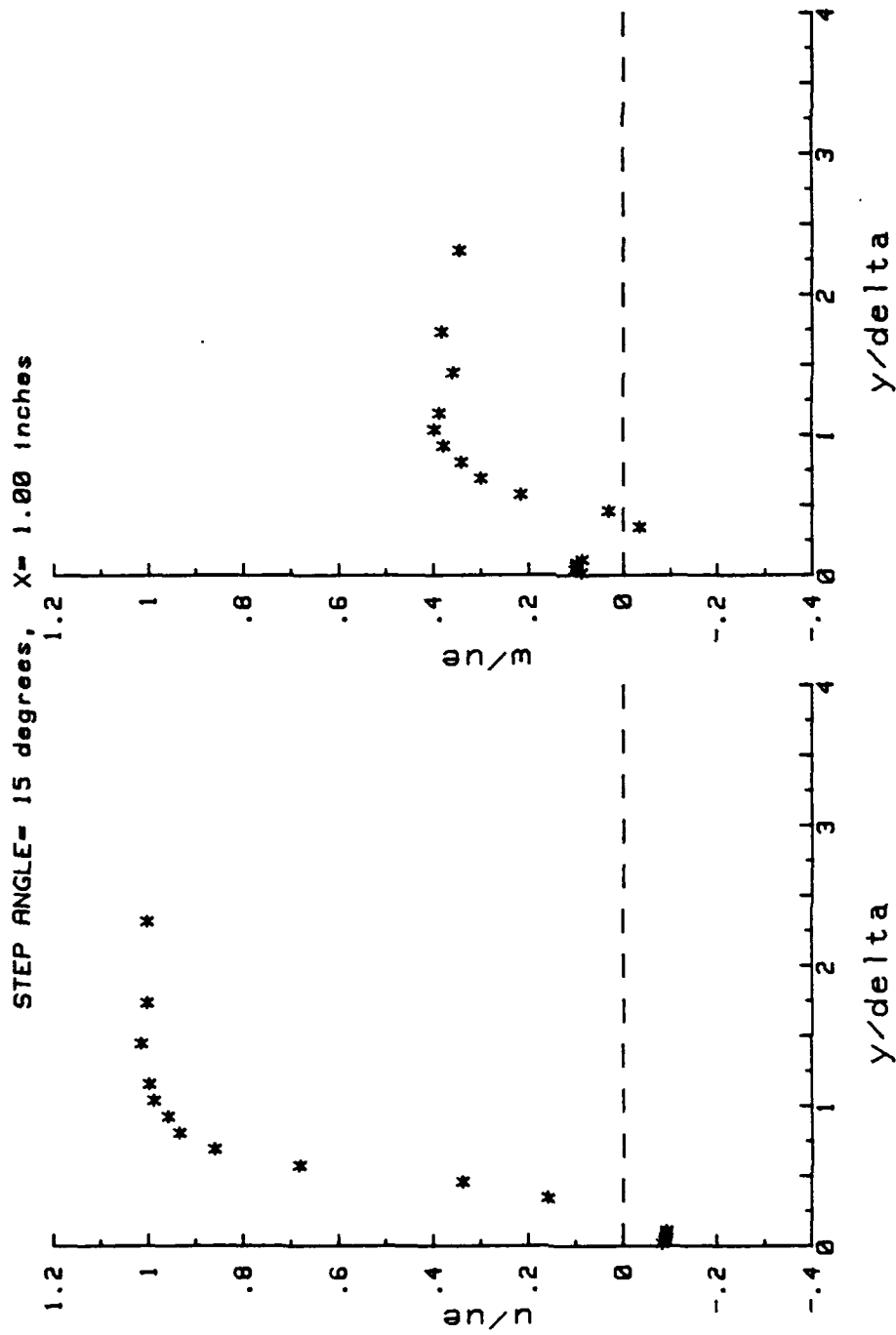


Figure 4.14 y/δ Versus u/u_e for
 $\Lambda = 15$ Degrees and
 $x/h = 2.0$

Figure 4.15 y/δ Versus w/u_e for
 $\Lambda = 15$ Degrees and
 $x/h = 2.0$

STEP ANGLE= 15 degrees, X= 1.00 inches

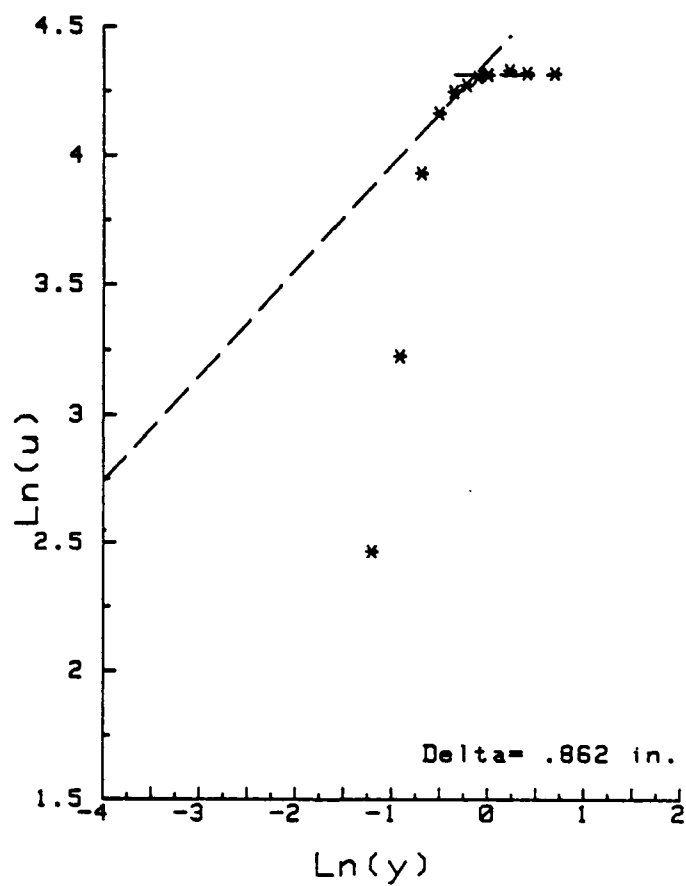


Figure 4.16 $\ln(y)$ Versus $\ln(u)$ for $\Lambda = 15$ Degrees and $x/h = 2.0$

Probe Positioning

The modified height gauge of the probe positioning mechanism had a resolution of 0.001 inches. Because of the problem of the relative movement of the model to the wind tunnel, described previously, the uncertainty of the probe position was ± 0.002 . The repeatability of probe positioning was very good and within the ± 0.002 uncertainty. The probe yaw angle was set by an yaw indicator wheel calibrated from 0 to 360 degrees in 1 degree increments.

Data Reduction - Total Velocity and Flow Direction

It was believed that the data reduction procedure could resolve the flow direction to within ± 2.0 degrees. From repeated velocity profiles at the same survey locations, the flow angle showed very good repeatability when the total velocity was above 10 fps. Below 10 fps the repeatability of the flow angle was poor, ± 10 degrees, but this was to be expected since these measurements were made at or below the lower limit of the calibration. The uncertainty of the data reduction procedure in determining the total flow velocity was estimated to be within ± 3 fps. The repeatability of the calculated total velocity between tests at the same survey location was very good with the velocities differing by only ± 1 fps.

Chapter 5 DISCUSSION OF RESULTS

Overview

The final part of this study, which is described in this chapter, was to interpret the results for the flow over a swept backward-facing step. Observations and analysis of the oil flow visualization tests are discussed first. Then an explanation of the velocity profile survey results is given. An overview of the flowfield in the vicinity of each step is presented in a carpet plot format. A more detailed look at the recirculation region behind each step is provided and discussed. A comparison of the test results from this study are made with other investigator's works. The results outside of the separated region are correlated in terms of Coles' incompressible law of the wall and wake. Finally, the Baldwin-Lomax algebraic turbulence model, modified for swept backward-facing steps, is investigated. An attempt is made to correlate the normal (u) and parallel (w) velocity components in terms of parameters of the Baldwin-Lomax model.

Oil Flow Results

0 Degree Step

The flow visualization studies indicated good agreement with the results presented by Selby (1982). Figure 5.1 is a typical photograph of the oil flow behind the 0 degree step. From this photograph the reattachment line is located approximately 2.5 inches or 5 step heights downstream of the step. Selby's (1982) results indicate reattachment at approximately 6.5 step heights downstream of the step. The actual flow directions can not easily be determined from the photographs but by observing and noting the movement of the oil behind the step during the tests the flow directions could be resolved. From the step face to the reattachment line the oil flowed back towards the step, and accumulated in a rather large puddle. Because of the excessive amount of oil put on the plate, the oil accumulation line extended from the step to approximately 1.0 inches downstream of the step. It is believed that because of the excessive amount of oil behind the step the flowfield was disturbed, but the extent of the interference is unknown. Downstream of the reattachment line the oil flowed in the freestream direction. The flow direction inside and outside of the recirculating region appeared to be perpendicular to the face of the step. The flow visualization indicated no wall interference for $z = \pm 16.0$ inches about the centerline of the model. The reattachment region also remained parallel to the step face over this same range.

15 Degree Step

Photographs showing the oil flow behind the 15 degree swept step were of poor quality and could not be photocopied to show any flow detail; therefore, they are not included. From the observations made during the testing, the reattachment line was approximately 2.5 inches (5.0 step heights) in the streamwise direction, downstream of the step (2.4 inches or

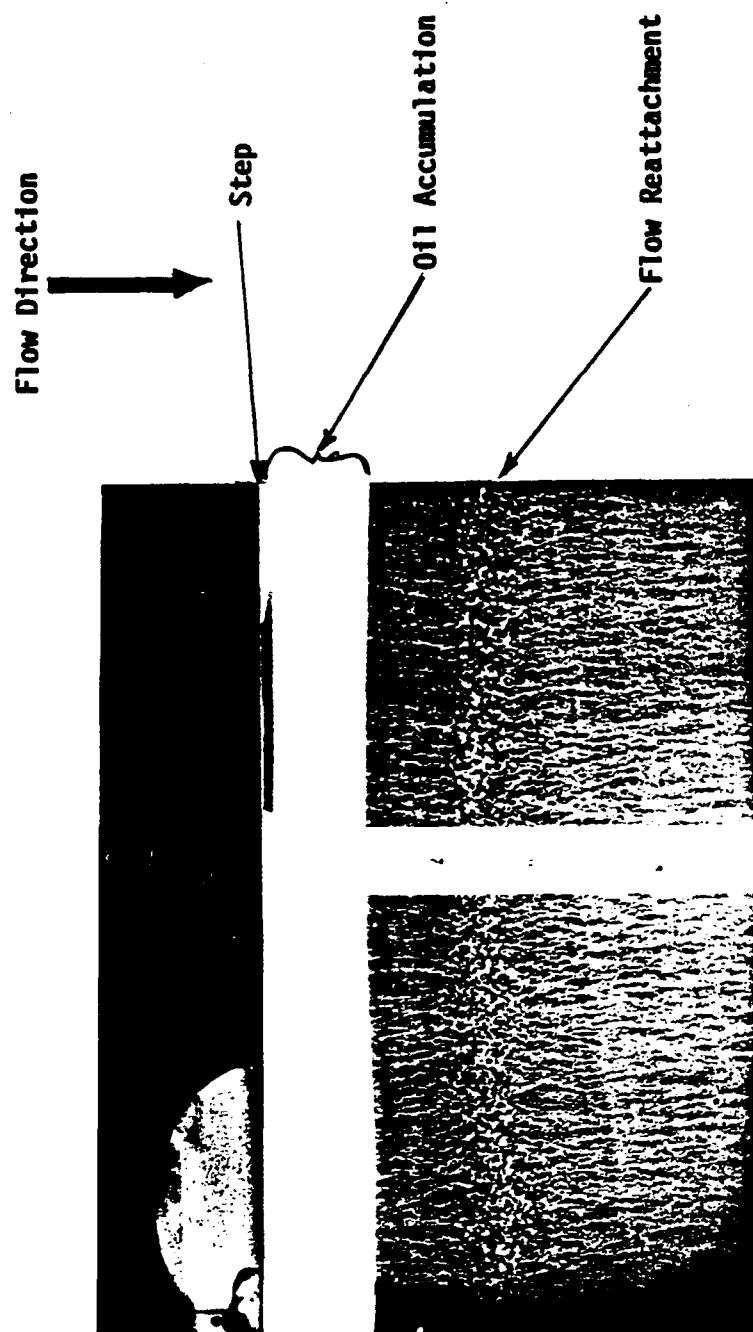


Figure 5.1 Oil Flow Visualization Downstream of the 0 Degree Step, $U_\infty = 73$ fps

4.8 step heights measured perpendicular to the step). Selby's (1982) reattachment point for the 15 degree step was approximately $x'/h=5.4$ downstream of the step. Between the step face and reattachment line, small ripples in the surface of the oil were seen moving parallel to the step face. The flow in this region was also moving toward the step as evidenced by the accumulation of the oil near the step face, similar to the result obtained in the zero degree step case. Downstream of the reattachment line, the flow again moved in the direction of the freestream. Wall effects had no influence on the flow between $z = \pm 12$ inches of the model centerline. The reattachment line remained parallel to the step over the same range of z .

30 Degree Step

Figures 5.2 and 5.3 show the oil flows behind the 30 degree step. From the photographs and the observations the reattachment line was determined to be approximately 3.2 inches (6.4 step heights) in the streamwise direction, downstream of the step face, or 2.8 inches (5.6 step heights) perpendicular to the step. Selby's (1982) analysis indicated a reattachment point of $x'/h=5.4$ downstream of the step. Figure 5.2 was taken 15 seconds after the tunnel was brought up to the test velocity of 50 mph. The formation of ripples moving parallel to the step face, and the accumulation of oil behind the step can be clearly seen. Thus, the oil was flowing both parallel and perpendicular to the step face. Within the recirculation region the flow was trying to turn so that it was perpendicular to the step. Within 2.0 inches downstream of the reattachment, the flow is again parallel to the freestream direction. No effect due to wall interference could be seen in the flow between $z = \pm 16$ inches of the centerline of the model. The reattachment line was parallel to the step over the same range of z .

Velocity Profile Results

Overview

The test results for the three backward-facing step configurations are presented and discussed in the following sections. The presentation of these results consists of two sets of four carpet plots each. The first set is an overview of the entire range, upstream and downstream of the step, with only selected profiles being shown in order to improve the clarity of the plots. The second set includes all of the profiles within the recirculation region of each step configuration. Each set was made up of the following carpet plot profiles: 1) total velocity; 2) total velocity flow direction; 3) u-component of the total velocity; and 4) w-component of the total velocity. To further improve the readability of the carpet plots, the individual profile data points are connected by straight lines and the zero position of each profile is indicated by a dotted line, thus making it easier to identify positive and negative values.

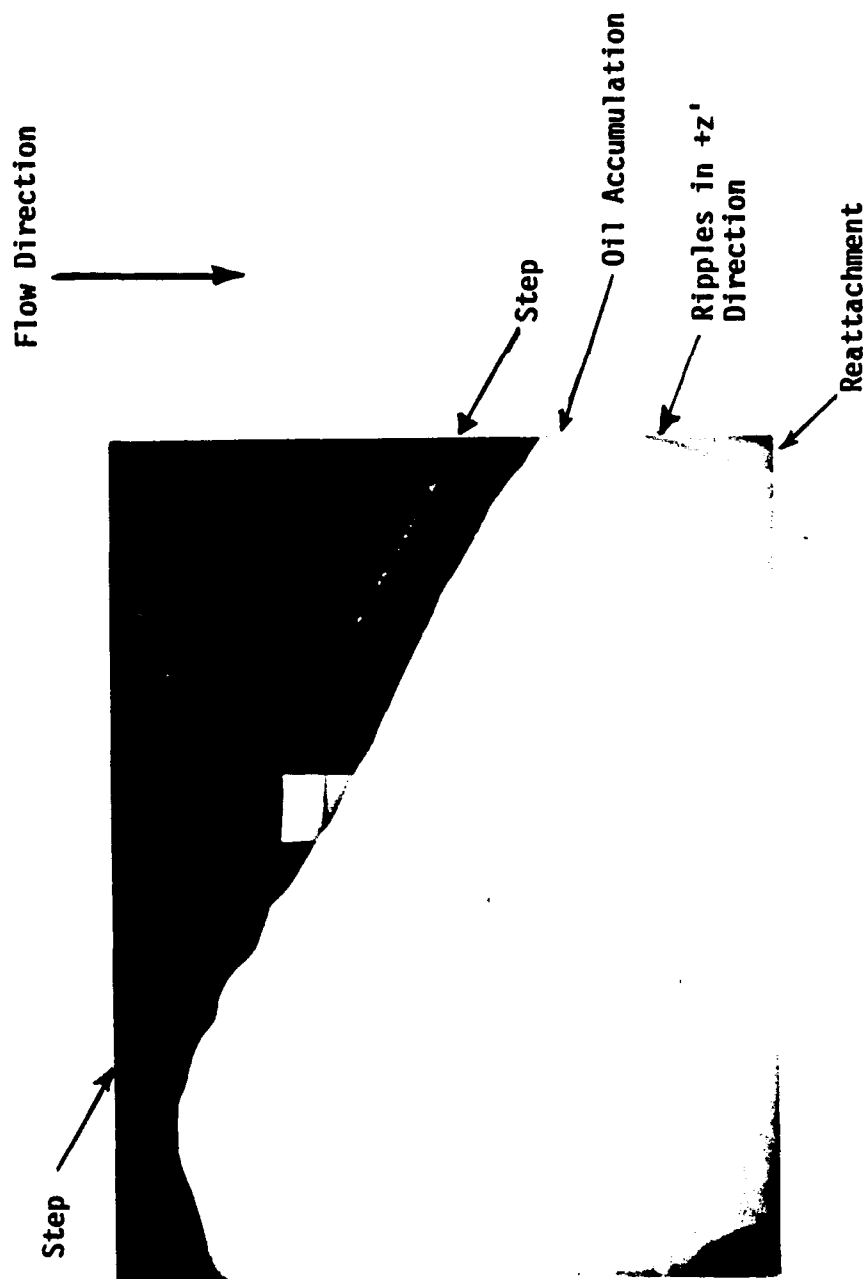


Figure 5.2 Oil Flow Visualization Downstream of the 30 Degree Step, $U_{\infty} = 73$ fps, (15 seconds after flow began)

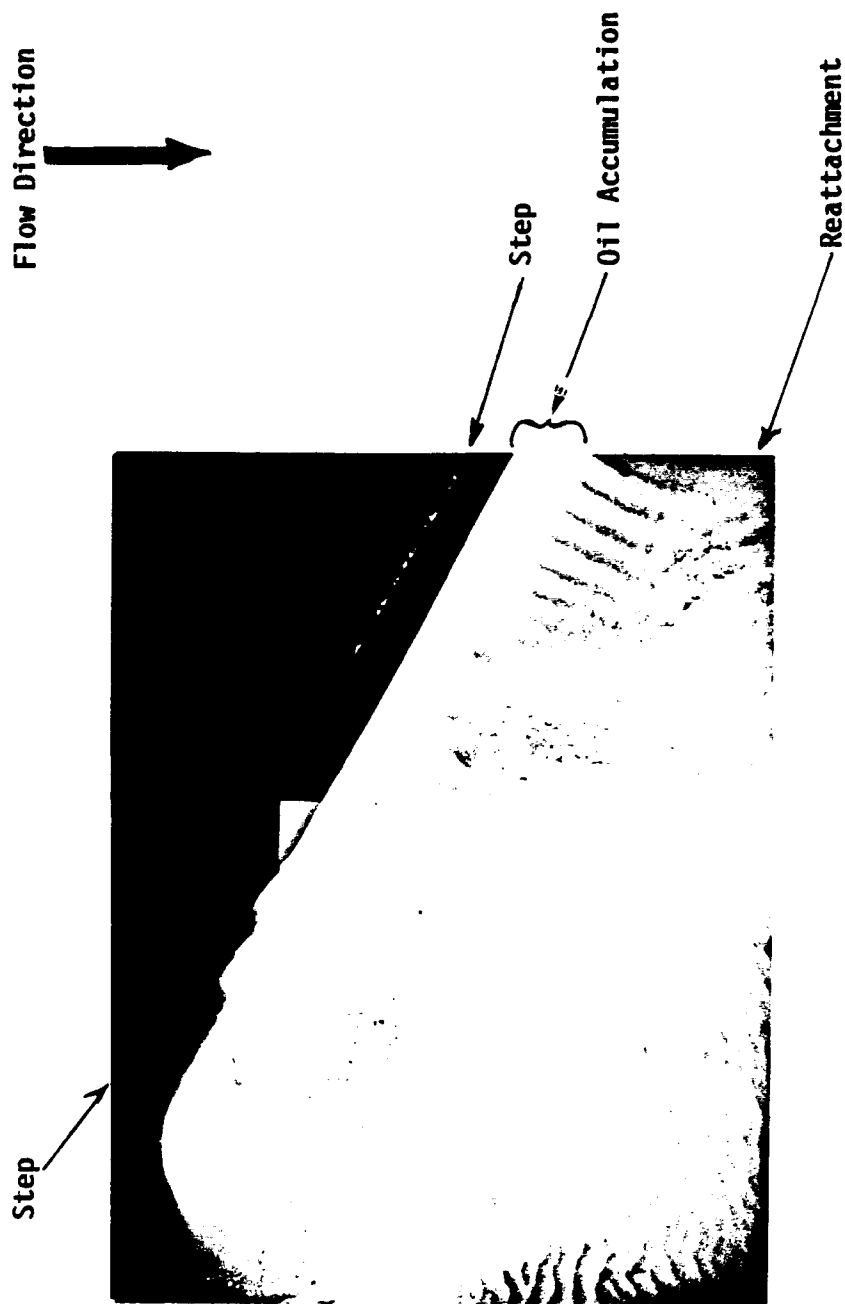


Figure 5.3 Oil Flow Visualization Downstream of the 30 Degree Step, $U_{\infty} = 73$ fps, (final results)

0 Degree Swept Step

Overview of Velocity Profiles. Because of the interest in the flow over a backward-facing unswept step an abundance of experimental results are available. Thus, by comparing the 0 degree step results with previously published data, a determination of the validity of the results from this study can be made. For the 0 degree step, velocity profiles were measured at the following x locations; -2.75, -1.5, -0.5, 0.0, 0.1, 0.25, 1.0 to 4.0 in steps of 0.5, 5.0, 6.0 and 7.5 inches. All survey locations were measured relative to the step, with negative measurements indicating profile locations upstream of the step.

Carpet plots of the 0 degree step profiles are presented in Figures 5.4 to 5.7. Figure 5.4 shows the non-dimensional total velocity profiles. The total velocity flow direction (α) carpet plot is shown in Figure 5.5, with all flow angles being approximately 0 degrees. The 0 degree flow angle implies that the flow remains in the free stream direction. Figure 5.6 shows the u velocity components. For this step the u component velocity is the same as the total velocity because of the near 0 degree flow angles. The w velocity components shown in Figure 5.7 are all practically zero, with a maximum value of $w/u_e = 0.08$.

Recirculation Region Velocity Profiles. The area of most interest is the recirculation region downstream of the step. Carpet plots of all velocity profiles from the $x/h = 0.0$ to 8.0 are presented in Figure 5.8 and 5.9. Only the total velocity and the flow angle carpet plots are shown. The u and w component plots provided no additional information, the u component is the same as the total velocity and the w components were all nearly zero. The velocity profiles in Figure 5.8, at $x/h = 0.2$ and 0.5, decrease to nearly zero velocity just below $y/h = 1.0$. The reattachment of the flow occurs between $x/h = 4$ and 5 and because of the large negative velocities present at $x/h = 4$ the reattachment is probably closer to 5. This result is in good agreement with the oil flows observations of this study. To precisely determine the reattachment point more surveys locations would be necessary. Downstream of the reattachment region, the effect of the step on the profile is slowly dissipated. At the reattachment point the velocity gradient dU/dy equals zero but as can be seen in Figure 5.8, dU/dy increases with increasing downstream distance. For the most part, the flow angles, Figure 5.9, above $y/h = 1.0$ are within the range of ± 4 degrees. Below $y/h = 1.0$ and within 3 step heights of the step, the flow angle has a range of approximately ± 20 degrees. The results for the two profiles, $x/h = 0.2$ and 0.5 and below $y/h = 1.0$, are questionable because the total velocity is outside of the calibration limits.

Comparison With Other Investigators' Results. A comparison between the 0 degree step results of this study and the results of other investigators was made. As discussed by Eaton and Johnston (1981), they listed five principal independent parameters that affected the reattachment point, and thus the flowfield in the vicinity of a backward-facing step. These

0 DEG. STEP, U/U_e VELOCITY PROFILES

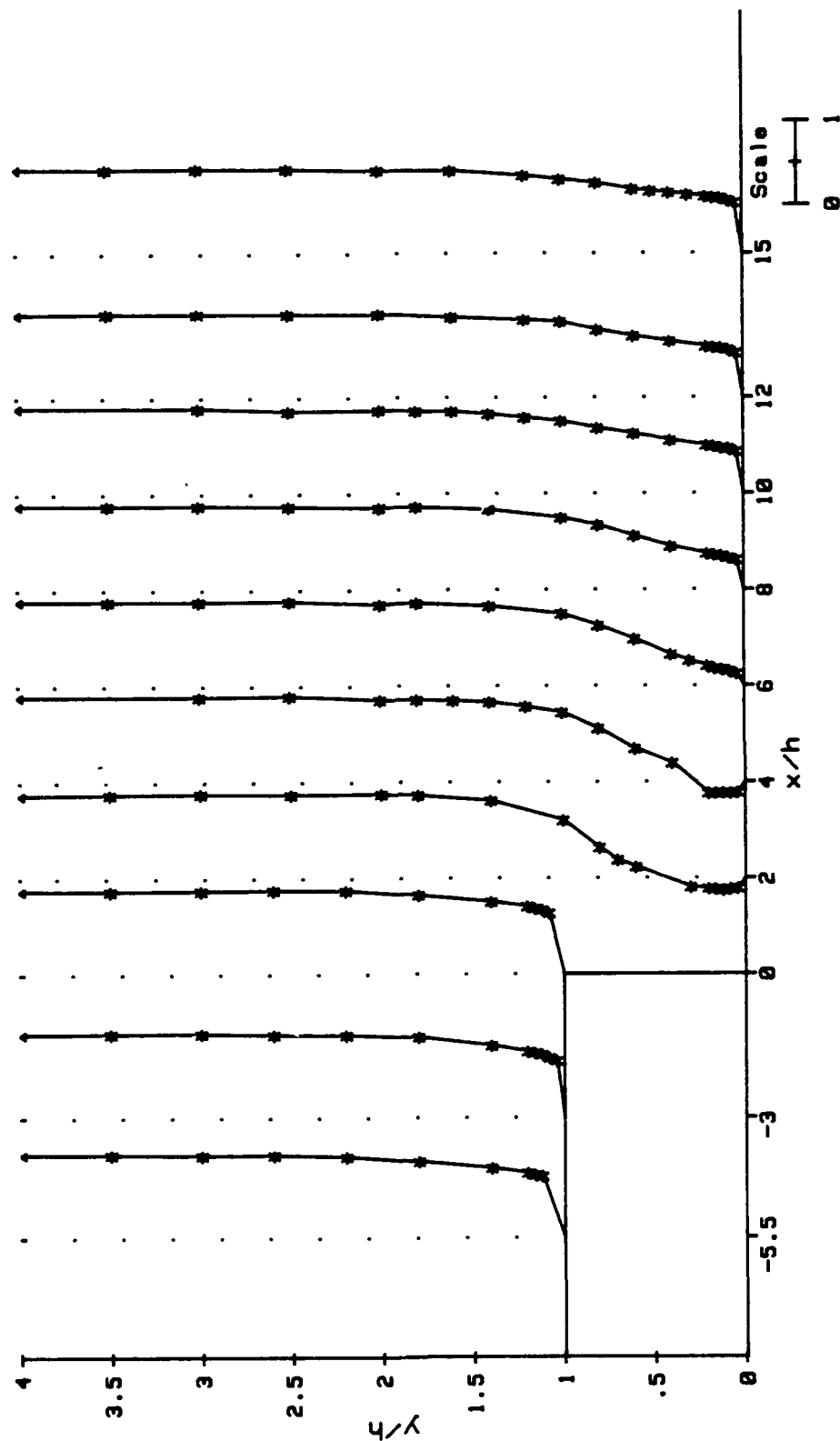


Figure 5.4 Carpet Plot of the U/U_e Profiles for $\Lambda = 0$ Degree, $x/h = -5.5$ to 15

0 DEG. STEP, alpha PROFILES

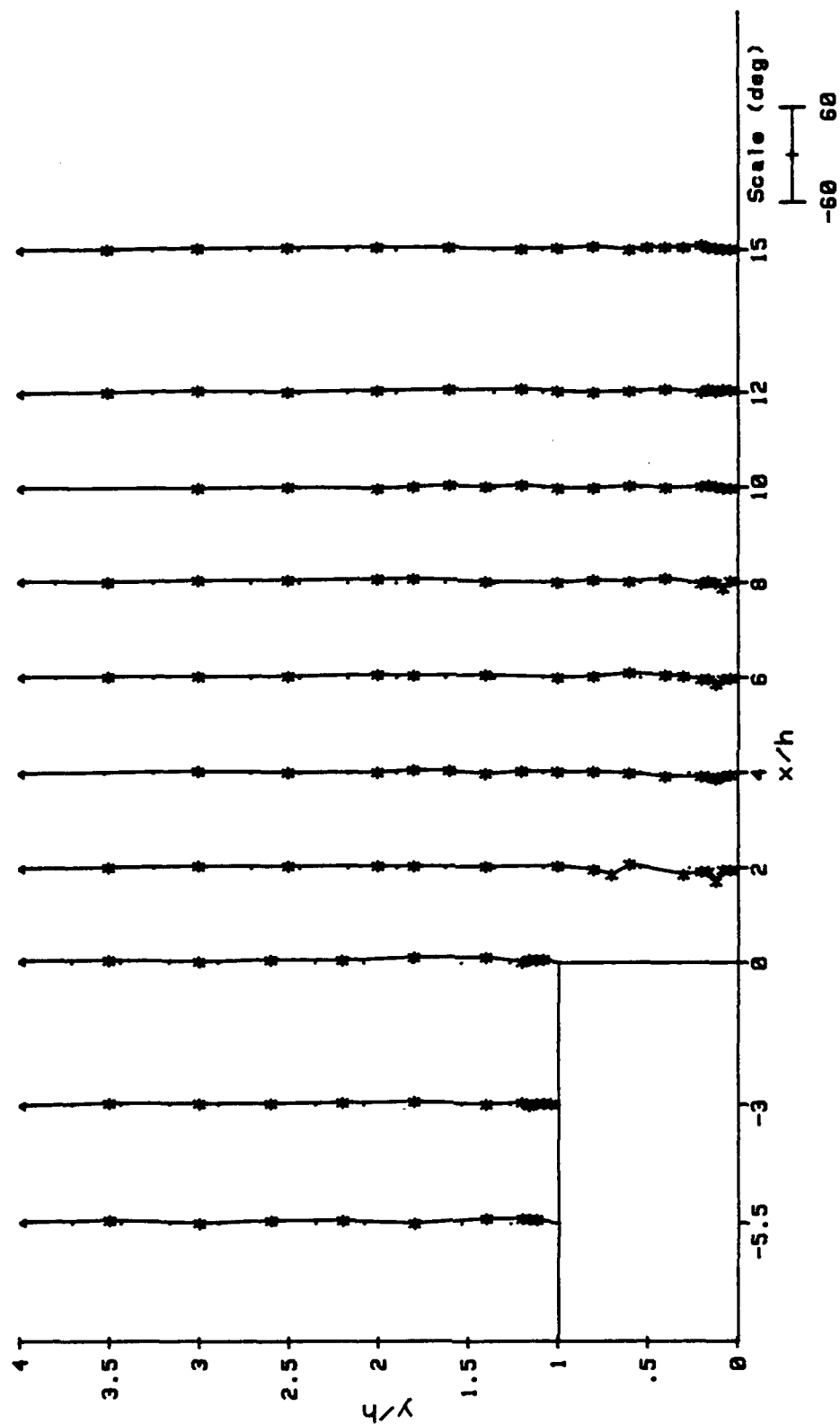


Figure 5.5 Carpet Plot of the α Profiles
for $\Lambda = 0$ Degree, $x/h = -5.5$ to 15

0 DEG. STEP, u/u_e VELOCITY PROFILES

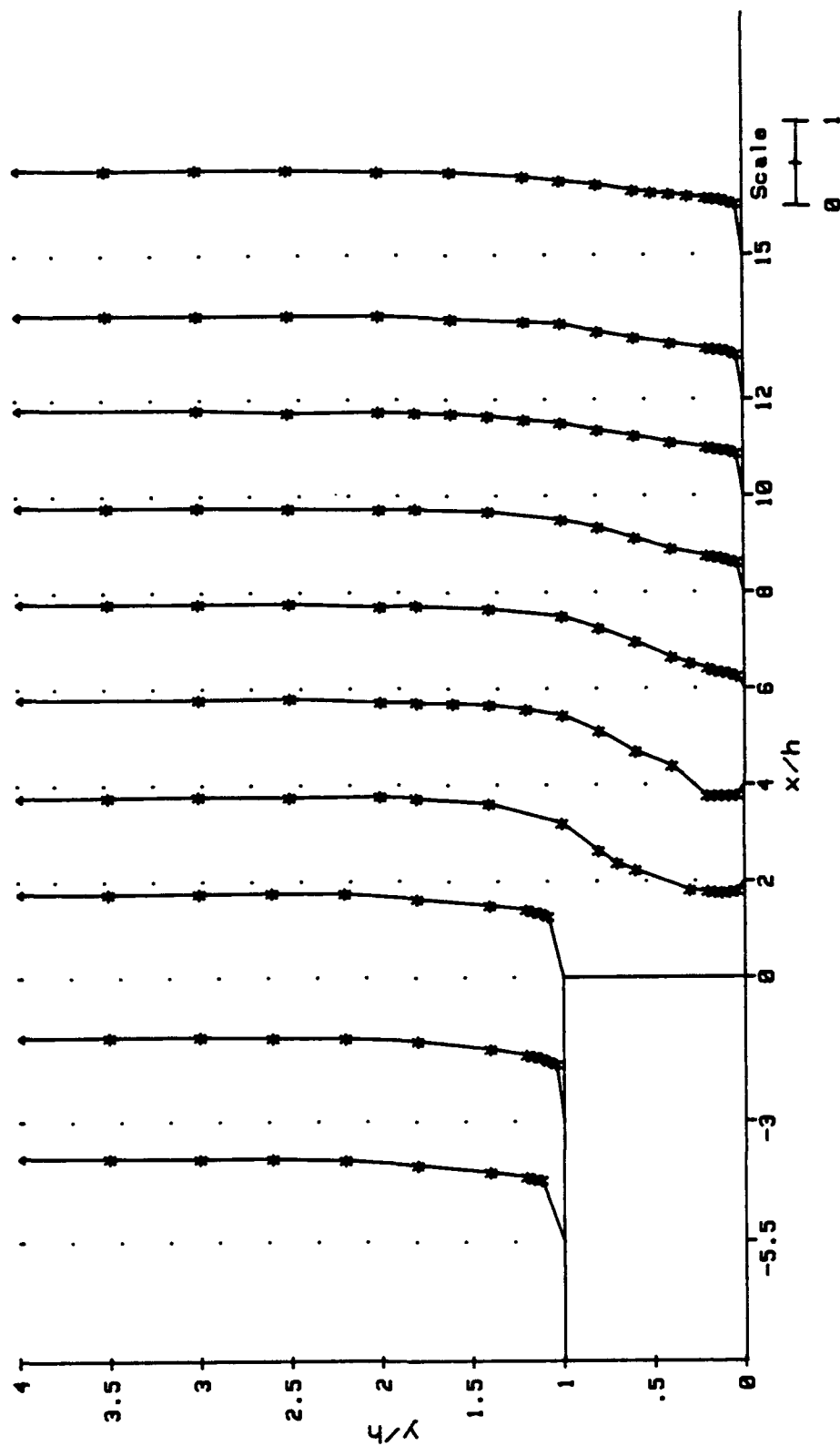


Figure 5.6 Carpet Plot of the u/u_e Profiles for $\Lambda = 0$ Degree, $x/h = -5.5$ to 15

0 DEG. STEP, w/u_e VELOCITY PROFILES

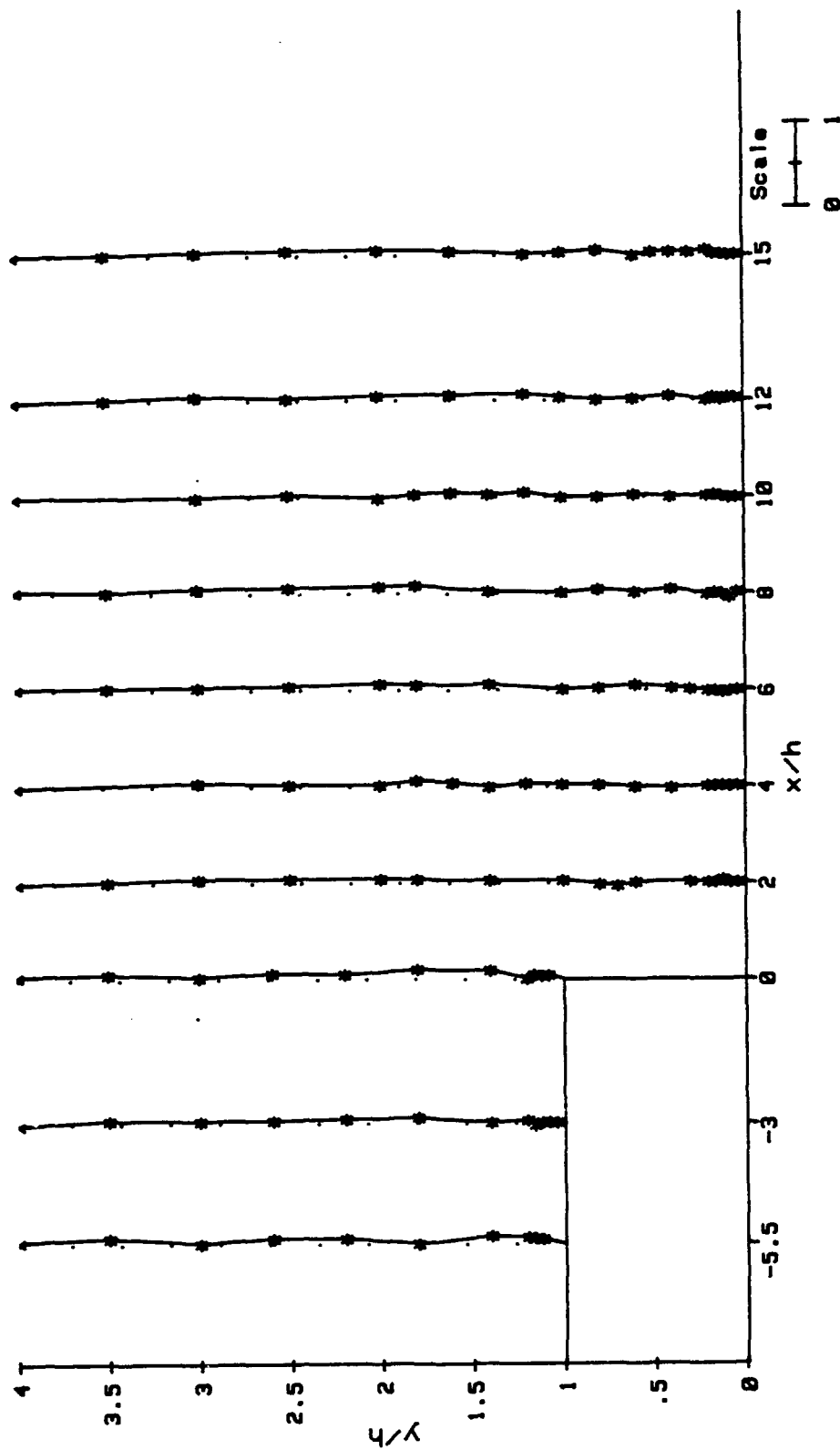


Figure 5.7 Carpet Plot of the w/u_e Profiles
for $\Lambda = 0$ Degree, $x/h = -5.5$ to 15

0 DEG. STEP, U/U_e VELOCITY PROFILES

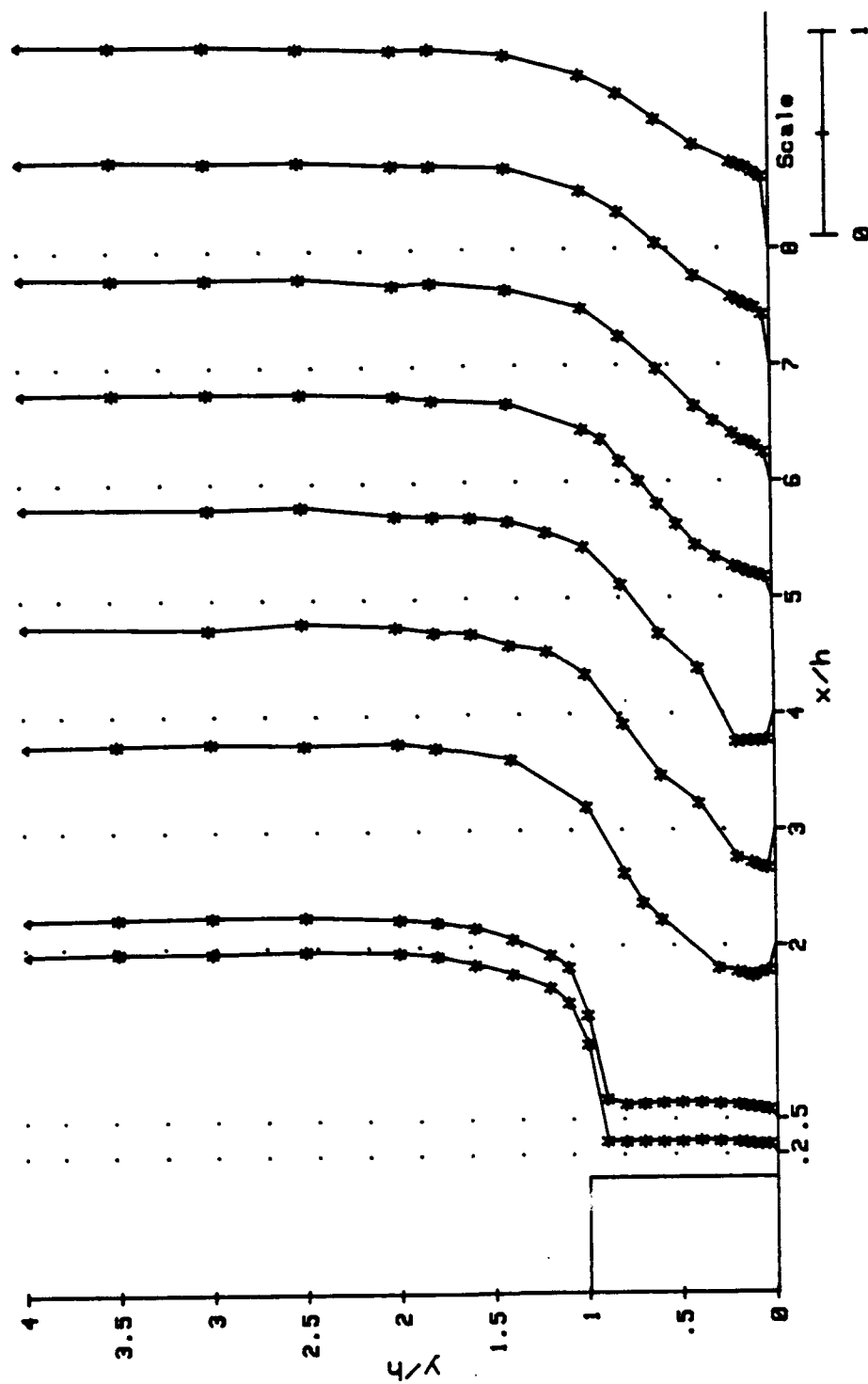


Figure 5.8 Carpet Plot of the U/U_e Profiles in the Recirculation Region for $\Lambda = 0$ Degree, $x/h = .2$ to 8.0

0 DEG. STEP, alpha PROFILES

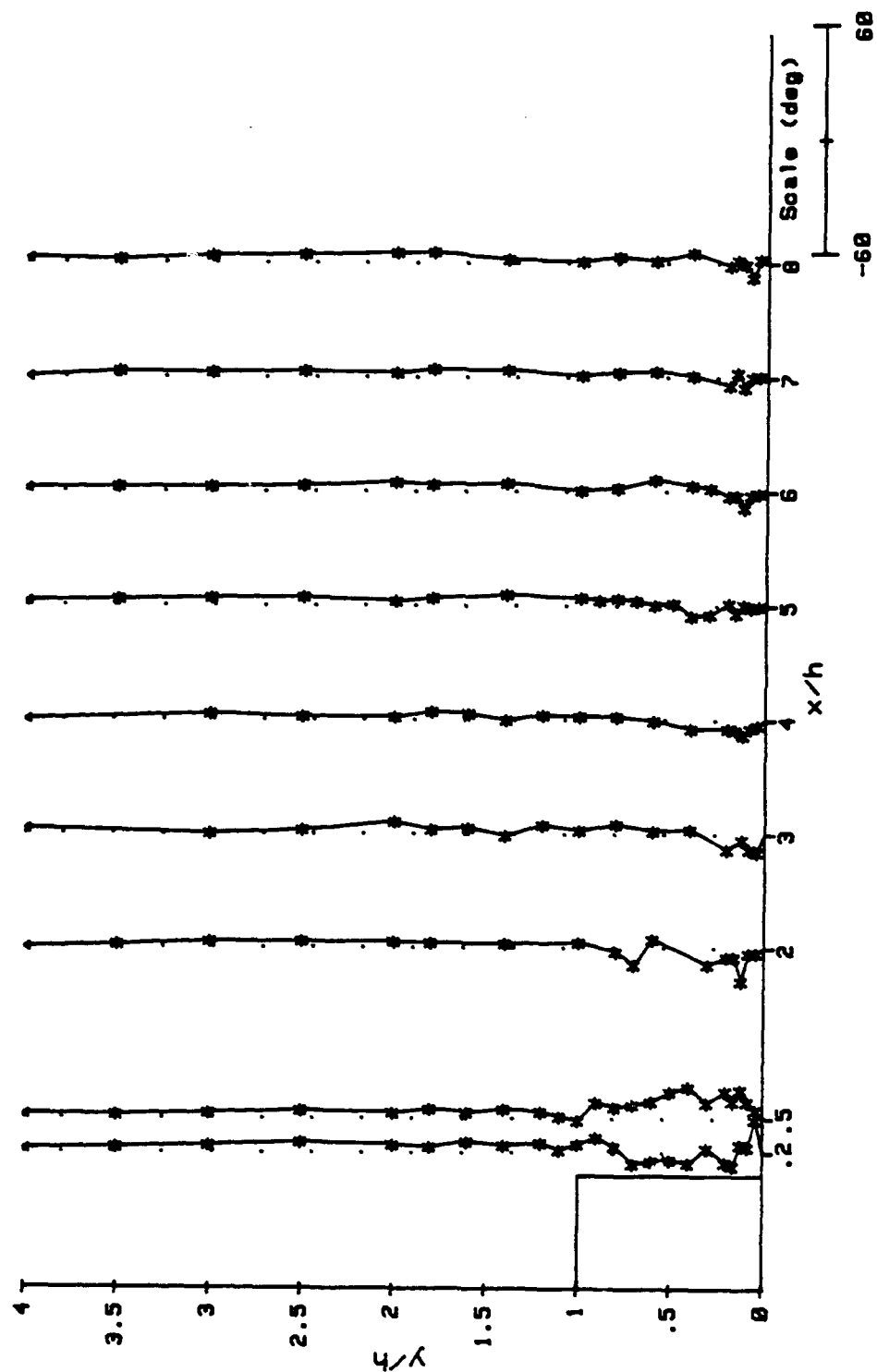


Figure 5.9 Carpet Plot of the α Profiles
in the Recirculation Region for
 $\Lambda = 0$ Degree, $x/h = .2$ to 8.0

five parameters are: 1) laminar or turbulent preseparation boundary-layer; 2) separation boundary layer thickness; 3) freestream turbulence; 4) streamwise pressure gradient; and 5) aspect ratio of the flow apparatus (channel width/step height). It is reasonable to assume that it would be nearly impossible for two investigators, at different facilities, to match all five parameters; consequently slight differences in the flowfields as well as the results must be expected. The amount that the results differ will depend on how close the parameters are matched.

A comparison of the mean velocity profiles of Eaton and Johnston (1980), Etheridge and Kemp (1978) and this study are presented in Figure 5.10. It should be noted that the Eaton and Johnston, and Etheridge and Kemp profiles are located at the reattachment point. The results from this study represent a survey location near, but downstream of the reattachment point. It also must be noted that the abscissa of the other investigators are shifted so that at $y/h=2$ the ratio of $u/u_e=1$. Taking into account the differences in survey locations, the agreement between the results is considered good. Bradshaw and Wong (1972) provided a mean velocity profile for a downstream location of $x/h=10$. The mean velocity profile from this study which best matches these results is located at $x/h=15$ and the comparison is shown in Figure 5.11. Once again, the agreement between these results is very good with a percent difference of less than 5%. From the above comparisons, it is felt that because of the good agreement with the results of several researchers the validity and accuracy of the results from this study are acceptable, especially when the problems involved with matching the flowfields are taken into account.

15 Degree Swept Step

Selected Velocity Profiles. There are no known experimental results available for comparison purposes for the flow over a swept backward-facing step. The 15 degree step velocity profiles were measured at the following x locations: -2.56, -1.5, -0.5, 0.0, 0.15, 0.25, 0.5 to 4.0 in steps of 0.5, 5.0, 6.0 and 7.5 inches. Selected profiles of the 15 degree swept step are presented in Figures 5.12 to 5.15. The total velocity carpet plot, Figure 5.12, indicates a reattachment point between $x/h=4$ and 6. The total velocity flow angles, Figure 5.13, are nearly zero everywhere except within and just downstream of the recirculation region. Figure 5.14 shows the u velocity component is equal to the total velocity except in and just downstream of the recirculation region. The negative u velocity component, due to flow reversal, can be seen below $y/h=0.25$ for the two profiles at $x/h=2$ and 4. The w velocity components, Figure 5.15, are positive everywhere except in the recirculation region.

Recirculation Region Velocity Profiles. A closer look at the recirculation region reveals more details of the flow over the 15 degree swept backward-facing step. The presence of the step greatly affects the total velocity profiles at $x/h=0.3, 0.5$ and 1.0, Figure 5.16. Just below the step surface, $y/h=1.0$, the total velocity decreases almost to zero. The profiles at

0 Degree Step at and Near Reattachment

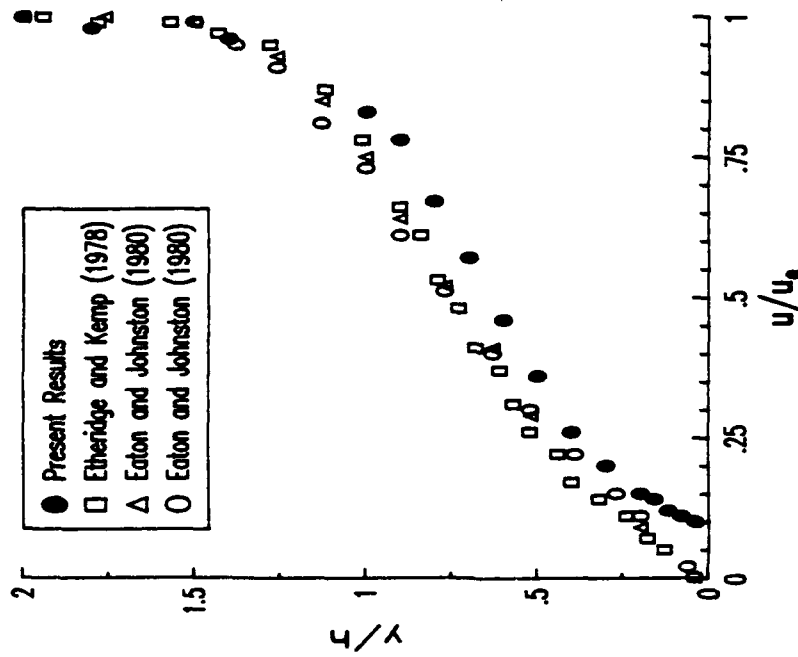


Figure 5.10 Comparison of Results at Reattachment to the Results of This Study Near Reattachment

0 Degree Step Downstream of Reattachment

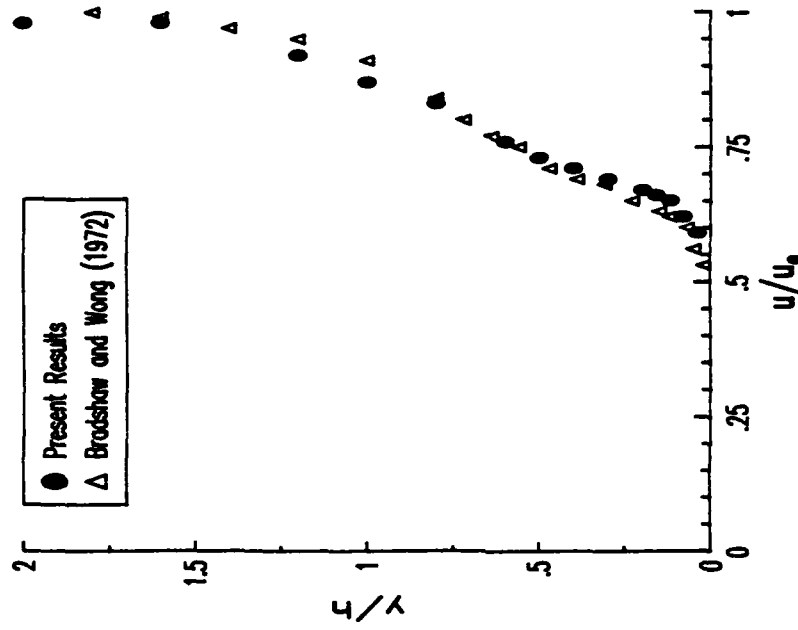


Figure 5.11 Comparison of Results Downstream of Reattachment

15 DEG. STEP, U/U_e VELOCITY PROFILES

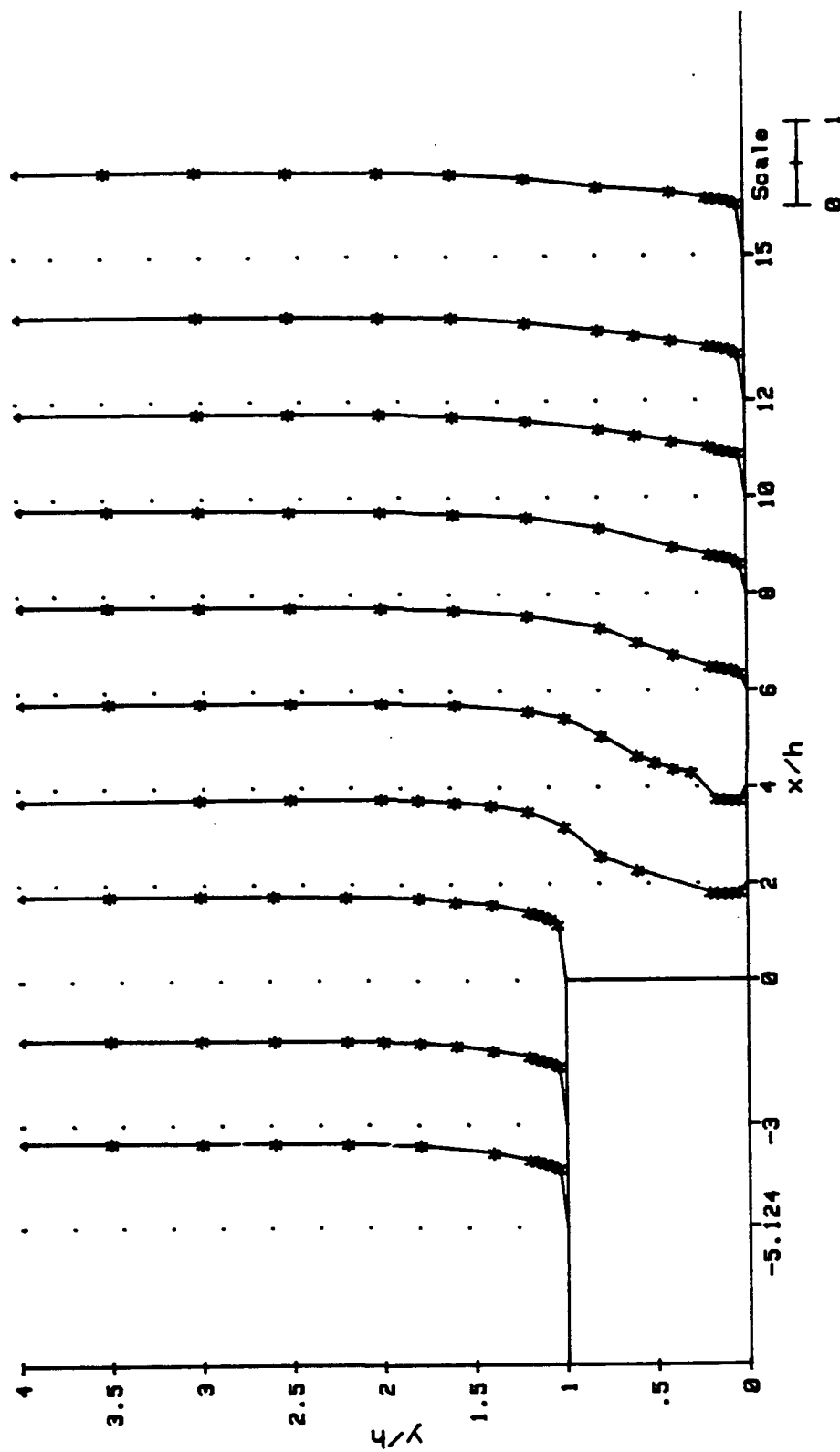


Figure 5.12 Carpet Plot of the U/U_e Profiles
for $\Lambda = 15$ Degrees, $x/h = -5.1$ to 15

15 DEG. STEP, alpha PROFILES

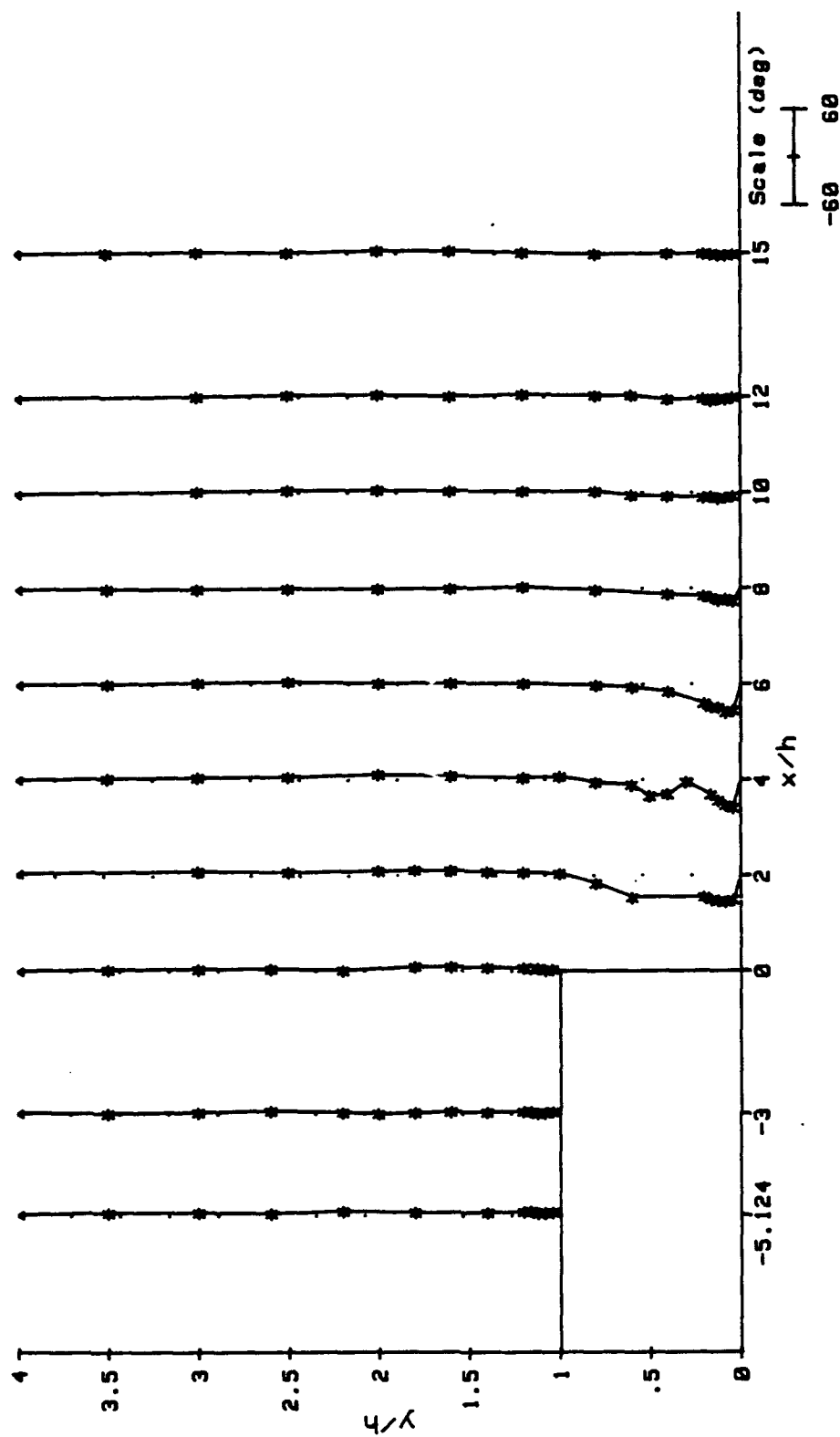


Figure 5.13 Carpet Plot of the α Profiles
for $\Lambda = 15$ Degrees, $x/h = -5.1$ to 15

15 DEG. STEP, u/u_e VELOCITY PROFILES

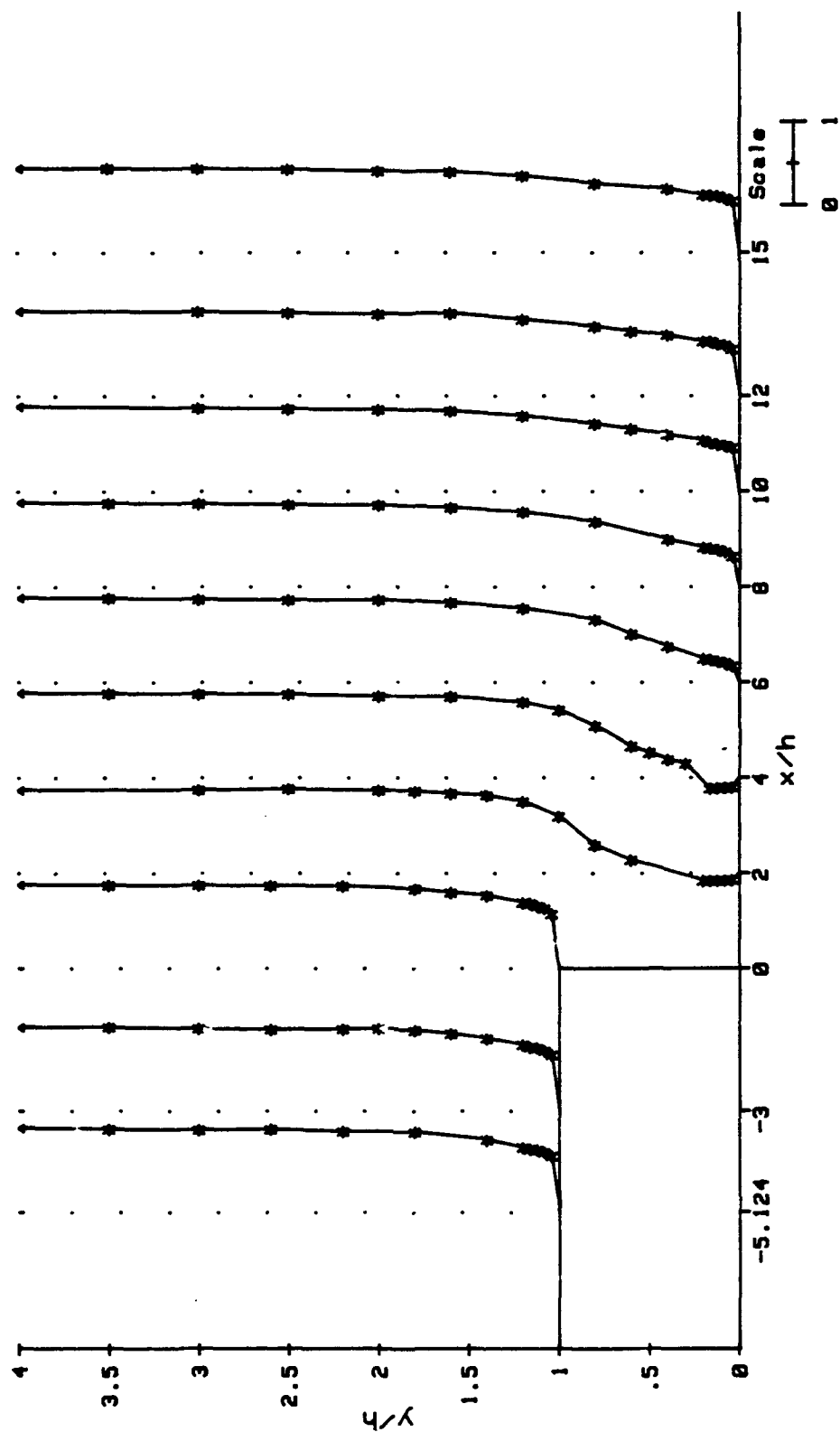


Figure 5.14 Carpet Plot of the u/u_e Profiles
for $\Lambda = \text{Degrees}$, $x/h = -5.1$ to 15

15 DEG. STEP, w/u_e VELOCITY PROFILES

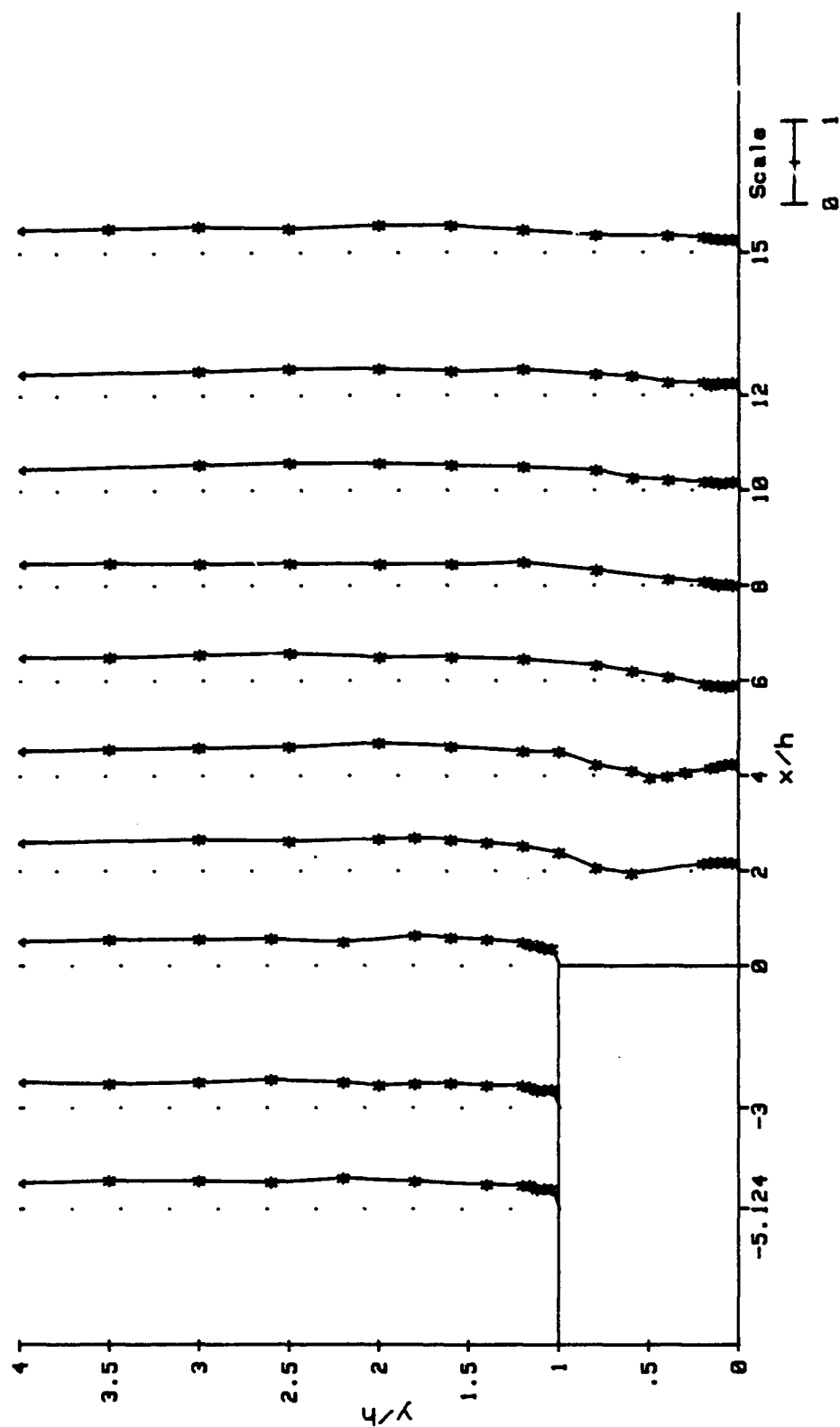


Figure 5.15 Carpet Plot of the w/u_e Profiles
for $\Lambda = 15$ Degrees, $x/h = -5.1$ to 15

15 DEG. STEP, U/U_e VELOCITY PROFILES

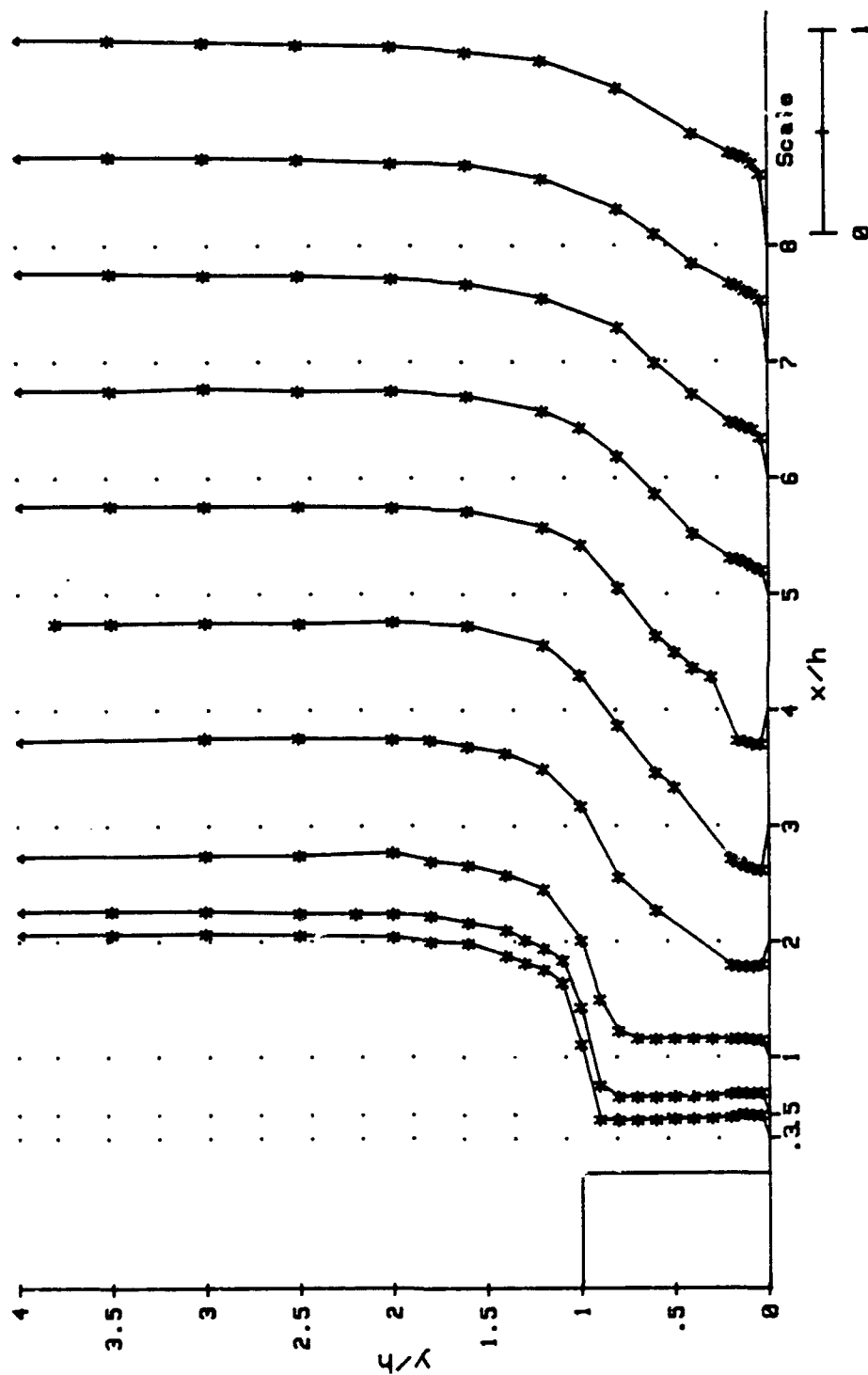


Figure 5.16 Carpet Plot of the U/U_e Profiles in the Recirculation Region for $\Lambda = 15$ Degrees, $x/h = .3$ to 8.0

$x/h=2.0, 3.0$ and 4.0 indicated a strong recirculation region, with the stagnation points at these location being approximately $y/h=0.38, 0.3, 0.22$, respectively. Flow reattachment occurs between $x/h=4$ and 5 , but probably closer to $x/h=4$. More survey locations are required to accurately determine the reattachment region. Similar to the 0 degree step, the velocity gradient near the wall increases with increasing distance downstream of the reattachment point.

As is expected the flow angles, Figure 5.17, are nearly zero in the freestream. The flow angles in the recirculation region and near the surface downstream of the reattachment point are all negative. For a given profile location, as y/h becomes less than 1.0 , the flow turns so that it is perpendicular to the step face. The flow angles for the three profiles at $x/h=0.3, 0.5$ and 1.0 and $y/h<1.0$ are questionable, due to the fact that the total velocities are so low and the flow reversal ambiguity could not be resolved. The next three profiles, $x/h=2.0, 3.0$ and 4.0 , the flow reversal was evident and the profiles have been modified accordingly. Once below $x/h=1.0$, the influence of the step on the profiles is to produce a negative flow direction angle. One important point that should be noted is that although the flow angle is negative between y/h of approximately 0.25 and the surface of the plate, the flow is actually 180 degrees from what is shown. This is due to the flow being reversal and the sign of the total velocity being negative. The influence of the step is still present in the flow angle data at $x/h=8.0$, but the effect is small and the flow is gradually realigning itself with the freestream flow direction.

The u velocity components are shown in Figure 5.18. The u component profiles at $x/h=0.3, 0.5$ and 1.0 decreases rapidly just below $y/h=1.0$ because of the presence of the step. Profiles at $x/h=2.0, 3.0$ and 4.0 indicates a strong recirculation region, while profiles beyond the reattachment point continue to show some influence due to the step.

The w velocity component, Figure 5.19, at $x/h=0.3, 0.5$, and 1.0 are essentially zero below $y/h=1.0$. Profiles between and including $x/h=2.0$ and 7.0 show the w component decreasing from the free stream value to zero or slightly negative and then increase again before becoming zero at the surface. The positive w velocity component, indicated in the recirculation region near the surface of the plate, is responsible for producing the ripples moving parallel to the step face which were observed in the oil flow studies. Beyond $x/h=7$, the influence of the step is small, with the w component profiles remaining constant within the free stream region but then decreasing to zero below $y/h=1.0$. The reason for the decrease in the w component with decreasing y/h is because the total velocity is also decreasing to zero.

15 DEG. STEP, alpha PROFILES

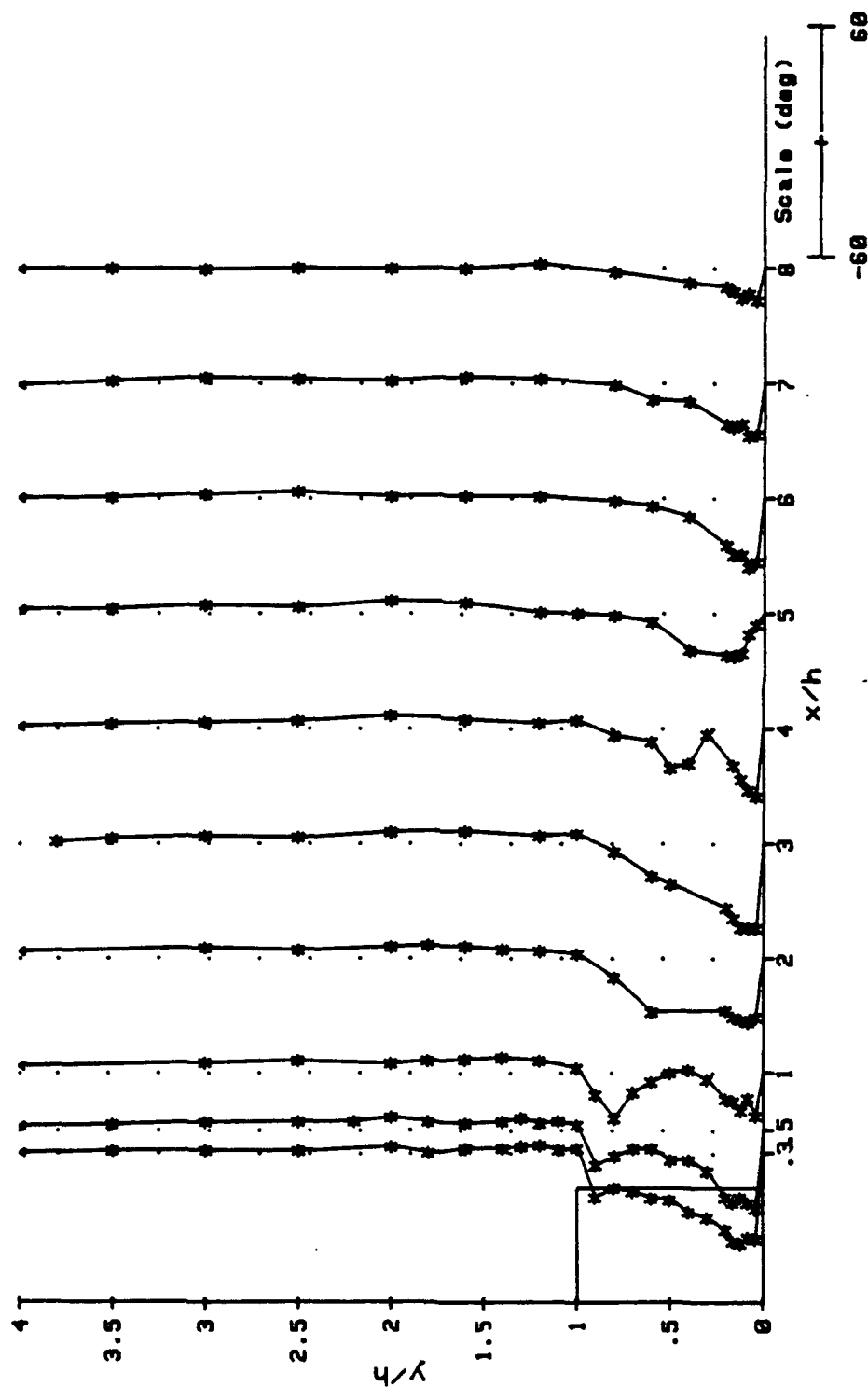


Figure 5.17 Carpet Plot of the α Profiles in the Recirculation Region for $\Lambda = 15$ Degrees, $x/h = .3$ to 8.0

15 DEG. STEP, u/u_e VELOCITY PROFILES

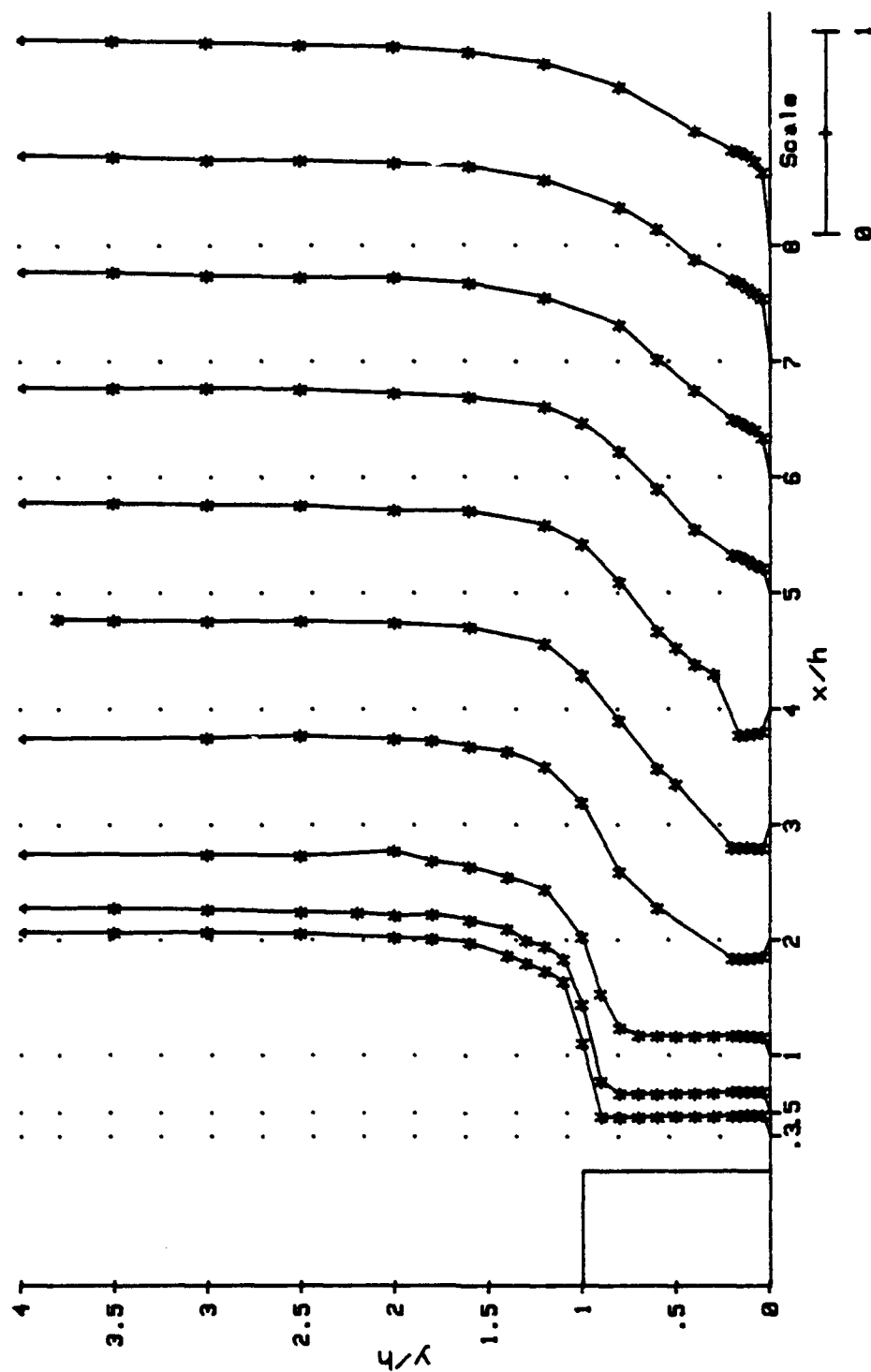


Figure 5.18 Carpet Plot of the u/u_e Profiles in the Recirculation Region for $\Lambda = 15$ Degrees, $x/h = .3$ to 8.0

15 DEG. STEP, w/u_e VELOCITY PROFILES

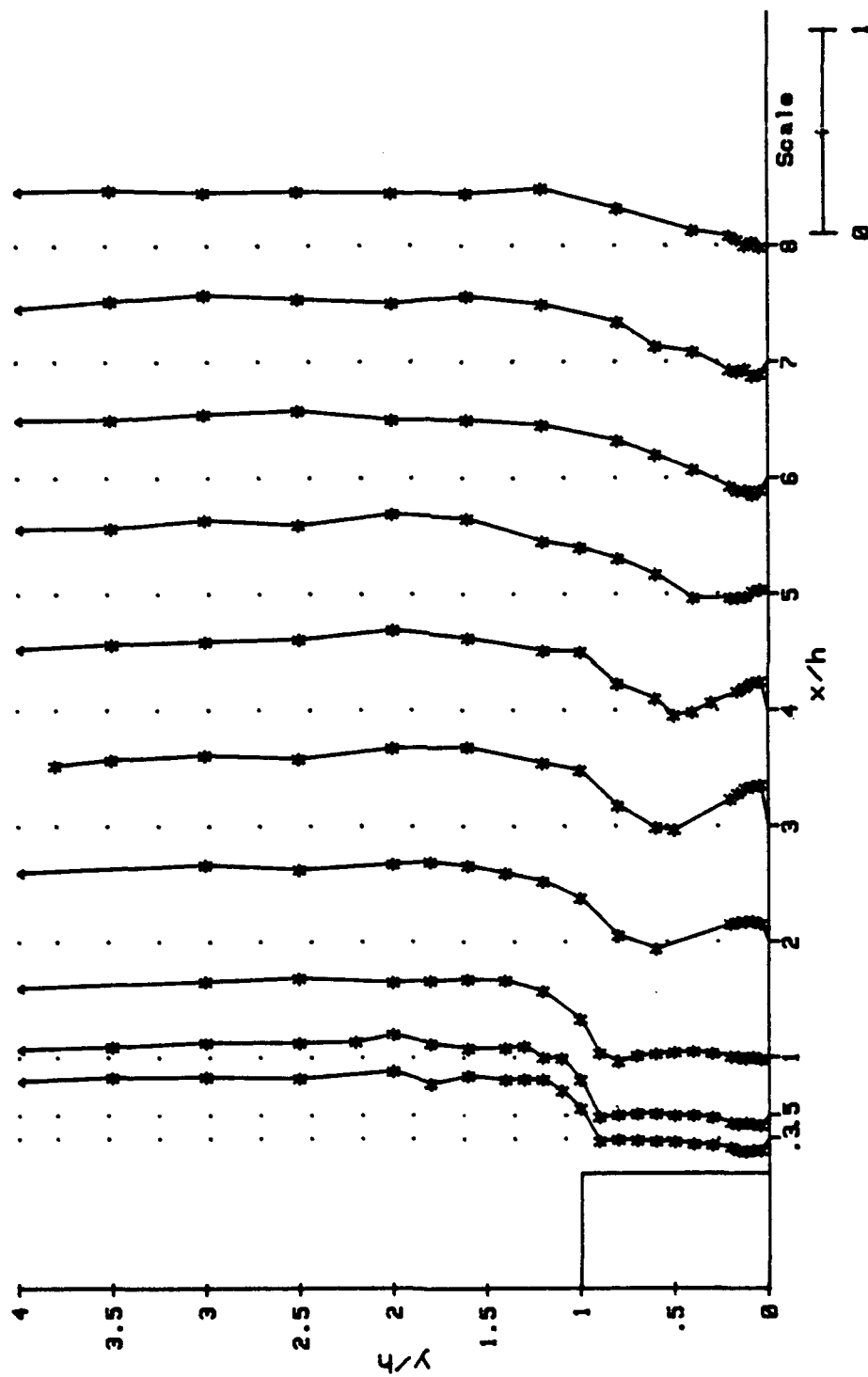


Figure 5.19 Carpet Plot of the w/u_e Profiles in the Recirculation Region for $\Lambda = 15$ Degrees, $x/h = .3$ to 8.0

30 Degree Swept Step

Selected Velocity Profiles. The 30 degree step was the most thoroughly tested configuration of the three. The same number of downstream locations was surveyed, but a more complete survey upstream of the step was performed in order to more accurately define the initial flow conditions. The following profile locations were surveyed: -2.5 to 0.0 in steps of 0.5, 0.15, 0.25; 0.5 to 4.0 in steps of 0.5, 5.0, 6.0 and 7.5 inches.

The overview of the total velocity profiles, Figure 5.20, reveals very little information. The upstream profiles are typical of the other two configurations. Downstream of the step, in Figure 5.20, no discernible recirculation region can be observed, but when all the profiles downstream of the step are examined the recirculation region becomes apparent. The flow reattachment point is believed to occur between $x/h=2$ and 4. Downstream of the reattachment point, the flow slowly dissipates the effect of the step, with the influence of the step still observable at $x/h=15$. The total flow angle, Figure 5.21, is basically zero at the following profile locations; $x/h=-5, -3, 0, 12$ and 15. At the remaining survey locations, the flow angle is zero in the freestream region but below $y/h=1.0$ the flow angle becomes negative. The overall u velocity component data, Figure 5.22, are similar to the total velocity profiles. Figure 5.23 displays the w velocity component carpet plots. The w components are positive everywhere except below $y/h=1.0$ and between $x/h=2$ and 6 where the component become slightly negative. A better view of the flow in the vicinity of the 30 degree step can be seen by examining the profiles between the step and $x/h=8$.

Recirculation Region Velocity Profiles. The total velocity profiles, Figure 5.24, shows a recirculation region with the reattachment region between $x/h=3.0$ and 4.0. More survey positions are necessary to accurately locate the reattachment region. The profile at $x/h=2$ has not been reversed because a definite flow reversal could not be detected from the total velocity profile. It is felt that the flow did reverse at this location, but it is not discernible from the measurements. The profiles at survey locations, $x/h=0.3, 0.5$ and 1.0 are greatly affected by the close proximity of the step. One noticeable difference is that the decrease in total velocity is not as great as for the same profiles of the 0 and 15 degree configurations. The total velocity ratio below $y/h=1$ for the 0 and 15 degree step was approximately 0.07, where as the ratio for the 30 degree step was 0.20 almost three times larger. As stated before, the results of this region are questionable due to the limits of the calibration and the lack of the ability to resolve the flow reversal ambiguity. Downstream of the reattachment region, the surface velocity gradient, dU/dy , increases with increasing streamwise distance.

The total flow angles, Figure 5.25, are approximately zero in the freestream, but become largely negative in the recirculation region. The three survey locations of $x/h=0.3, 0.5$ and 1.0 below $y/h=1.0$ have a constant flow angle of approximately -50 degrees. It must be noted, that because of the choice of $\theta=15$ degrees, if $|\alpha|>45$ degrees then this particular

30 DEG. STEP, U/U_0 VELOCITY PROFILES

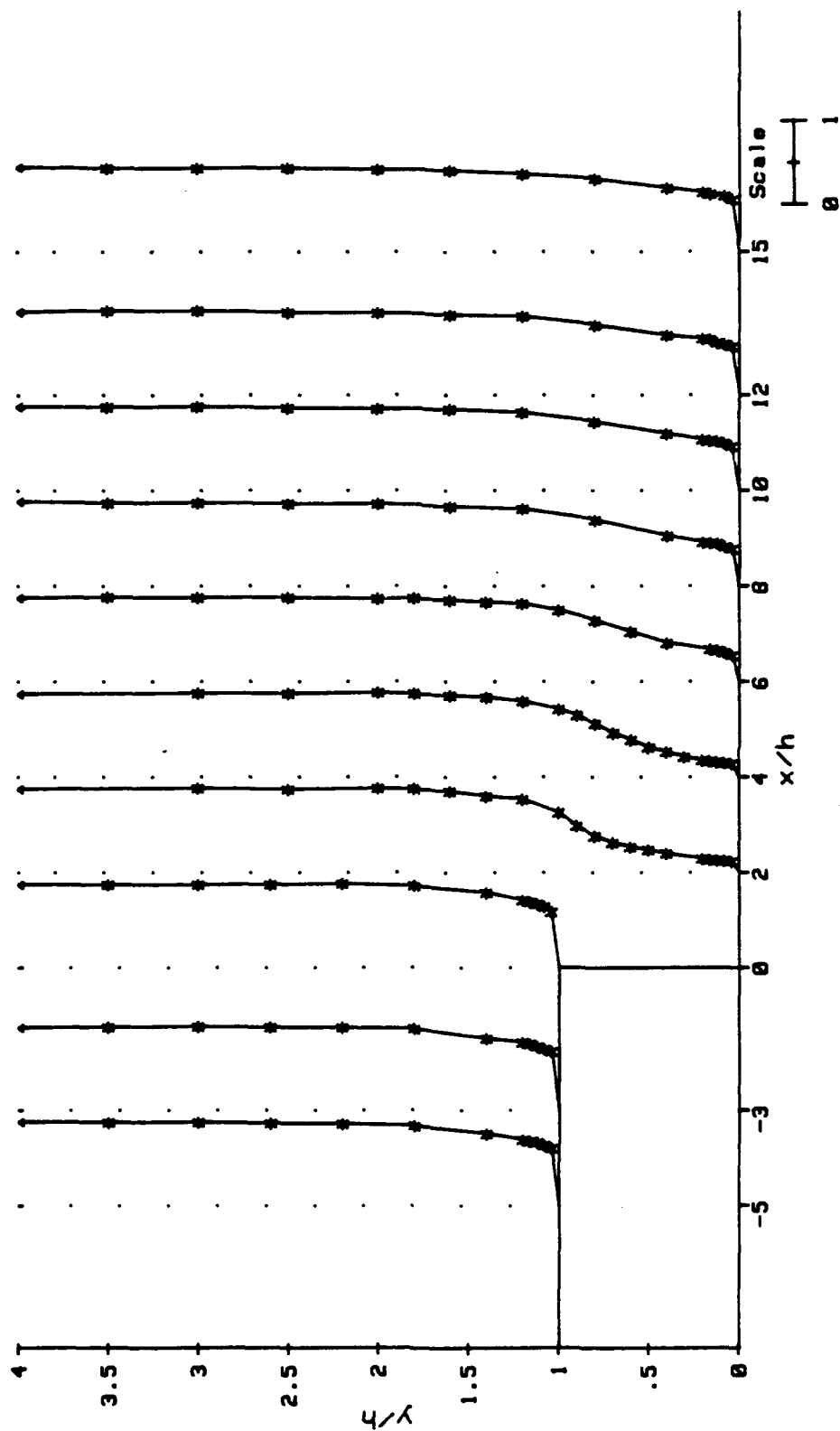


Figure 5.20 Carpet Plot of the U/U_0 Profiles for $\Lambda = 30$ Degrees, $x/h = -5$ to 15

30 DEG. STEP, alpha PROFILES

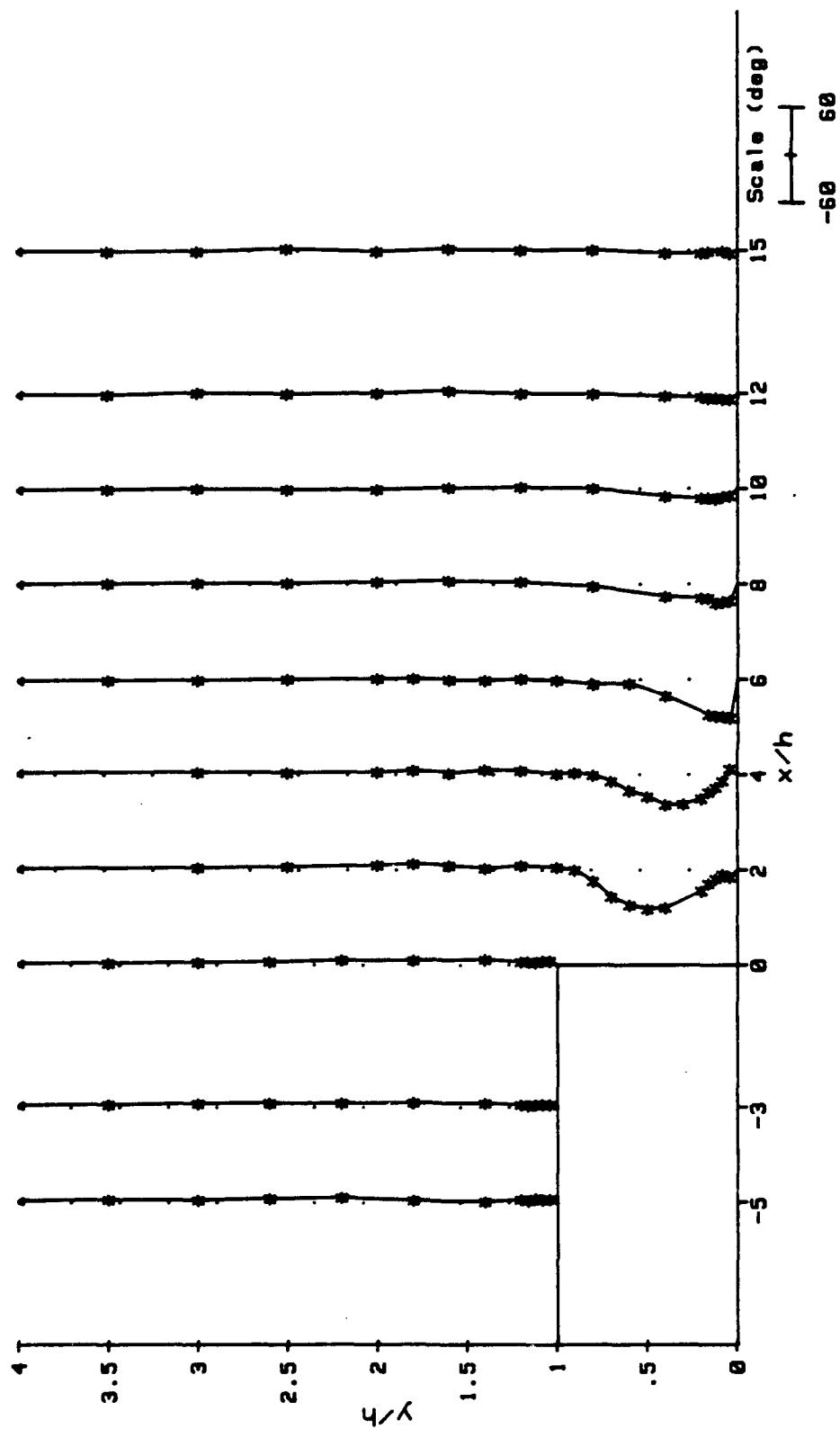


Figure 5.21 Carpet Plot of the α Profiles
for $\Lambda = 30$ Degrees, $x/h = -5$ to 15

30 DEG. STEP, u/u_e VELOCITY PROFILES

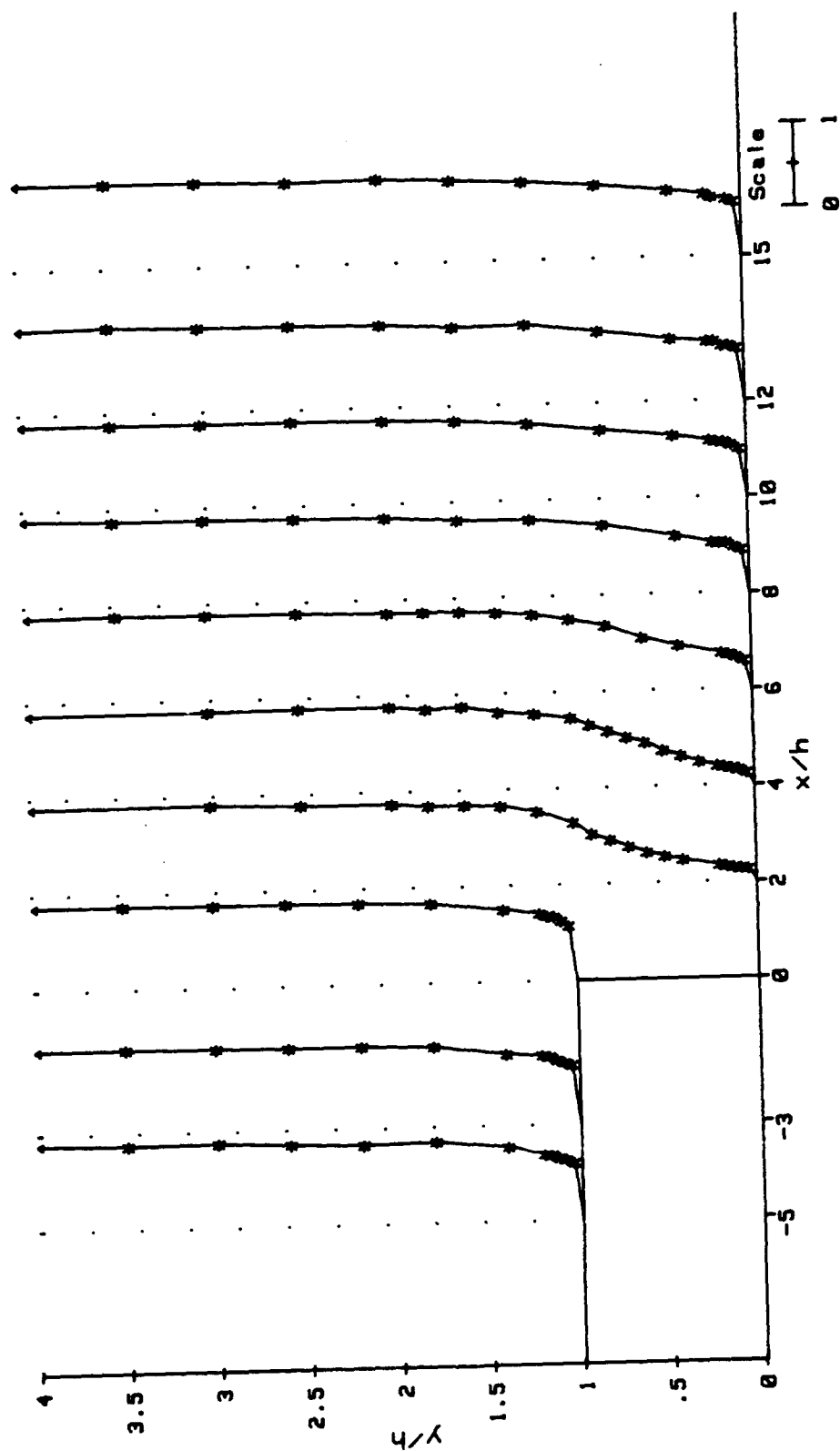


Figure 5.22 Carpet Plot of the u/u_e Profiles for $\Lambda = 30$ Degrees, $x/h = -5$ to 15

30 DEG. STEP, w/u_e VELOCITY PROFILES

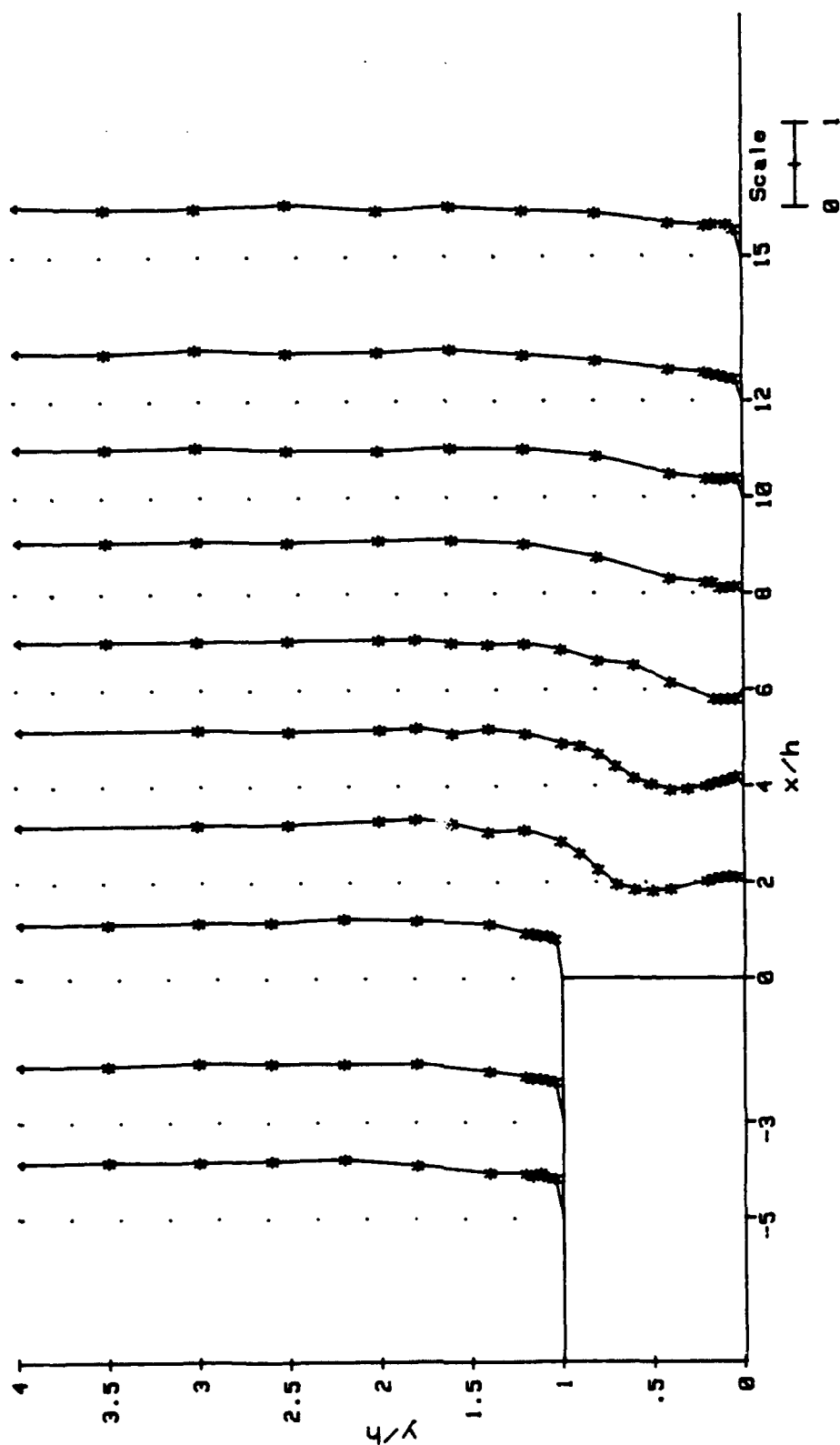


Figure 5.23 Carpet Plot of the w/u_e Profiles for $\Lambda = 30$ Degrees, $x/h = -5$ to 15

30 DEG. STEP, U/U_e VELOCITY PROFILES

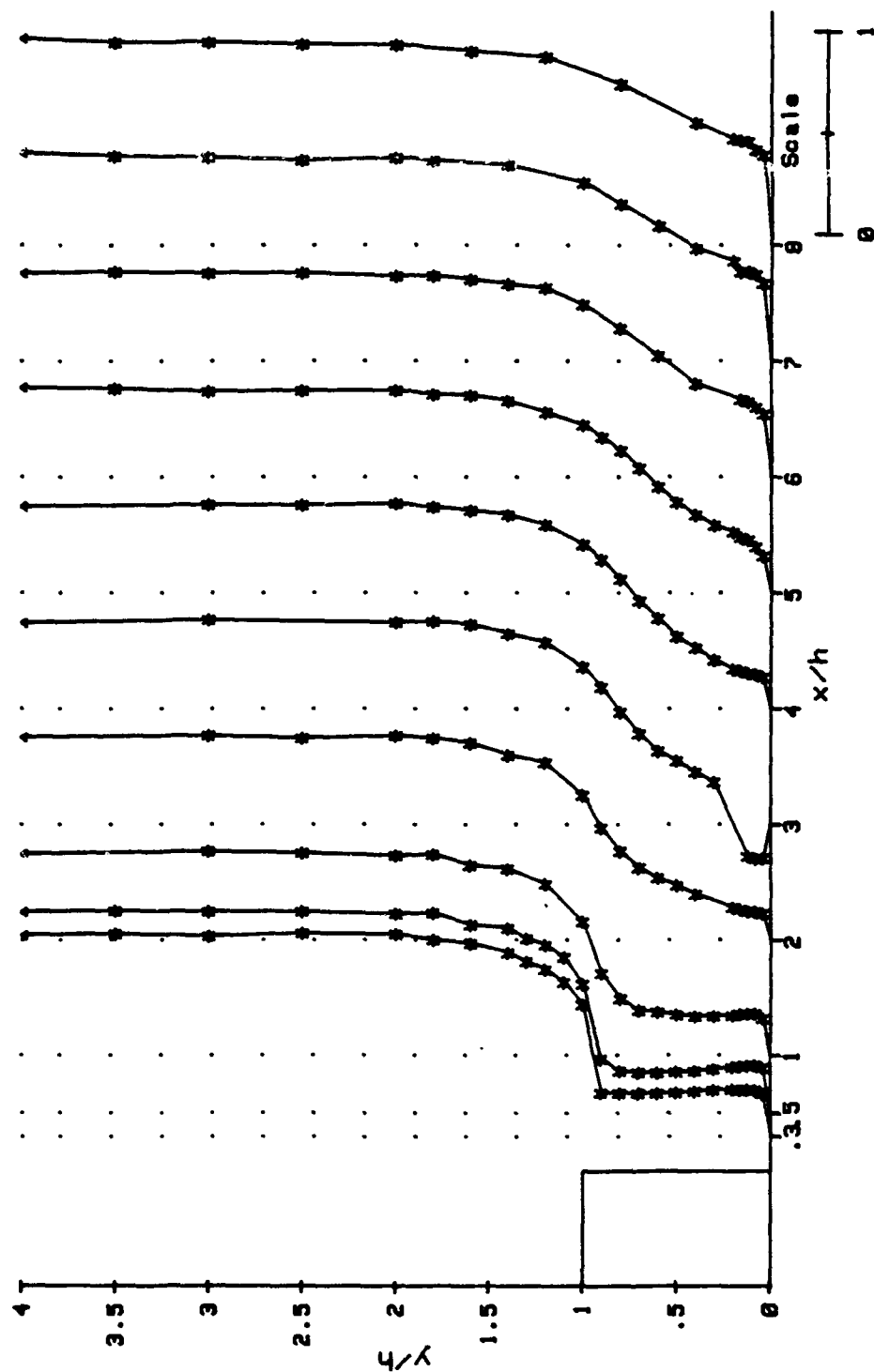


Figure 5.24 Carpet Plot of the U/U_e Profiles in the Recirculation Region for $\Lambda = 30$ Degrees, $x/h = .3$ to 8.0

30 DEG. STEP, α PROFILES

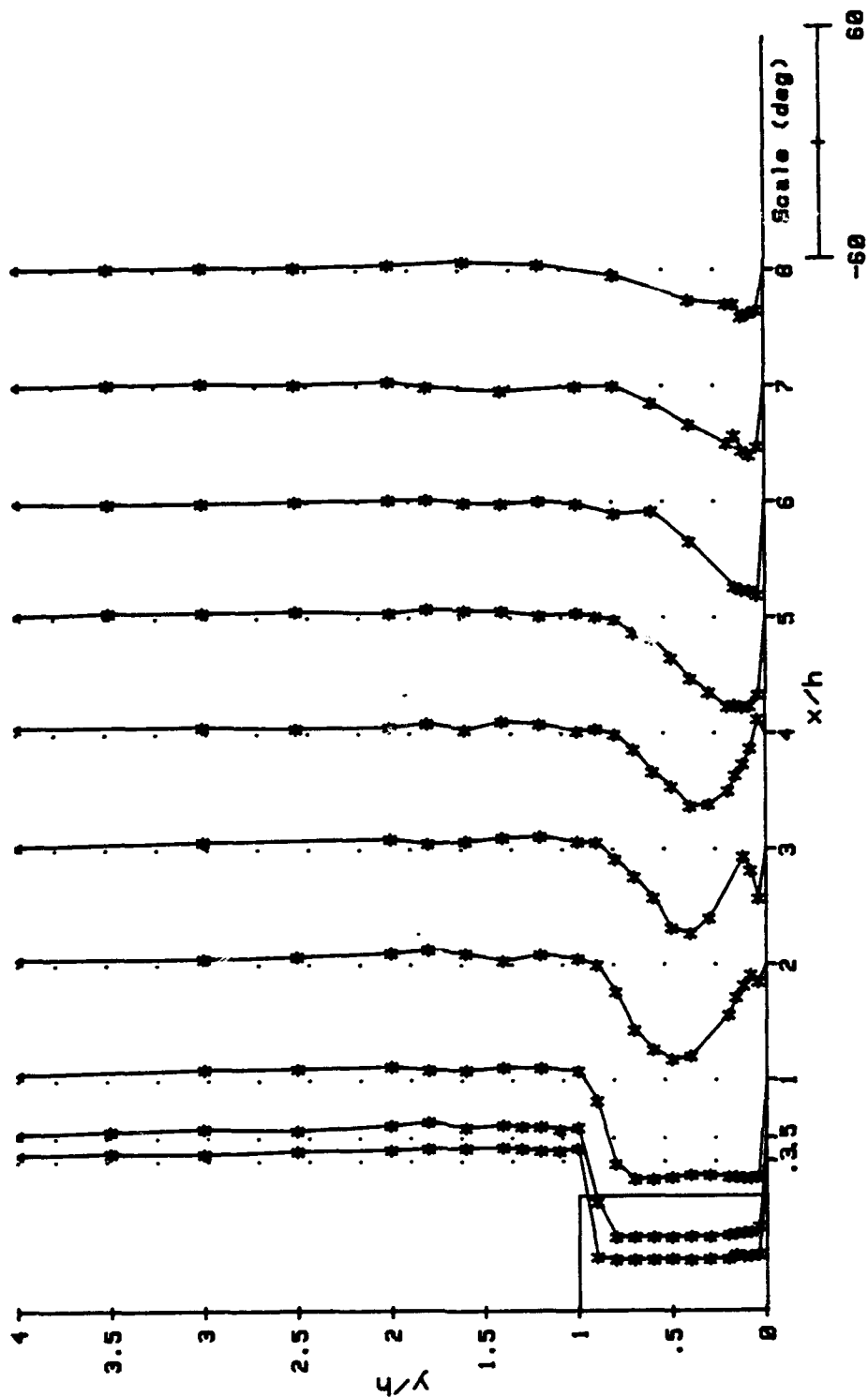


Figure 5.25 Carpet Plot of the α Profiles in the Recirculation Region for $\Lambda = 30$ Degrees, $x/h = .3$ to 8.0

α is only an estimate. This is a requirement of the yaw calibration curve, which was discussed in the Yaw Calibration section of Chapter 4. At survey locations, $x/h=2, 3$ and 4 , and below $y/h=1.0$, the flow angle becomes negative decreasing to a minimum, then increasing towards zero degrees and finally decreasing again. For $x/h=2$, a minimum flow angle of -50 degrees at $y/h=0.5$ is achieved. As y/h continues to decrease the flow angle increases to a maximum within the shear layer of -5.3 degrees at $y/h=0.08$ and then decreases to -9.3 at $y/h=0.04$. The survey location at $x/h=3$, yields a minimum flow angle of -44 degrees at $y/h=0.4$ which increases to a maximum of -4 degrees at $y/h=0.12$ and then finally decreases to -26 at $y/h=0.04$. The stagnation point for each profile occurs at the maximum flow angle within the shear layer. Below the stagnation point, the flow angle again decreases, but now the total velocity is negative, meaning the flow is moving toward the step. For $x/h=4$ the minimum flow angle of -38 degrees occurs at $y/h=0.40$ and then increases to $+7$ degrees at $y/h=0.04$. The remaining locations, $x/h=6, 7$ and 8 continues to show a strong influence on the flow angle due to the presence of the step. By location $x/h=8$ the effect of the step is beginning to dissipate. For profiles $x/h=6, 7$ and 8 the minimum flow angle occurs much closer to the surface of the plate than the profiles further upstream.

The u velocity component profiles, Figure 5.26, are similar to the total velocity profiles. One noticeable difference is that the transition from the freestream to the shear layer is not as smooth for the u component as for the total velocity.

The more interesting results are the w velocity component, Figure 5.27. The carpet plot indicates a positive w component outside of the shear layer with the component becoming negative below $y/h=1$ at survey locations $x/h=0.3, 0.5$ and 1.0 . The profiles at $x/h=2, 3$ and 4 and within the shear layer show the w velocity component suddenly decreasing and becoming negative. The minimum velocity for the three profiles occurred at $y/h=0.5, 0.4$ and 0.4 , respectively. The w component then increases to a positive value as the surface of the plate is approached. This supports the observations made during the oil flow studies which indicated that the oil flowed in the positive w direction within the recirculation region (see Figure 5.2). Once the w components at locations $x/h=5, 6$ and 7 enter the shear layer they become negative and remain negative to the surface of the model. For the $x/h=8$ the w velocity components are positive along the entire profile.

Comparison of Results

Initially there was a concern that because of the three different leading edge and step configurations, identical flowfields could not be reproduced. However, the reduced data show that the total velocity profiles at $x/h=0.0$ agree to within about 4% for the three configurations. From Schlichting (1979) the following relation was used to estimate the turbulent boundary-layer thickness at the edge of the step:

30 DEG. STEP, u/u_e VELOCITY PROFILES

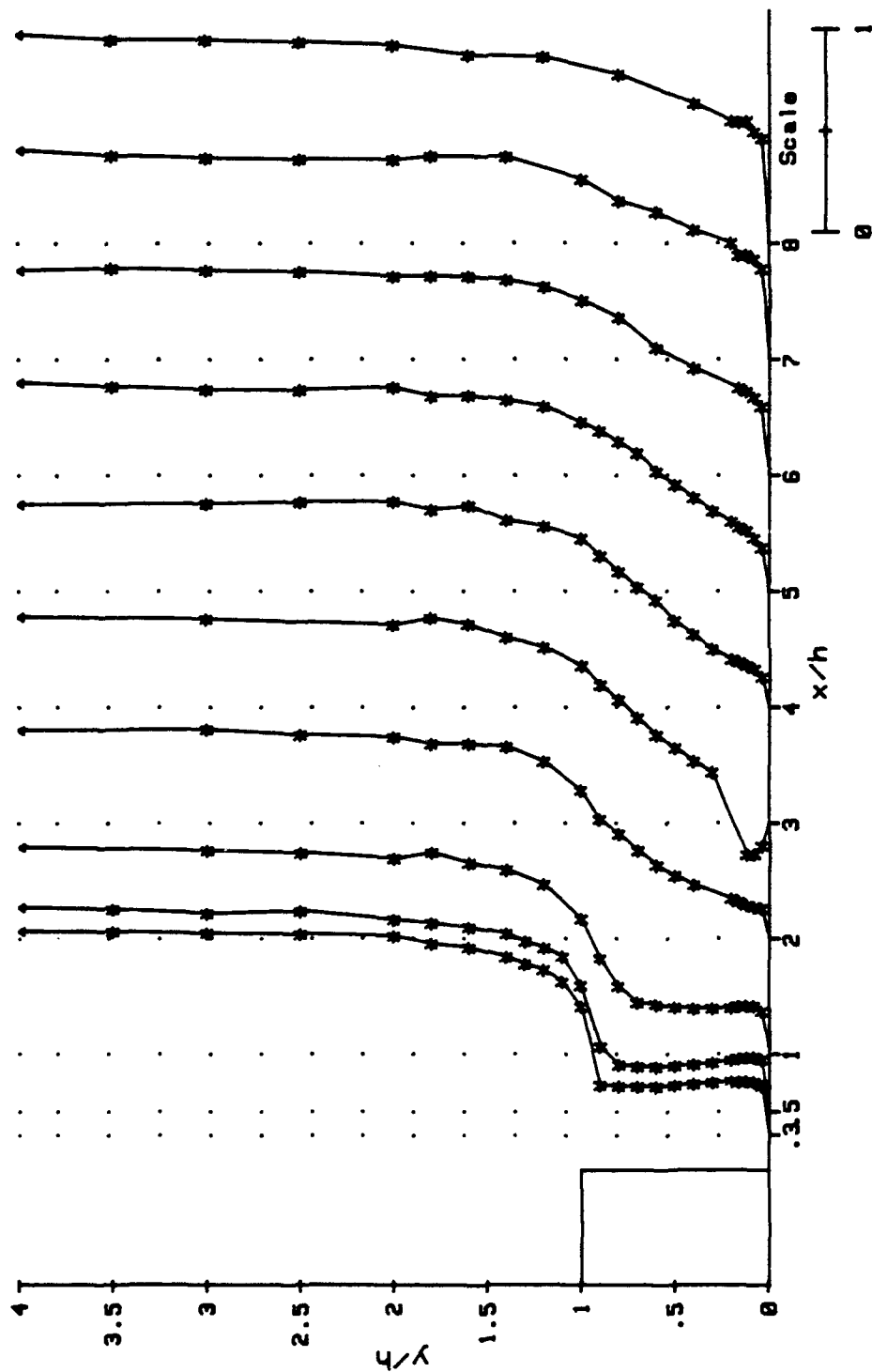


Figure 5.26 Carpet Plot of the u/u_e Profiles in the Recirculation Region for $\Lambda = 30$ Degrees, $x/h = .3$ to 8.0

30 DEG. STEP, w/u_e VELOCITY PROFILES

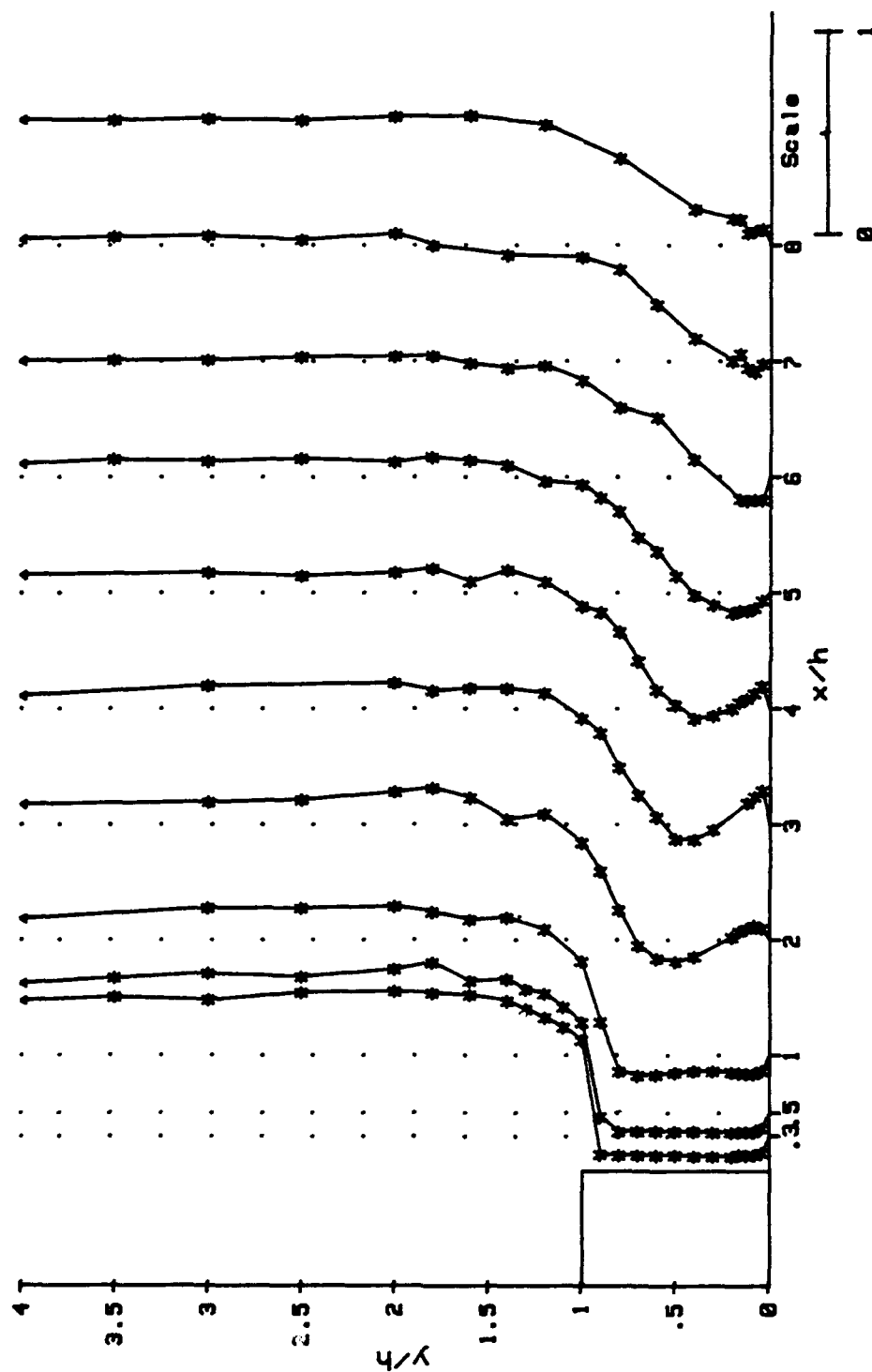


Figure 5.27 Carpet Plot of the w/u_e Profiles in the Recirculation Region for $\Lambda = 30$ Degrees, $x/h = .3$ to 8.0

$$\delta = 0.37 \left(\frac{u L_{sep}}{\nu} \right)^{-1/5} L_{sep} \quad (5.1)$$

where $u = 50$ mph or 73.3 fps, $\nu = 1.57 \times 10^{-4}$ ft²/sec and $L_{sep} = 2.25$ ft. This equation yields a δ of 0.052 ft or 0.62 inches. The agreement between the experimental and theoretical is good with an approximate 5% difference.

Using the procedure described in Chapter 4, the boundary-layer thickness was estimated for each profile surveyed. A plot of δ versus x' for each swept step configuration is shown in Figure 5.28. The results upstream of the step indicate a growing boundary-layer thickness as the step is approached, with $\delta + h = 1.15$ inches at $x/h = 0.0$. It should be noted that the boundary-layer thickness is indicated with respect to the lower surface. Thus, the δ 's upstream of the step are 0.5 inches thicker to account for the height of the step. The furthest upstream result for the 0 degree step is questionable. Downstream of the step, $x/h = 0.0$ to 6.0 , δ decreases to approximately 0.70 inches. Beyond the recirculation region, $x/h > 6.0$ the boundary-layer thickness again begins to increase as the flow recovers from the separation caused by the step. In the recovery region, δ generally increases with increasing sweep angle for a specific survey position.

Estimation of Stagnation Line Within the Recirculation Region. An attempt was made to determine the position of the stagnation line for both the u and w velocity components within the recirculation region. For the u component, this was accomplished by examining the total velocity profiles that showed evidence of flow reversal. Then, by linear interpolating between the two data points on either side of the u component stagnation line, a value of y when $u=0$ was determined. The results are presented in Figure 5.29. The results for the 0 , 15 and 30 degree step are fitted to separate second degree polynomials using a least squares method. The results for the 0 degree step at $x/h = 2.0$ and the 15 degree step at $x/h = 3.0$ and 4.0 are neglected because it is not clear where the flow reversal occurs. However from the curve fits, an estimate of the location of the reverse flow region can be made. The general trend is that the reattachment length decreases as the sweep angle increases.

The w component stagnation line was found by noting, for each survey, the height above the wall where $w=0$ for the first time as y/h decreased from 4.0 to 0.0 . Since the w component is essentially zero for the 0 degree step, only results from the 15 and 30 degree steps are shown in Figure 5.30. From these results the stagnation line for w component is linear. Figure 5.30 indicates that within the reattachment region (where $u=0$) the w component still has finite magnitude. The w component is also negative at this location which means the external flow has been turned beyond normal to the step by the pressure gradient acting normal to the step, so that at reattachment the flow is moving in the negative z' direction. This is consistent with the oil flow observation, presented in Figure 5.3.

Boundary-Layer Thicknesses

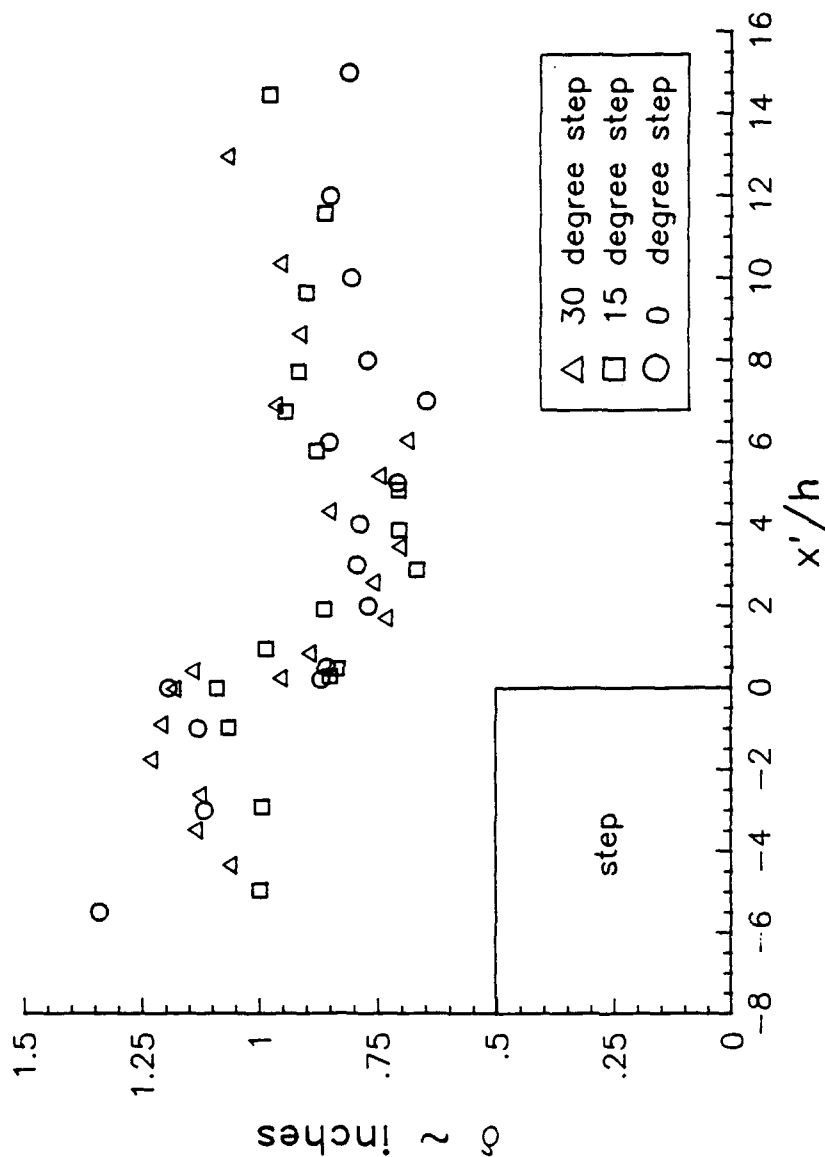


Figure 5.28 Boundary-Layer Thickness as a Function of x'/h for the Three Step Sweep Angles

Downstream Heights of $u/u_e = 0.0$

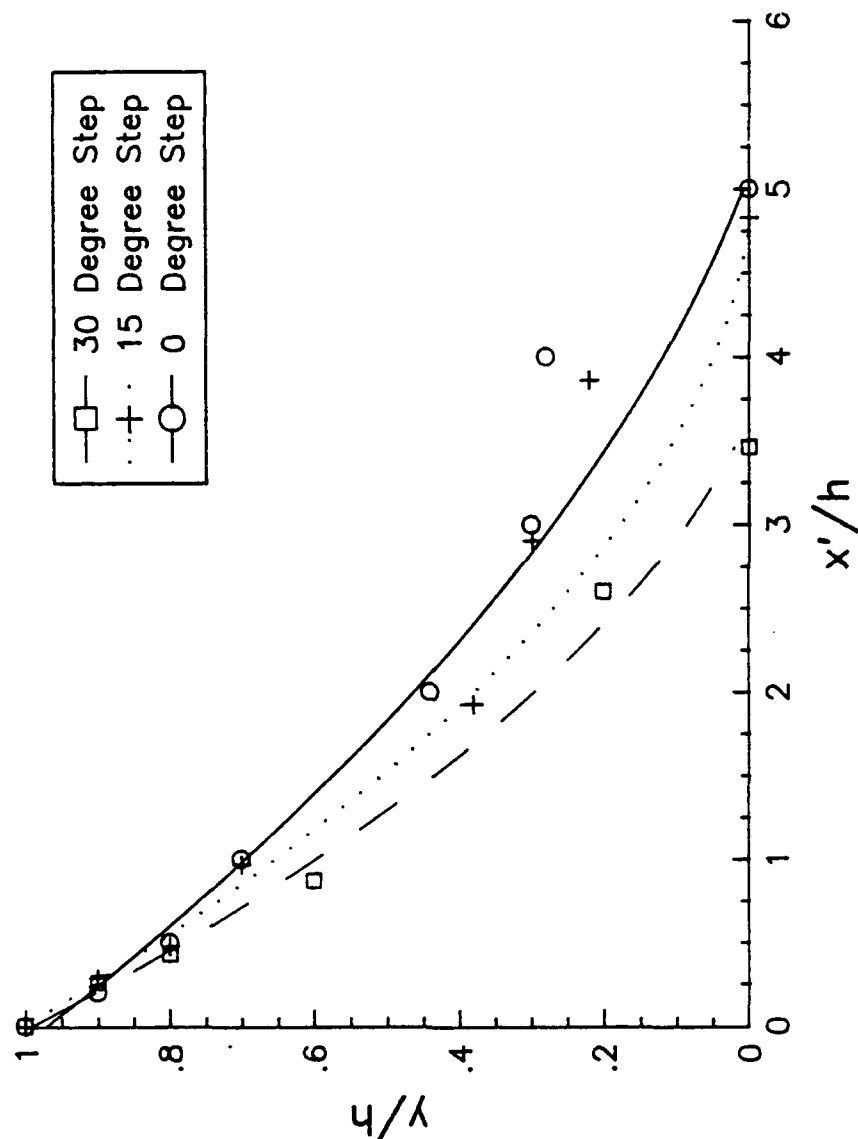


Figure 5.29 Location of the u/u_e Stagnation Line Within the Recirculation Region for the Three Swept Step Configurations

Downstream Heights of $w/u_e = 0.0$

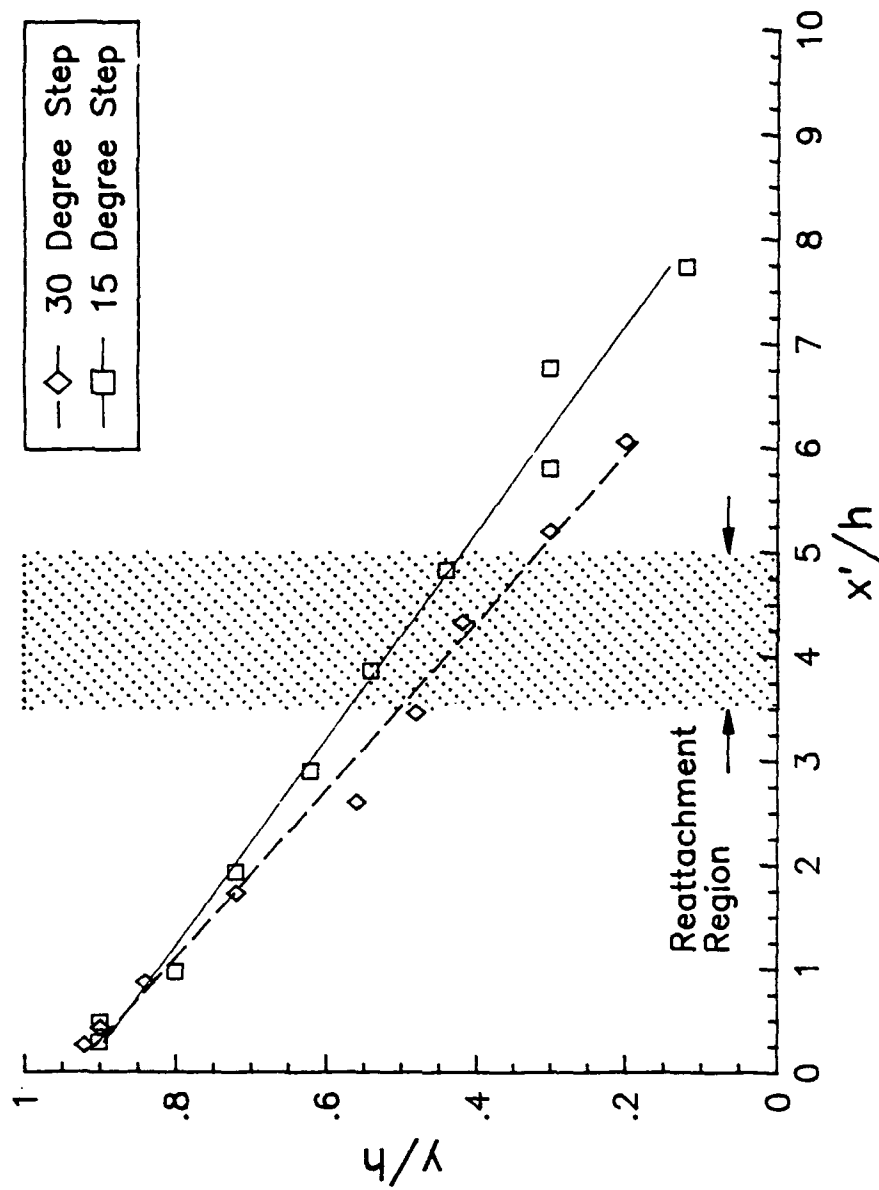


Figure 5.30 Location of the w/u_e Stagnation Line Downstream of the Step for the 15 and 30 Degree Step Configurations

Correlation of Results to Computational Turbulence Models

Overview.

Turbulent boundary-layers are made up of two regions: an inner or wall region and a outer or wake region. The inner region, which consists of only about 10 to 20% of the total turbulent boundary-layer, may be further broken down into three sublayers. The layer closest to the wall is the laminar or viscous sublayer where the viscous shear dominates. This layer extends from the wall to approximately $y^+ = 5$, where $y^+ = y u_\tau / \nu$. The buffer sublayer, where viscous and turbulent stresses are approximately equal, extends from $5 < y^+ < 35$. The turbulent stresses are dominant in the final sublayer of the inner region, the fully turbulent layer, which extends from $35 < y^+$ to $y/\delta \approx 0.2$. The outer or wake region makes up approximately 80% to 90% of the turbulent boundary-layer. This layer is characterized by the intermittency of turbulent flow. The outer region is more sensitive to external parameters, especially the pressure gradient. The main reason for needing an inner and outer region to numerically approximate turbulent boundary-layers is because they are based on different length scales. The inner region length scale, ν/u_τ , depends on the wall shear stress and the outer region length scale is the total boundary-layer thickness, δ .

One aspect of this study was to investigate the correlation of the results with the widely used turbulent boundary-layer law of the wall and law of the wake to swept backward-facing step flows.

Coles' Law

Description of Coles' Law. The first approximation examined was Coles' incompressible law of the wall and wake for attached flows as described by Cebeci and Smith (1974). Coles' equation is written as:

$$u^+ = \frac{1}{\kappa} \ln(y^+) + C + \frac{2\Pi}{\kappa} \sin^2 \left(\frac{\pi y}{2\delta} \right) \quad (5.2)$$

where $u^+ = u/u_\tau$ and $u_\tau = \sqrt{\tau/\rho}$. Coles' law is valid for the fully turbulent sublayer and across most of the outer region. The first two terms on the right hand side of the equation represent the semi-logarithmic form of the law of the wall. κ , the von Karman constant, is the inverse of the slope and C is the intercept of the semi-logarithmic law of the wall curve. The last term is Coles' wake function, which accounts for the wake defect of the velocity in the outer region of the boundary-layer.

The four constants in (5.2) are determined for the present data by a least squares technique. This is accomplished by rewriting Coles' equation in the following form which was used by Danberg (1971):

$$u/u_e = a_1 \ln(y) + a_2 + a_3 \sin^2(a_4 y) \quad (5.3)$$

The a 's are four profile constants to be determined by the least squares fit. A general, nonlinear least squares fit routine was used to compute the four constants from four initial estimates by assuming small perturbations to the a 's. This allowed the equations to be expressed by a linear Taylor series expansion, whereby an improved estimate of the a 's was obtained to start a new iteration. The procedure was repeated until a predetermined degree of accuracy was achieved. With the four values of a 's known, the constants u_τ/u_e , C , Π , and δ could be determined. It is not possible to determine κ independently and the normal value of $\kappa = 0.43$, used by Danberg (1971), was assumed.

Results from Coles' Law. After applying the procedure described above to the results of this study, up and downstream of the recirculation region, the four constants u_τ/u_e , C , Π and δ were determined. Instead of u_τ/u_e the skin friction coefficient, C_f , was calculated. C_f is related to u_τ/u_e by the following relation:

$$C_f = 2 \left[\frac{u_\tau}{u_e} \right]^2 \quad (5.4)$$

The values of C_f for the three configurations are plotted in Figure 5.31. The C_f 's upstream of the step indicate the presence of a pressure gradient acting on the three different step configurations. For the 0 degree step the C_f 's decrease as they approach the edge of the step indicating an adverse pressure gradient acting on the flow. A favorable pressure gradient acts upstream of the 15 degree step with C_f increasing as the step is approached. The 30 degree case indicates a zero pressure gradient or a slight favorable pressure gradient. C_f 's upstream of the 30 degree step remain nearly constant. Downstream of reattachment the C_f 's for the 0 degree step are approximately a factor of 3 smaller than the values obtained upstream. The C_f 's for the 15 and 30 degree steps are only slightly lower downstream when compared to the values upstream. At reattachment the values of C_f is 0 because the velocity gradient at the wall is 0. As x'/h increases from reattachment to approximately 5 step heights downstream, C_f also increases and then remains nearly constant with further increases of x'/h . The effect of sweep angle on the value of C_f indicates that as sweep angle increases so does C_f .

Figure 5.32 shows the various values of the intercept C as a function of survey location for various sweep angles. Upstream, C for the 0 degree step, under an adverse pressure gradient, increases with increasing x'/h . The upstream C 's, for 15 degree step, decrease as the step is approached, indicating a favorable pressure gradient. For the 30 degree step with a zero or slightly favorable pressure gradient the values of C remain nearly constant. Downstream of reattachment the C 's tend to decrease with increasing sweep angle. The value of C is zero at reattachment and then increases with increasing downstream distance. A typical value of C according to Cebeci and Smith (1974) is 5.0 for a two-dimensional flat plate. The comparison between their value and the value of C from this study shows the effect of separation and

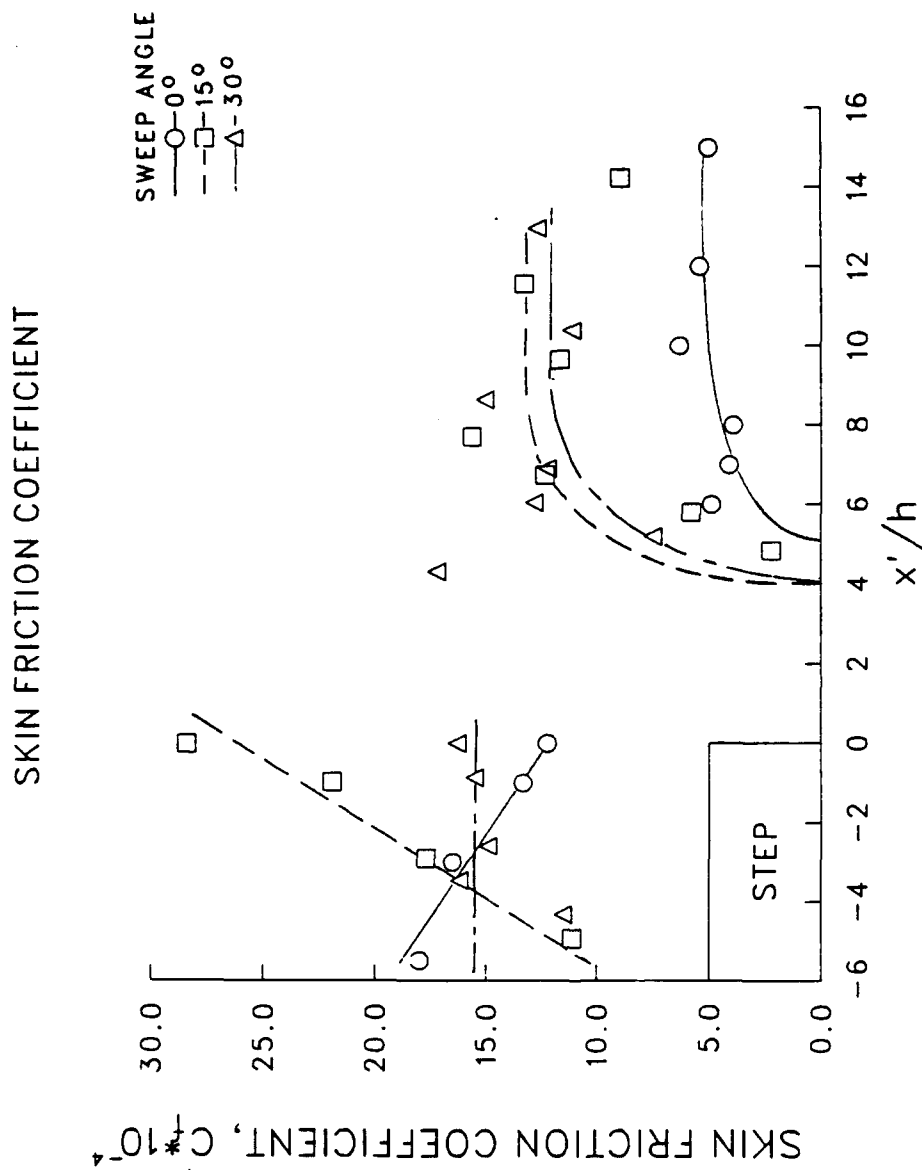


Figure 5.31 Skin Friction Coefficient as a Function of x'/h for the Three Step Sweep Angles

INTERCEPT IN LAW OF THE WALL, C

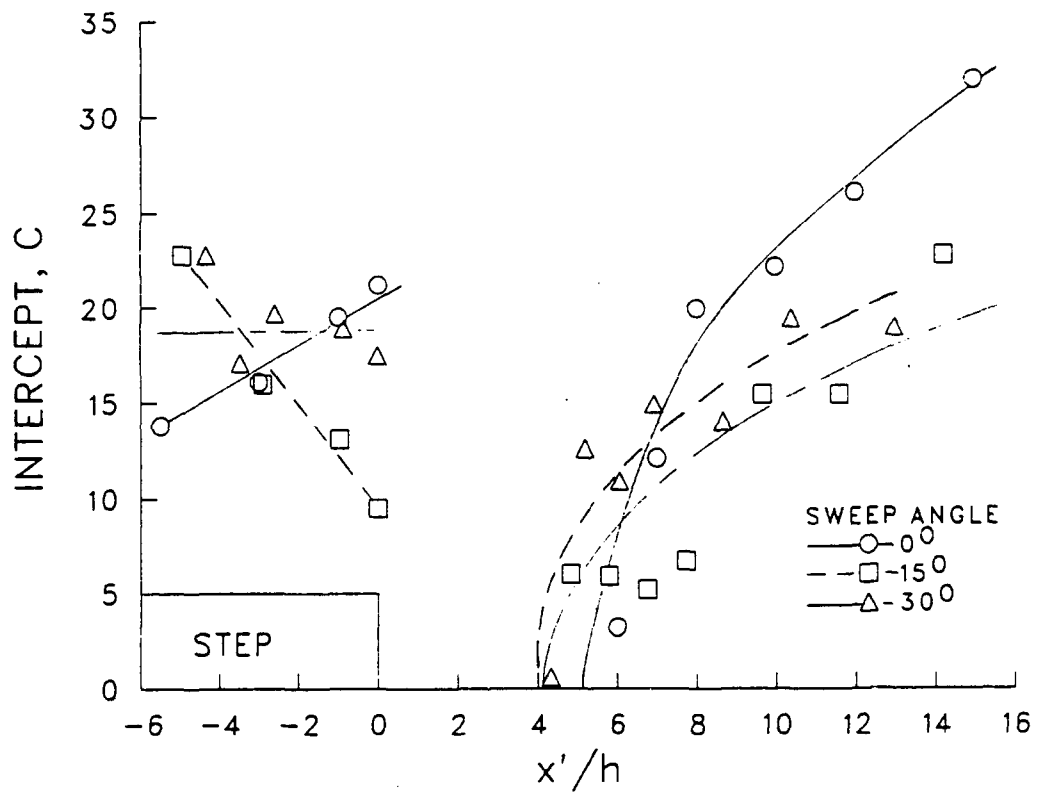


Figure 5.32 The Law of the Wall Intercept, C , as a Function of x'/h for the Three Step Sweep Angles

the three-dimensional flow caused by sweep.

The wake parameter, Π , is shown in Figure 5.33, for the three sweep angles and the different survey locations. Π is a function of the pressure gradient acting on the viscous flowfield. Coles (1968) evaluated a large number of incompressible turbulent boundary-layer profiles on flat plates at high Reynolds numbers ($Re > 3000$) to obtain a value for Π of 0.55. In the present case, upstream of the step, an average value of 0.71 for Π was determined. If the two highest values are neglected, the average Π is 0.61. Upstream of the step, the trends for the various sweep angles can be better seen in the expanded scale of Figure 5.34. The general trend of Π is very similar to the trend of C in Figure 5.32 and is consistent with the skin friction coefficient data. Π increases with increasing x'/h for the 0 degree step. For the 15 degree step, Π decreases as the step is approached, and in the 30 degree case Π remains nearly constant or decreases slightly.

Downstream of reattachment (Figure 5.33) the wake is the dominant component of the boundary-layer. The inner or wall layer effectively disappears at reattachment. Coles' profile equation becomes,

$$\frac{u}{u_e} = \frac{2 u_r \Pi}{u_e \kappa} \sin^2 \left(\frac{\pi y}{2 \delta} \right) \quad (5.5)$$

where in the limit as τ_w tends towards zero at reattachment the term

$$\lim_{\tau_w \rightarrow 0} \frac{2 u_r \Pi}{u_e \kappa} = 1 \quad (5.6)$$

Thus Π goes to infinity as u_r goes to zero. This is only true in the limit and as the boundary-layer develops downstream of reattachment the effects of the wall layer become important again. This result is evident in the calculated values of Π downstream of reattachment. Near reattachment Π is quite large with values around 10.0. As the downstream distance increases the magnitude of Π decreases to 3.45, 1.89 and 1.01 for 0, 15 and 30 degree sweep angles, respectively. Although Π is slowly decreasing it is still much larger than its' pre-step value. The results also indicate that Π decreases as sweep angle increases.

The final parameter, Coles' δ , is plotted in Figure 5.35. Also shown in this figure are the boundary-layer thicknesses from Figure 5.28. The agreement between the two procedures for determining the boundary-layer thicknesses is quite good with the general trend of the results being similar between the two procedures. The general trend of Coles' δ , upstream of the step for all sweep angles, is to increase as the step is approached, and except for a few points, the agreement is good. No δ 's are determined from Coles' law in the recirculation region. In the recovery region the boundary-layer continues to grow with increasing x'/h . The effect of sweep angle on δ in the recovery region, is that for a specific location, δ increases with increasing Λ .

LAW OF THE WAKE PARAMETER, Π

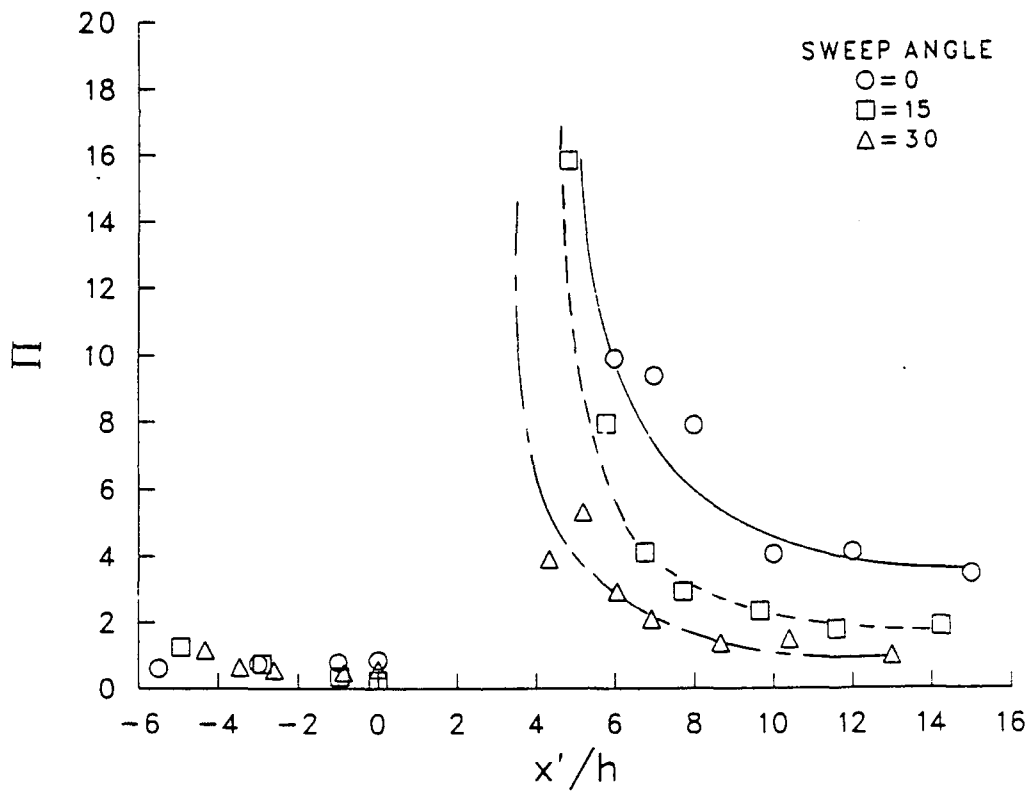


Figure 5.33 Coles' Wake Parameter as a Function of x'/h for the Three Step Sweep Angles

LAW OF THE WAKE PARAMETER, Π AHEAD OF SEPARATION

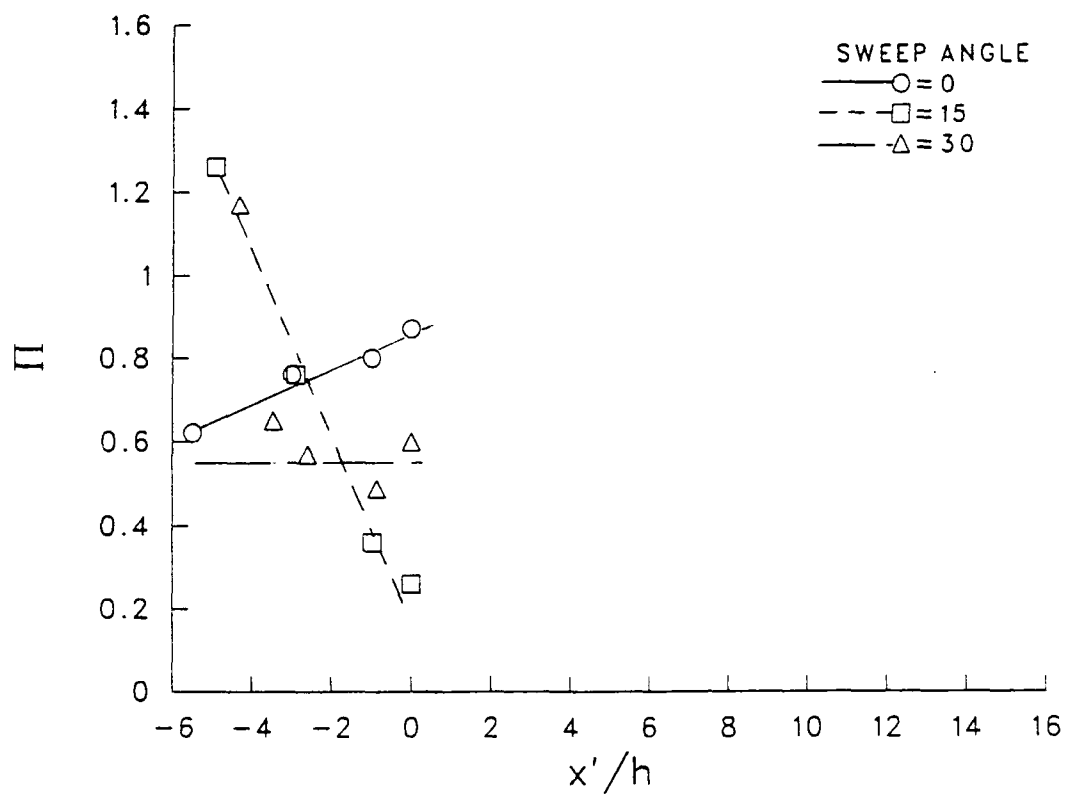


Figure 5.34 Coles' Wake Parameter Upstream of the Step,
Plotted on an Expanded Scale

Boundary-Layer Thicknesses

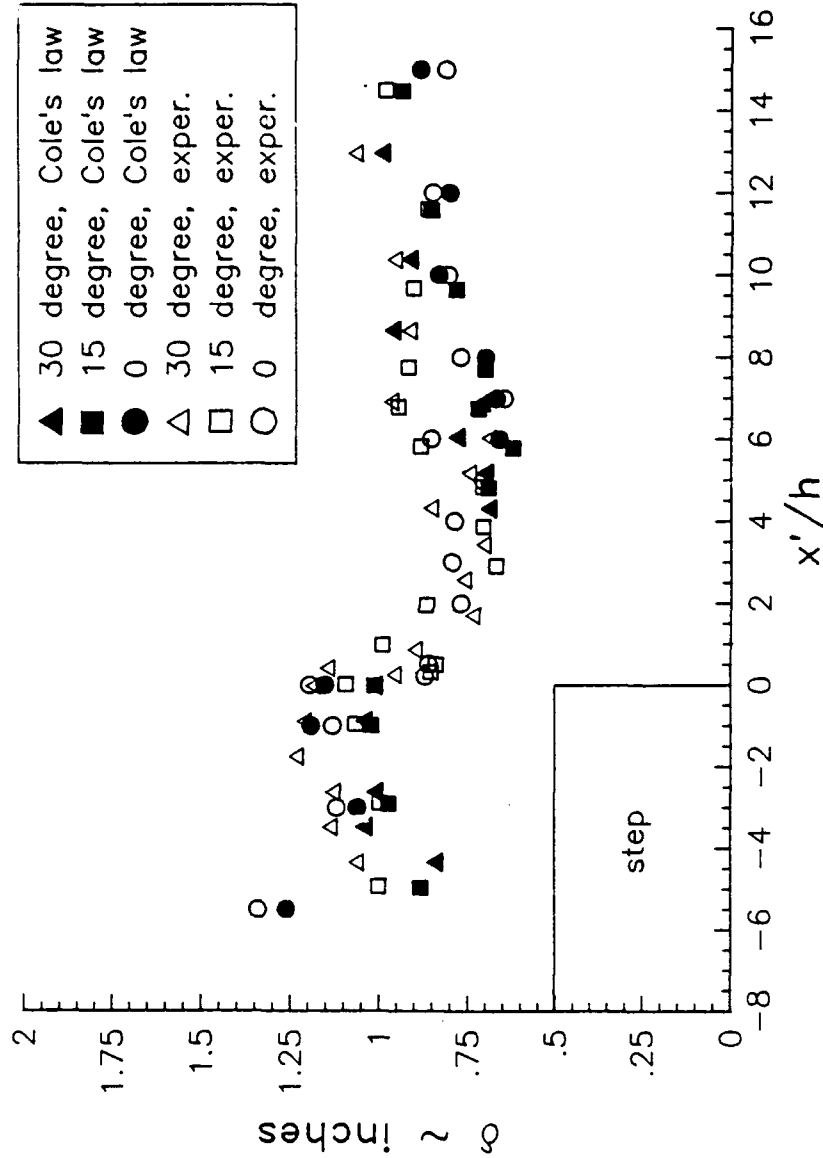


Figure 5.35 Comparison of Coles' Law Boundary-Layer Thickness and Those Determined Directly From the Experimental Results

Another way of examining the results from the Coles' law analysis is by looking at the semi-log profiles. The semi-log profiles at the step ($x'/h = 0.0$) are shown in Figure 5.36 for the three Λ 's. As pointed out earlier, the profiles u/u_e versus y/δ show very little differences, $\approx 4\%$, but the log profiles show considerable difference because they present the profiles in a more sensitive manner. The relative magnitude of the wake defect is consistent with the previous discussion of the coefficients of Coles' law. The $\Lambda = 0$ degree profile is characteristic of an adverse pressure gradient because of the large wake defect, whereas the $\Lambda = 15$ degrees profile shows evidence of a favorable pressure gradient. The $\Lambda = 30$ degrees also has a slight favorable pressure gradient but is more representative of an equilibrium flow. It is not clear whether these gradients are entirely due to initial conditions or if the sweep induces them. Figure 5.37 presents three typical semi-log profiles after flow reattachment for $\Lambda = 30$ degrees. The three profile locations are $x/h=6.0$, 7.0 and 10.0. These three profiles illustrate the recovery of the flow after reattachment. The wake effect is quite large in the profile at $x/h=6.0$. At $x/h=7.0$ the wake effect has been reduced by 50% and at $x/h=10.0$ the wake effect is approximately 25% of what it was at $x/h=6.0$.

The resulting velocity profiles produced from Coles' equations are shown in Figure 5.38 through 5.41 along with the experimental results of this study. Since the upstream velocity profiles are similar for the three configurations only the $\Lambda = 15$ degrees results are presented in Figure 5.38. All profiles upstream of the step collapse into approximately a single curve, with the solid lines representing Coles' law and the symbols indicating the experimental data. Figures 5.39 to 5.41 show the profile from Coles' law downstream of reattachment. All Λ 's show recovery from separation. At separation the logarithmic terms of Coles' equation (5.3) are zero and the separation profile is just the wake component. As the downstream distance increases the profiles become fuller indicating an increasing importance of the logarithmic terms.

Baldwin-Lomax Method

General Baldwin-Lomax Method. The method as described by Baldwin and Lomax (1978) is a two-layer algebraic turbulence model which is widely used in computational fluid dynamics. The model works well for two- and three-dimensional attached flows. Basically the model evaluates the turbulent shear stresses in terms of an eddy viscosity. The major advantage of this model is that the boundary-layer thickness does not have to be known explicitly and thus the arbitrariness and potential error associated with this quantity is eliminated.

In the Baldwin-Lomax model the eddy viscosity, μ_t , is represented by two values, one for the inner and one for the outer regions. The inner region uses the Prandtl-Van Driest formulation for μ_t . For this study, only the outer region formulation was used, since no measurements were obtained within the inner region. The value of the outer region eddy viscosity coefficient depends on whether the flow is attached or separated. For attached flow the outer

LAW OF THE WALL - WAKE PROFILE
 $x'/h=0.0$

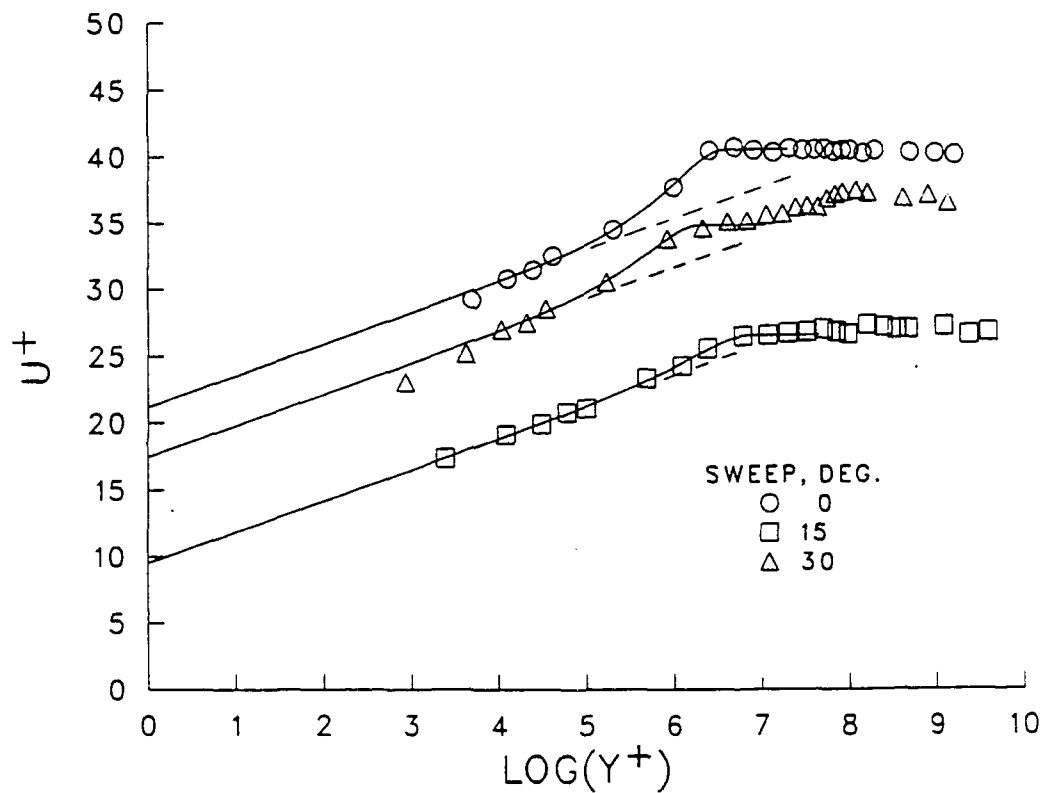


Figure 5.36 Law of the Wall Semi-Logarithmic Wake Profiles at $x'/h = 0.0$ for the Three Step Sweep Angles (symbols are experimental data)

LAW OF THE WALL - WAKE PROFILE AFTER REATTACHMENT

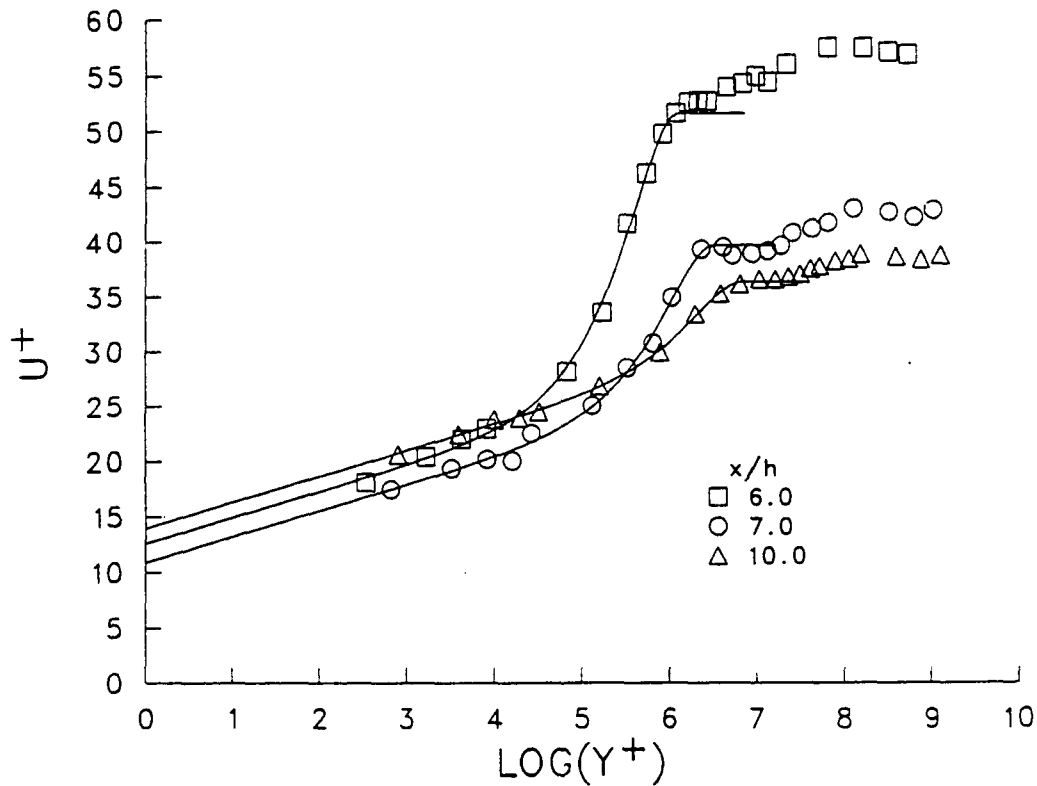


Figure 5.37 Law of the Wall Semi-Logarithmic Wake Profiles
After Reattachment for $\Lambda = 30$ Degrees
(symbols are experimental data)

VELOCITY PROFILES AHEAD OF SEPARATION
SWEEP=15 DEG.

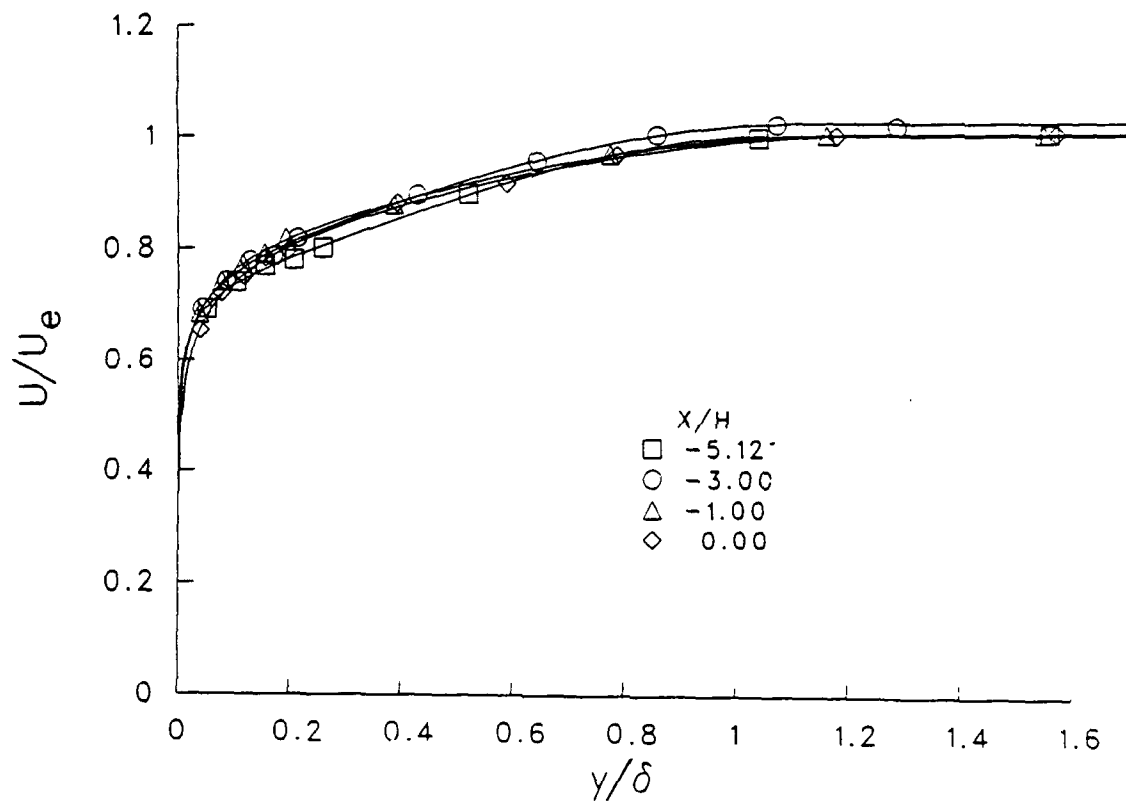


Figure 5.38 Typical Coles' Law Velocity Profiles
Ahead of Separation for $\Lambda = 15$ Degrees
(symbols are experimental data)

VELOCITY PROFILES AFTER REATTACHMENT
SWEEP=0 DEG.

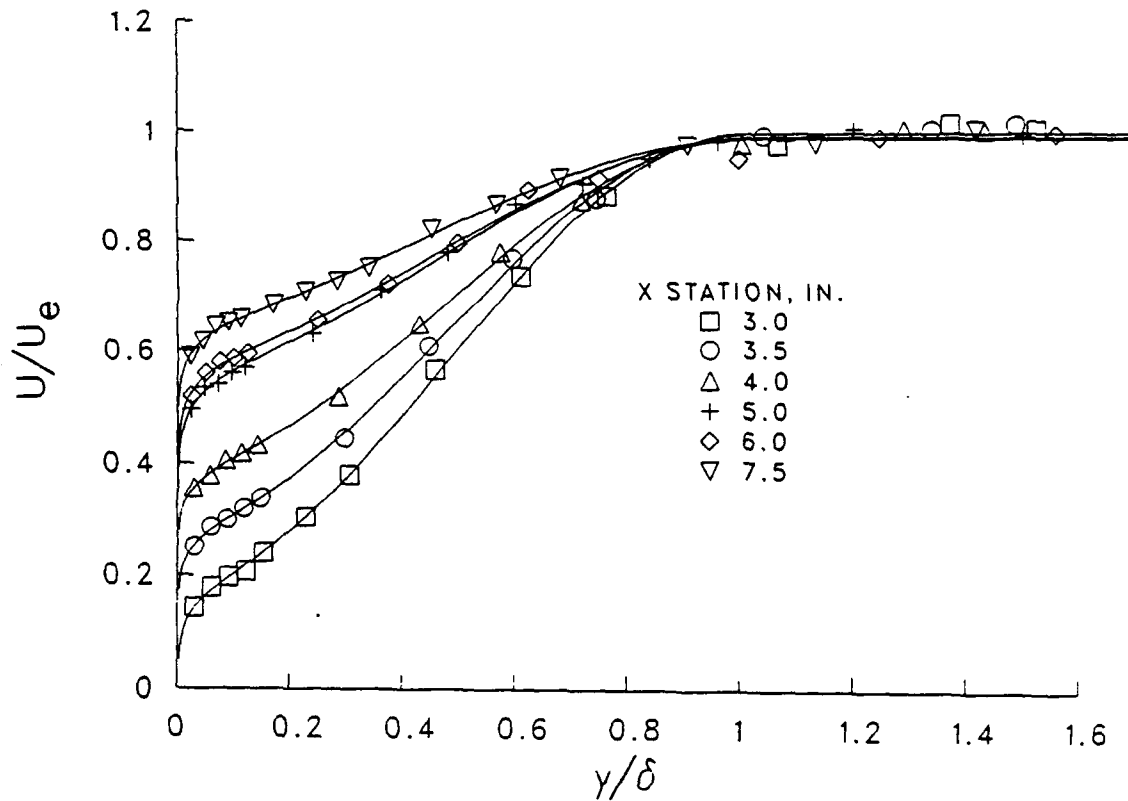


Figure 5.39 Coles' Law Velocity Profiles After Reattachment for $\Lambda = 0$ Degree (symbols are experimental data)

VELOCITY PROFILES AFTER REATTACHMENT
SWEEP=15 DEG.,

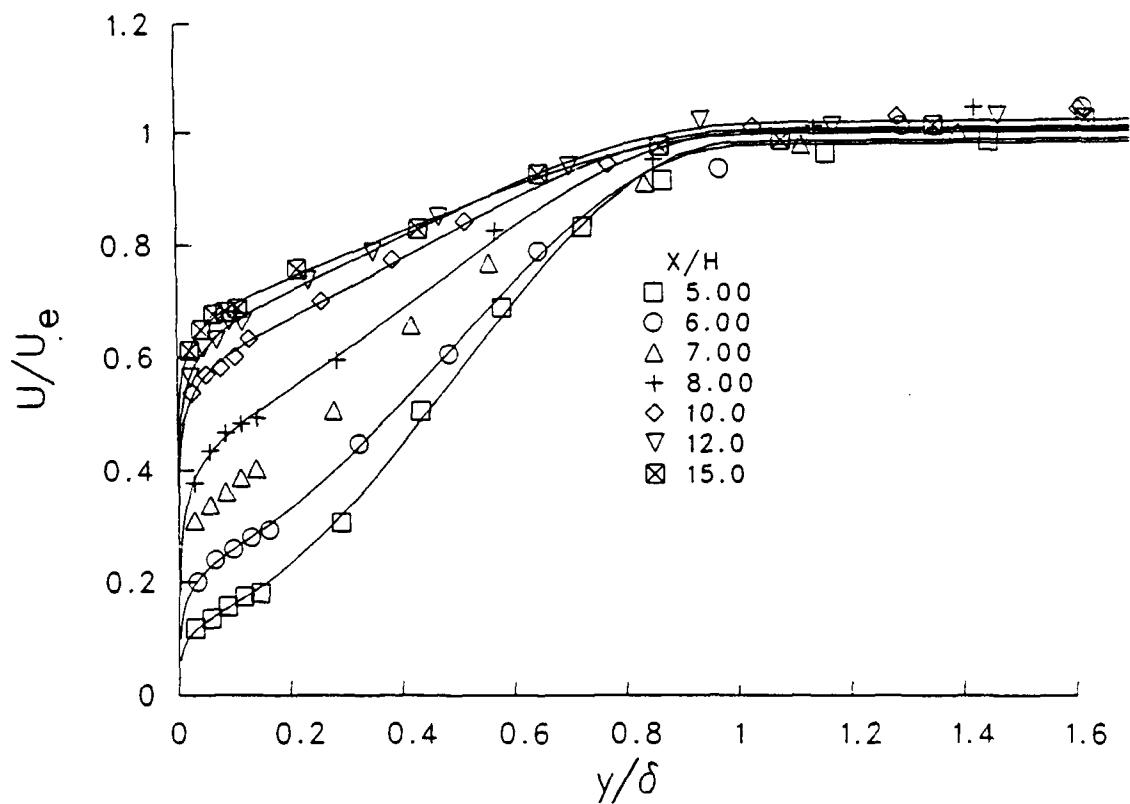


Figure 5.40 Coles' Law Velocity Profiles After Reattachment for $\Lambda = 15$ Degrees (symbols are experimental data)

VELOCITY PROFILES AFTER REATTACHMENT
SWEEP=30 DEG.

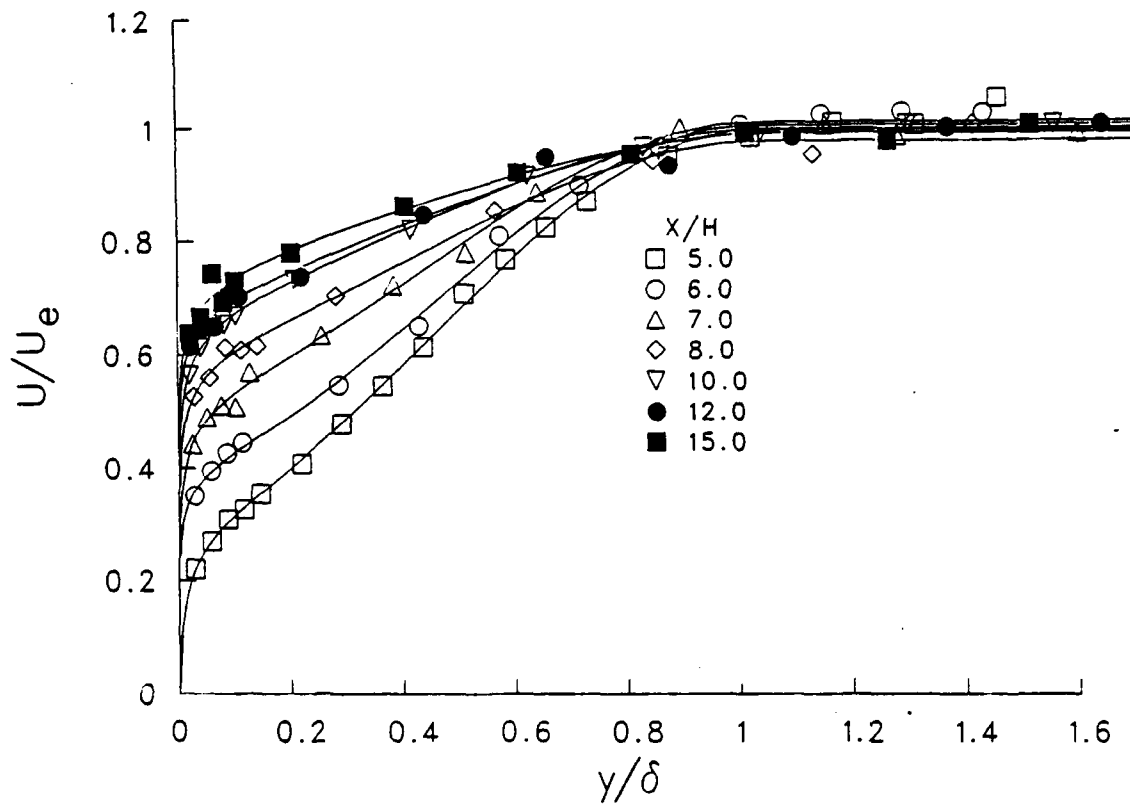


Figure 5.41 Coles' Law Velocity Profile After Reattachment for $\Lambda = 30$ Degrees (symbols are experimental data)

eddy viscosity is given by;

$$\mu_t^o = K C_{cp} \rho y_{max} F_{max} \gamma \quad (5.7)$$

where K is the Clauser constant equal to 0.0168, C_{cp} is a constant equal to 1.6, ρ is the density, y_{max} is the normal distance to F_{max} and F_{max} is determined from the moment of vorticity equation:

$$F(y) = y |\omega| \left[1 - e^{(-y^+/A^+)} \right] \quad (5.8)$$

where ω is the vorticity and A^+ is a constant equal to 26. γ is the Klebanoff's intermittency factor defined by the following equation:

$$\gamma = \left[1 + 5.5 \left(\frac{C_{kleb} y}{y_{max}} \right)^6 \right]^{-1} \quad (5.9)$$

where $C_{kleb} = 0.3$.

The outer layer eddy viscosity for a separated flow is given by the following relation:

$$\mu_t^o = K \rho C_{cp} C_{wk} \left[\frac{U_d^2 y_{max}}{F_{max}} \right] \gamma \quad (5.10)$$

$$U_d = \sqrt{(u^2 + v^2 + w^2)_{max}} - \sqrt{(u^2 + v^2 + w^2)_{min}} \quad (5.11)$$

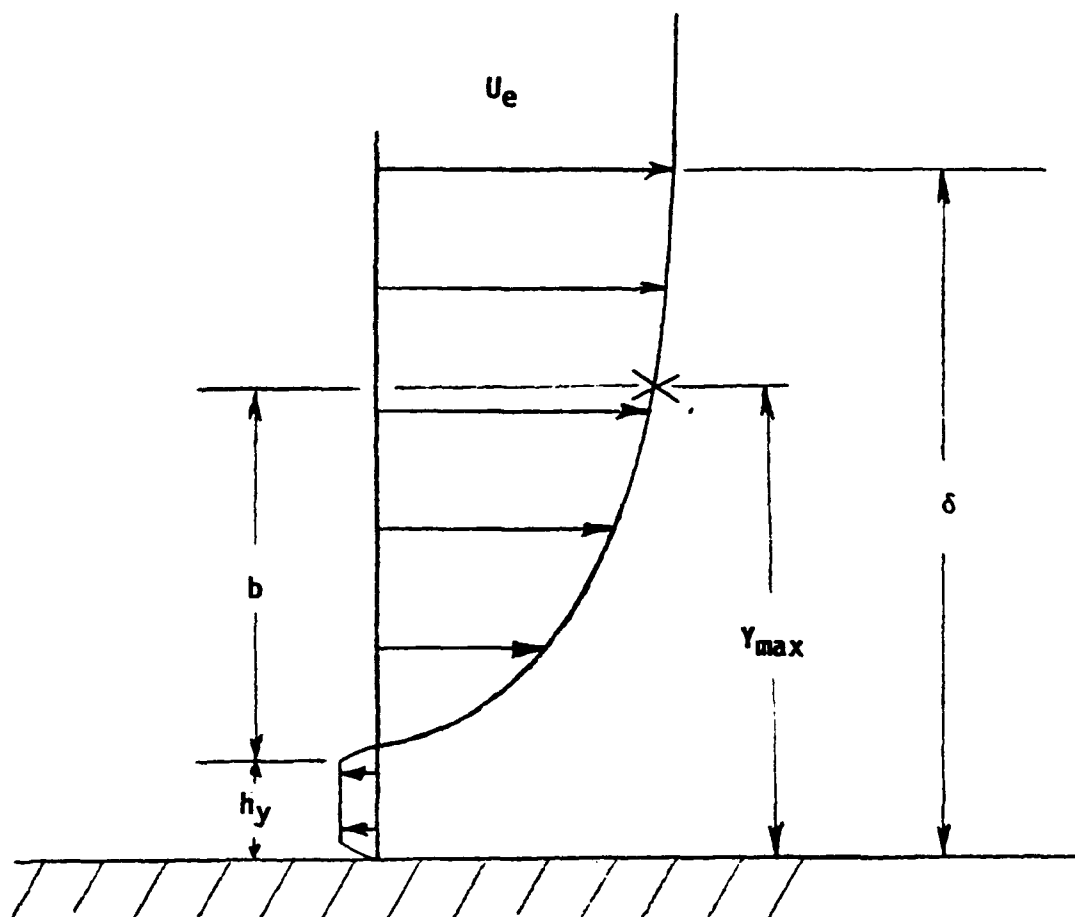
where the constant $C_{wk} = 0.25$

U_d is the difference between the maximum and minimum velocity across the profile and $U_{min} = 0$ for attached flow due to the no slip boundary condition.

Qualification to the Baldwin-Lomax Model. In order to achieve satisfactory results with the Baldwin-Lomax turbulence model several qualification, presented by Danberg and Patel (1988), need to be made to the model. First, the equation defining the eddy viscosity for the separated or wake flow case must be modified. The necessary changes to equation (5.8), which defines the moment of vorticity, $F(y)$, is given as follows:

$$F(y) = (y - h_y) (du/dy) \left[1 - e^{(-y^+/A^+)} \right] \quad (5.12)$$

The first difference between (5.12) and (5.8) is that in (5.12), the quantity $(y - h_y)$ has replaced y , with h_y being defined as the vertical height above the surface to the position of the minimum velocity, see Figure 5.42. The purpose of (5.8) or (5.12) is to determine the appropriate length and



NOTE: For typical attached profiles $y_{max} \approx .65 \delta$

Figure 5.42 Typical Separated Profile Illustrating Terms Important to Modification to the Baldwin-Lomax Model

velocity scale for evaluating the eddy viscosity. If the equation is left unchanged, as stated in (5.8), then an incorrect value of y_{\max} is obtained. This can be seen by considering two typical profiles; one just upstream of separation and the other immediately after separation. In the first case, y_{\max} is roughly 65% of the boundary-layer thickness, which is characteristic of the thickness of the wake layer. Note that the maximum vorticity occurs at the wall but the moment arm is zero there, and thus the maximum of the moment of vorticity occurs away from the wall at a point characteristic of the wake region.

Immediately after separation the maximum vorticity still occurs near the top of the step, but now the corresponding moment arm is large and the maximum in $F(y)$ occurs at that point. The characteristic length scale suddenly jumps from 65% of δ to the step height, H . As a result there is a discontinuity in the length scale y_{\max} and F_{\max} , which is physically unrealistic. By evaluating the moment of vorticity relative to a line, displaced h_y above the wall, the outer flow is separated from the inner recirculation region and thus, the difficulty of determining the proper y_{\max} and F_{\max} is avoided.

The second difference between (5.8) and (5.12) is the substitution of du/dy for the $|\omega|$. Since the derivatives of the v and w components contribute very little to the vorticity compared to the du/dy term, the vorticity in the boundary-layer model is approximated by du/dy . By making these changes, equation (5.12) provide more realistic values of y_{\max} and F_{\max} for the separated flow case.

The Klebanoff intermittency factor, γ , given by (5.9) must also be modified to take into account the displacement of the shear layer from the wall by the distance h_y . If γ remains the same function of y/δ , the intermittency is too high at the outer edge of the shear layer in the separated region. This problem can be avoided by letting $\gamma=1.0$ for all values of y less than h_y . h_y can be approximated by $(y_{\max} - b)$, where b is the half width of the shear layer, see Figure 5.42, and is estimated for separated flows from the following expression:

$$b = \frac{\pi}{4} \frac{(u_e - u_{\max})}{F_{\max}} (y_{\max} - h_y) \quad (5.13)$$

After modifying the length scale of (5.9) to account for the displacement of the shear layer in separated flows the intermittency factor now becomes:

$$\gamma = \left\{ 1.0 + 5.5 \left[C_{\text{kleb}} \frac{(y - y_{\max} + b)}{2b} \right]^6 \right\}^{-1} \quad (5.14)$$

For separated flows, the intermittency, as defined by (5.14), decreases the eddy viscosity to approximately the same value at the shear layer outer edge as it would have achieved at the outer edge of an attached boundary-layer.

A correlation equation for the experimental profiles in the separated or recirculation region has been developed in order to estimate the moment of vorticity. This procedure was necessary because of the limited number of measurements within the shear layer which makes a direct determination of du/dy difficult. The correlation equation assumes the following polynomials with the appropriate boundary conditions:

$$\tilde{u} = a e(\eta) + (1 - a) f(\eta) + c g(\eta) \quad (5.15)$$

where \tilde{u} and η are given by:

$$\tilde{u} = \frac{u - u_{\min}}{u_e - u_{\min}} \quad (5.16)$$

$$\eta = \frac{y - h_y}{\delta - h_y} \quad (5.17)$$

Consider the following polynomial functions $e(\eta)$, $f(\eta)$ and $g(\eta)$ which must satisfy the boundary conditions describing the separated profiles.

$$e(\eta) = \eta + \eta^2 - \eta^3 \quad (5.18)$$

$e(\eta)$ must satisfy the boundary conditions at $\eta=0$, $e=0$ and at $\eta=1$, $e=1$ and $e'=0$. Note that in the limit, as $\eta \rightarrow 0$, equation (5.15) is linear with slope of a . The $f(\eta)$ polynomial is defined as:

$$f(\eta) = \eta^2 + 2\eta^3 - 2\eta^4 \quad (5.19)$$

with the boundary conditions at $\eta=0$, $f=0$ and at $\eta=1$, $f=1$ and $f'=0$. Thus, the first two terms on the right hand side of (5.15), when combined, satisfy the outer boundary conditions at $\eta=0$. The final polynomial, $g(\eta)$, provides some control over the shape of the profile without affecting the boundary conditions and has the following form:

$$g(\eta) = \eta^2 - 2\eta^3 + \eta^4 \quad (5.20)$$

Note that g must satisfy the homogeneous boundary conditions, at $\eta=0$, $g=0$, and at $\eta=1$, $g=0$, $g'=0$.

The polynomial-fitted, separated profiles for the 15 degree step are presented in Figure 5.43. The agreement between the curve-fits and the experimental results are typical of the separated profiles for all three configurations, so only the 15 degree results are shown. A minor problem exists with the present curve-fitting method. For the profiles near the step, the slope, a , becomes very large which causes the curve-fitted polynomials to overshoot the outer boundary conditions. Thus, the boundary conditions are satisfied by being approached from above. This is undesirable, but only complicated

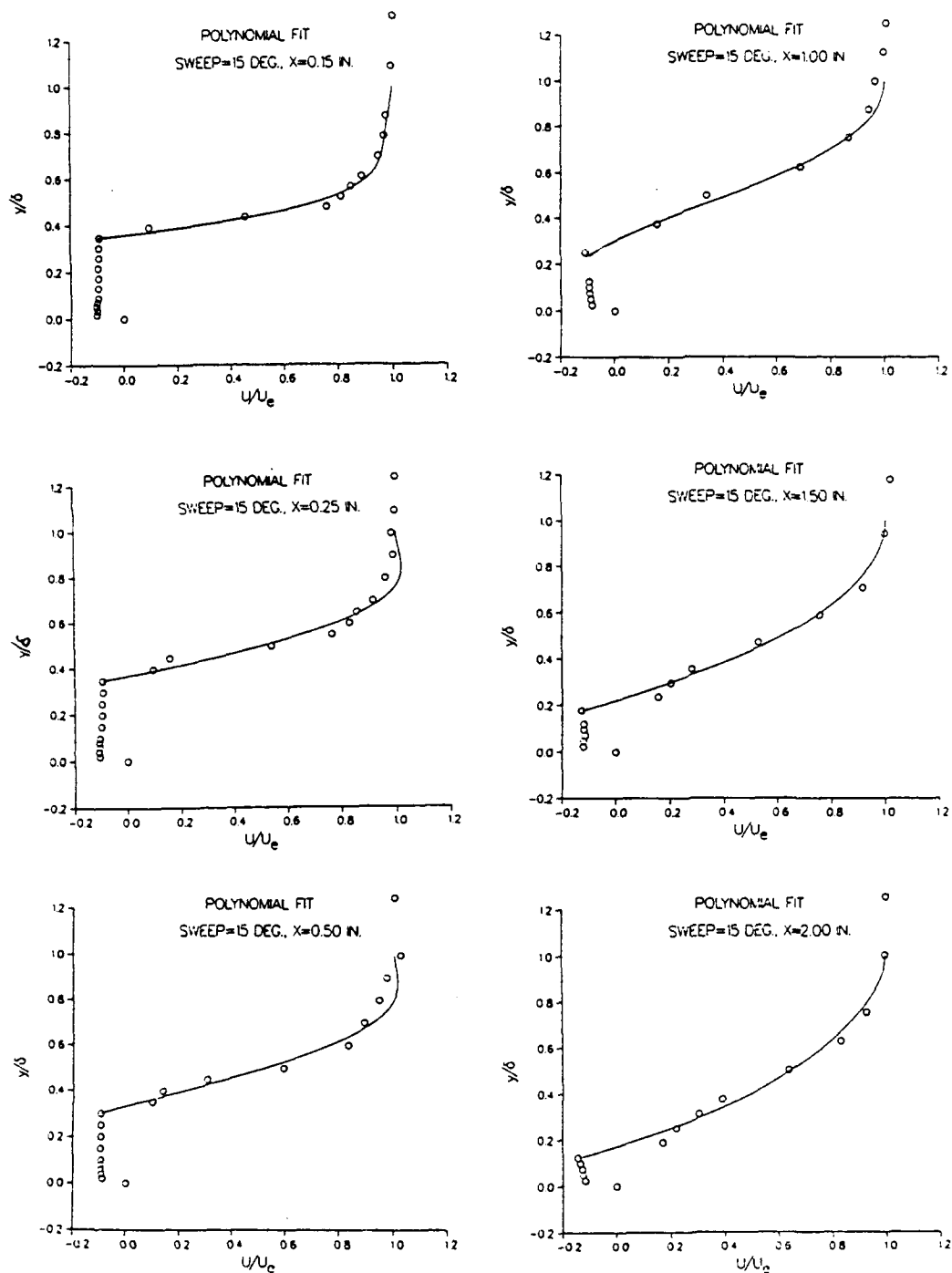


Figure 5.43 Typical Polynomial Fit for the Separated Profiles, $\Lambda = 15$ Degrees

transcendental relations are able to avoid this overshoot problem. The curve-fitted profiles also can not approximate the reverse flow region with any reasonable degree of accuracy. Although there are some problems with the present curve fitting procedure, the resulting polynomial profiles are still useful for the evaluation of the Baldwin-Lomax parameters because it is only necessary to adequately describe the middle layer of the profile, not the region near the reverse flow or at the outer edge. The curve-fitted profiles shown in Figure 5.43 illustrate how well the center of the profiles are described.

Comparing C_{cp} and C_{wk} . Ideally, a comparison should be made between the shear stress computed using the Baldwin-Lomax method and an experimentally measured stress. This is beyond the scope of the present study. Therefore, an indirect procedure has been used which is based on a fundamental assumption in formulating the Baldwin-Lomax method. It is assumed that the Baldwin-Lomax method is derived from the empirical observation of Clauser that the outer layer eddy viscosity is determined from:

$$\mu_t^o = K \rho \delta_k^* u_e \gamma \quad (5.21)$$

where

$$\delta_k^* = \int_0^{\infty} (1 - u/u_e) dy \quad (5.22)$$

Since the velocity profiles, at least in the outer layer, have been measured, the value of δ_k^* can be calculated using the estimates of δ and u_e which have already been discussed. Equating the Baldwin-Lomax formulas for μ_t^o to Clauser's, (5.21), the constants C_{cp} for attached flow and $C_{cp} C_{wk}$ for separated flow, can be determined from the following relations:

$$C_{cp} = \frac{\delta_k^* u_e}{F_{\max} y_{\max}} \quad (5.23)$$

$$C_{cp} C_{wk} = \frac{\delta_k^* u_e F_{\max}}{U_d^2 y_{\max}} \quad (5.24)$$

From the above procedure the constants for the Baldwin-Lomax method were determined for the u velocity components of all three step configurations and are presented in Figure 5.44. The dashed lines indicate Baldwin-Lomax's (1978) recommended results for the two constants. The comparison of C_{cp} upstream of the step is good, with an average result of approximately 1.4. Downstream of reattachment the average value of C_{cp} , approximately 1.1, is considerably lower than the 1.6 suggested by Baldwin-Lomax (1978) for attached flow. As the flow continues downstream, C_{cp} continues to increase. This result suggests that at 10 step heights downstream of reattachment the flowfield has not totally recovered from the flow separation at the step.

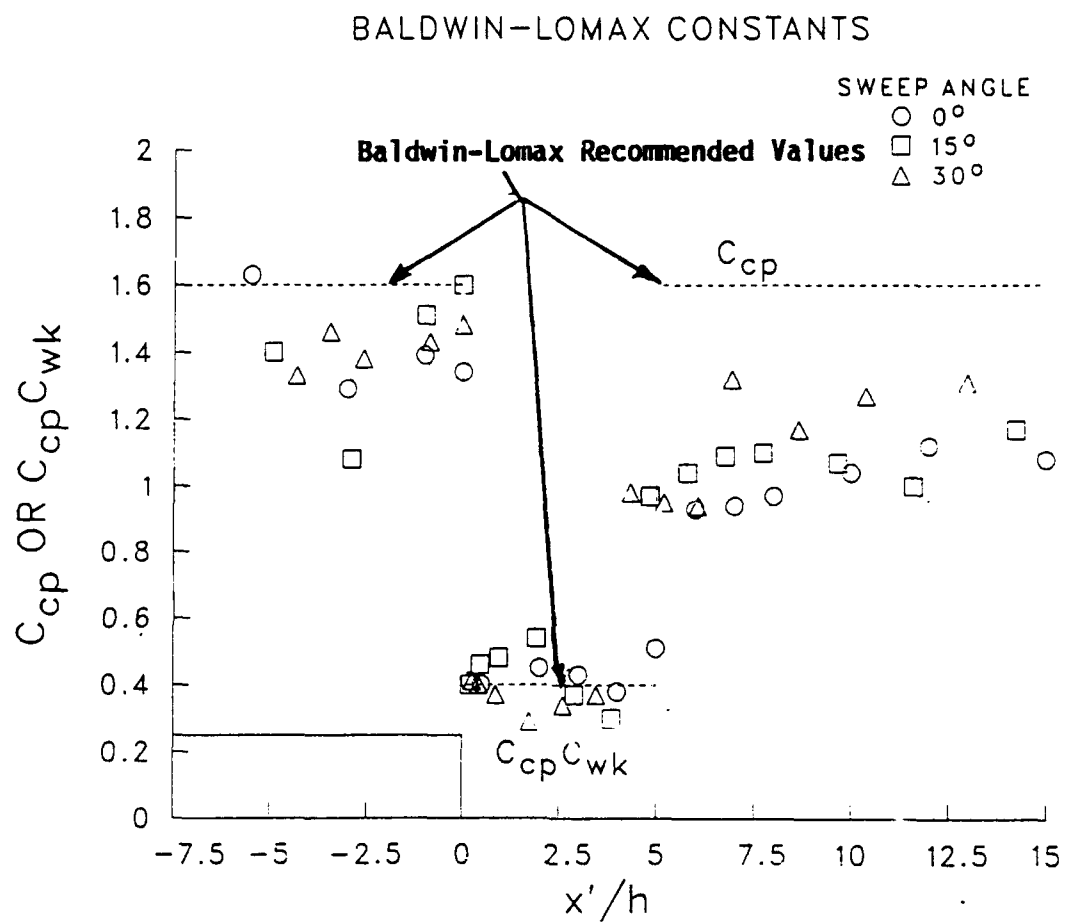


Figure 5.44 Baldwin-Lomax Constant for the Attached and Separated Profiles

There is no observable effect of sweep angle on C_{cp} upstream of the step. The results seem to be evenly scattered about 1.4 without a noticeable trend. For a given survey location downstream of reattachment, the effect of increasing the sweep angle is to increase C_{cp} . These results indicate that as the step sweep angle increases, the flow in the recovery region recovers sooner from the effects of the flow separation at the step. This is in agreement with the results from the Coles' law analysis, where the wake parameter, Π , decreased faster with increasing step sweep angle in the recovery region.

The agreement between the calculated $C_{cp} C_{wk}$ and the suggested results of 0.4 is very good, with the average of $C_{cp} C_{wk}$ being just slightly higher. The 0 degree step results remain nearly constant at a value of approximately 0.4. The results for the 15 degree step increased slightly just downstream of the step before decreasing at a $x'/h \approx 2.5$. The values of $C_{cp} C_{wk}$ for the 30 degree step exhibit a trend opposite to that of the 15 degree step. With increasing downstream distance from the step, $C_{cp} C_{wk}$ decreases until a location of $x'/h \approx 2.5$, then for the remainder of the recirculation region the values increase.

Correlation of Profiles With Baldwin-Lomax Variables. The final analysis was to examine the correlation of the separated profiles of both the u and w velocity components with the Baldwin-Lomax variables. Figures 5.45 to 5.47 are the correlation profiles for the u components within the recirculation region for each step, respectively. The profiles are plotted with respect to a nondimensional velocity scale variable, $(u - u_{min})/(u_e - u_{min})$ and a length variable, $(y - h_y)/b$. The 0 degree step results, Figure 5.45, show that the six separated profiles have collapsed into a single curve within the scatter of the data. The results for the 15 degree step, Figure 5.46, show slightly less similarity. This is because the results near the step, within the recirculation region are near the lower limit of the calibration and are questionable. The similarity of the results, shown in Figure 5.47 for the 30 degree step, is the poorest. As for the 15 degree case, the accuracy of the 30 degree profiles at $x/h=0.3$ to 1.0 and below $y/h=1.0$ are questionable. There is no strong trend evidenced in the correlation with downstream distance using the Baldwin-Lomax variables.

The correlations of the w velocity components using the Baldwin-Lomax variables are shown in Figures 5.48 and 5.49. The w components are all equal to zero for the 0 degree step, so only the results from the 15 and 30 degree steps can be examined. The length scale used for the w component was the same as for the u component plots. A different velocity scale was used and is given by w/w_e , where $w_e = u_e \tan(\Delta)$. Figure 5.48 presents the w velocity component within the separation region of the 15 degree step. The similarity of the results is fair. Figure 5.49 presents the correlation of the w components for the 30 degree step. Again the similarity is fair. One noticeable result from these two plots is that the ratio of w/w_e obtains a value larger than 1. For the 15 degree step the velocity ratio at the edge of the boundary-layer is approximately 1.25 and for the 30 degree step it is about

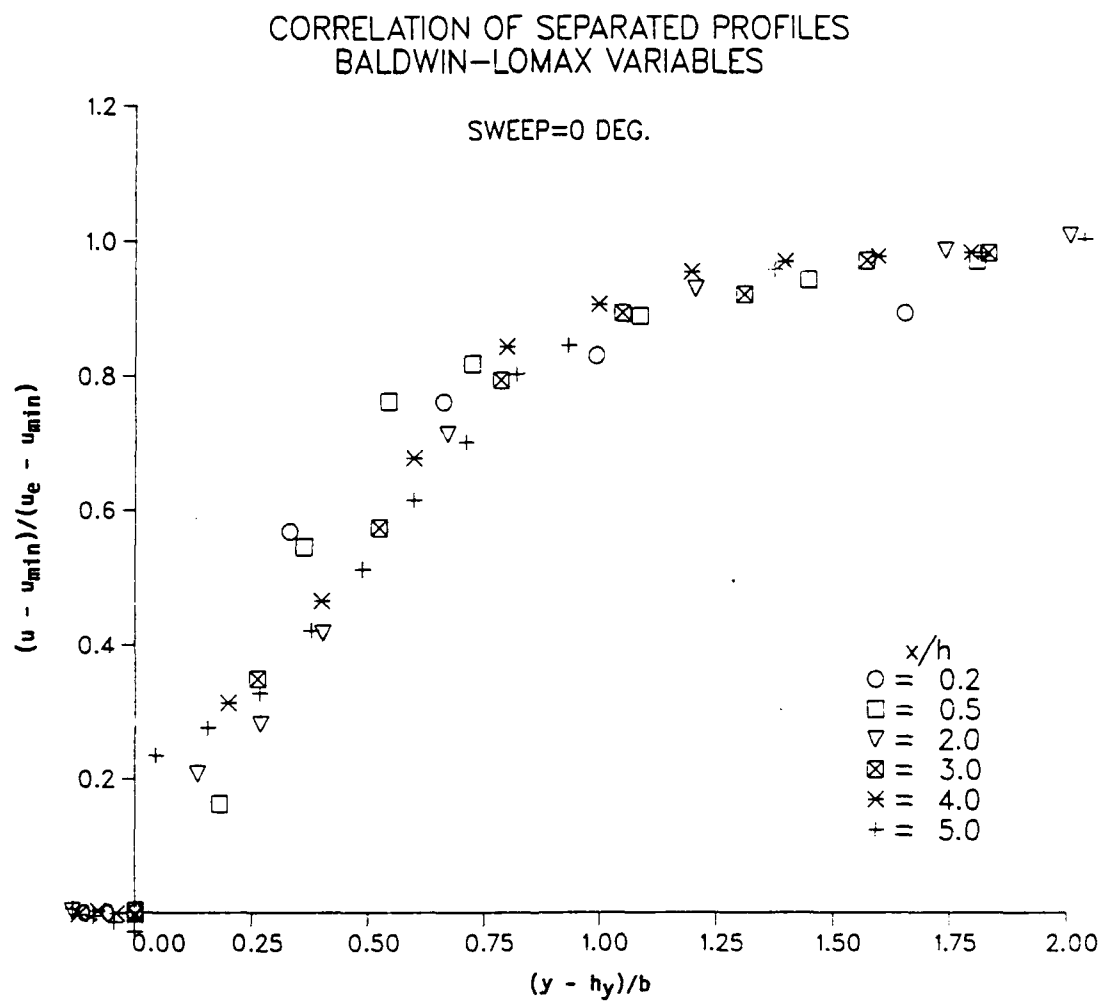


Figure 5.45 Correlation of the u Component Separated Profiles With the Baldwin-Lomax Variable for $\Lambda = 0$ Degree

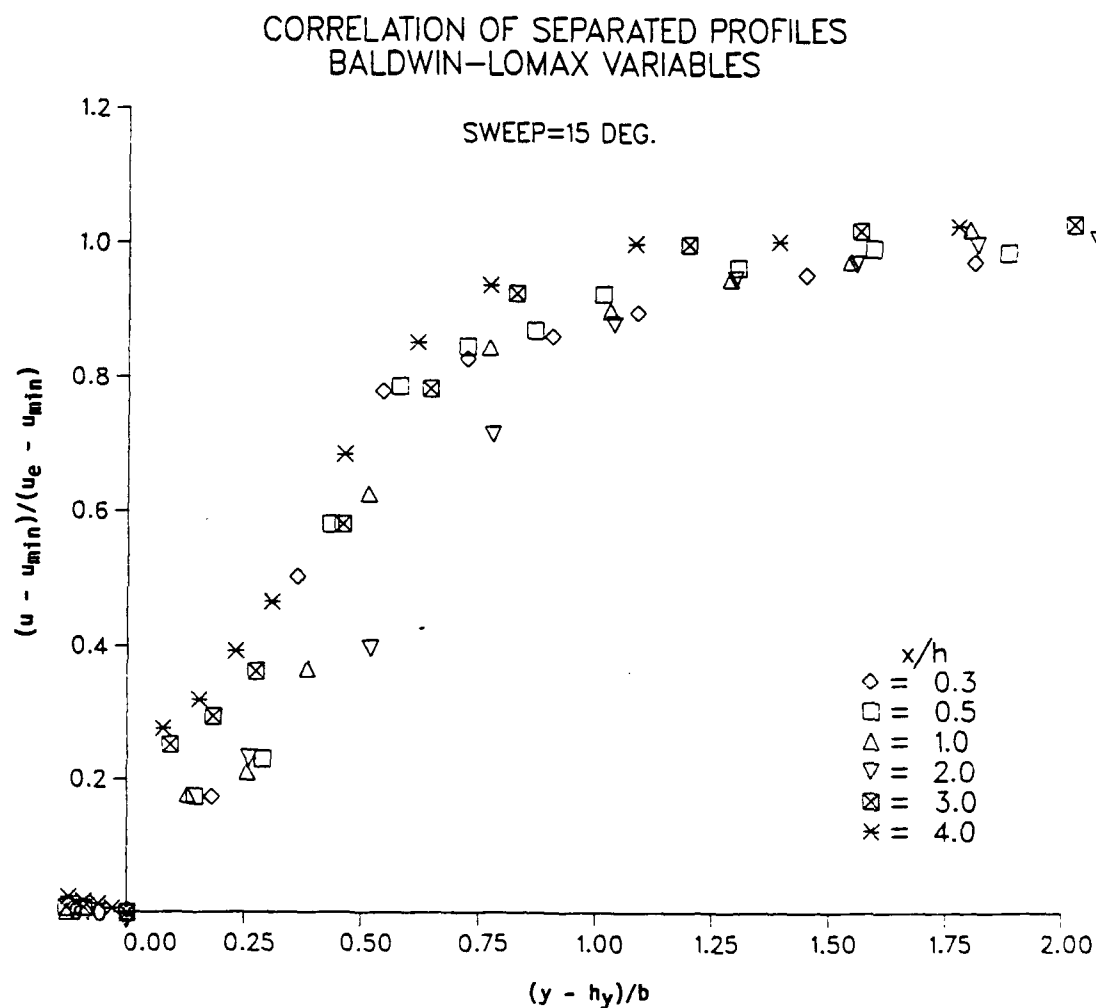


Figure 5.46 Correlation of the u Component Separated Profiles With the Baldwin-Lomax Variable for $\Lambda = 15$ Degrees

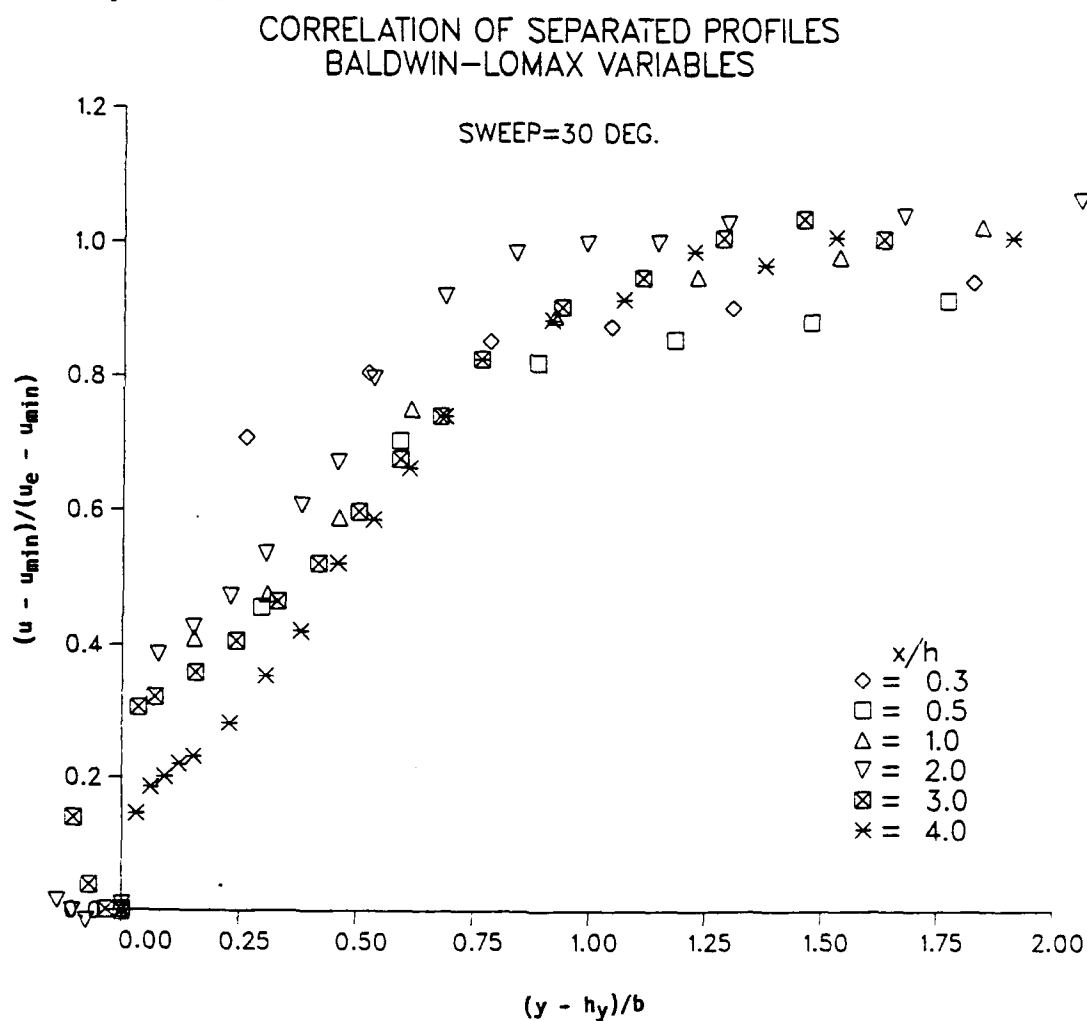


Figure 5.47 Correlation of the u Component Separated Profiles With the Baldwin-Lomax Variable for $\Lambda = 30$ Degrees

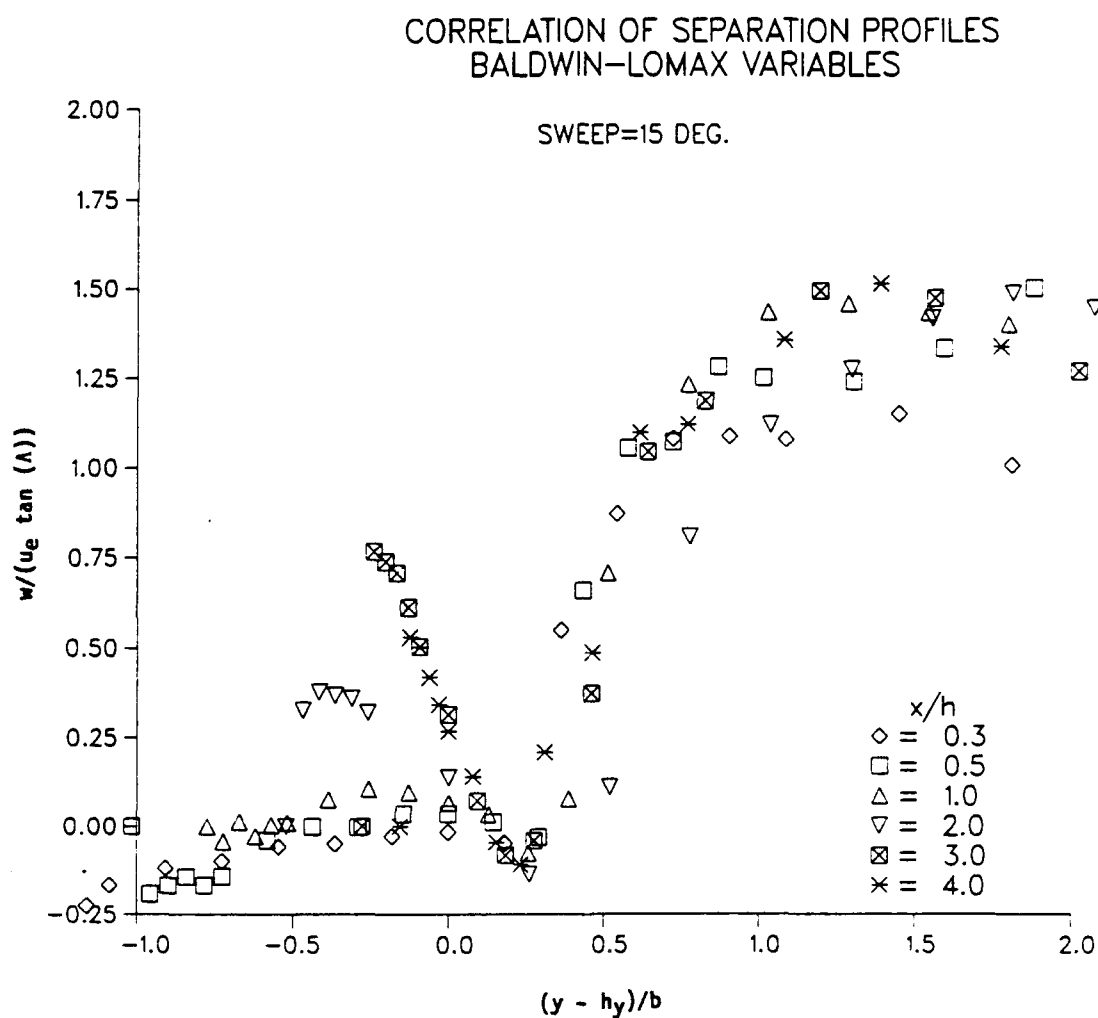


Figure 5.48 Correlation of the w Component Separated Profiles With the Baldwin-Lomax Variable for $\Lambda = 15$ Degrees

CORRELATION OF SEPARATION PROFILES BALDWIN-LOMAX VARIABLES

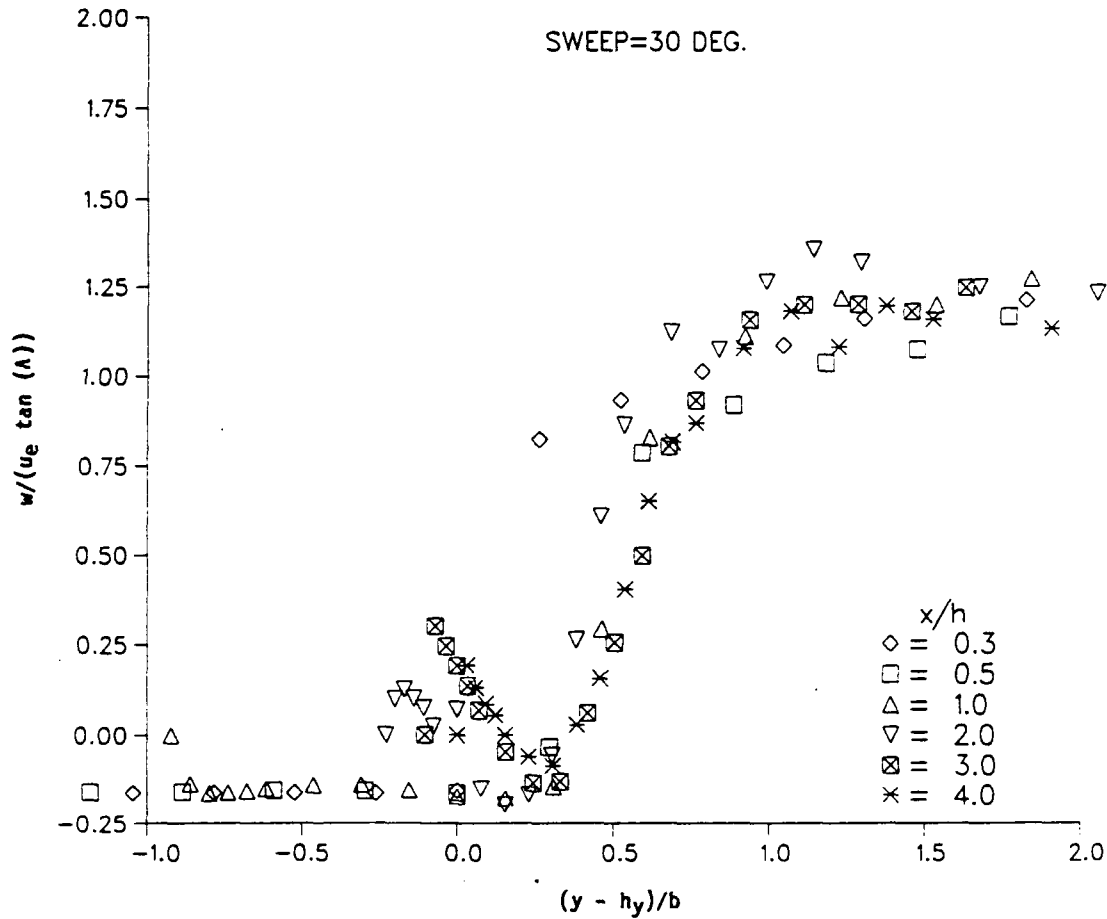


Figure 5.49 Correlation of the w Component Separated Profiles With the Baldwin-Lomax Variable for $\Lambda = 30$ Degrees

1.15. The difference seems to be due to a turning of the free stream so that the velocity is directed along the step. This is contrary to the flow in the recirculation region which turns so that the w component is flowing in the negative direction, along the step. The reason for this is not clearly understood.

Coles' law and the modified Baldwin-Lomax variables have been shown to provide techniques for correlating the data from this study. It has also been shown that the flow over the swept backward-facing step wind tunnel model was influenced by pressure gradients acting in the flow and it is not clear whether these gradients are due to initial conditions or whether the step sweep induces them. A major finding from the Baldwin-Lomax analysis was that all length scales used in the separated flow region must take into account the displacement of the shear layer from the wall by the distance h_y .

Chapter 6 SUMMARY, CONCLUSIONS AND RECOMMENDATIONS

Summary

The objectives of studying the flowfield behind a swept backward-facing were:

- (1) to provide preliminary mean flow measurements behind a swept backward-facing step.
- (2) to determine the magnitude of the velocity components parallel and normal to the step face.
- (3) to examine the effect of step sweep angle on the velocity field.
- (4) to examine the use of Coles' law of the wall and wake in the attached boundary-layer region of the present swept step data.
- (5) to examine the use of a modified version of the Baldwin-Lomax algebraic turbulence model for the flow over a backward-facing step.
- (6) to correlate the spanwise separated flow u and w velocity components using the Baldwin-Lomax variables.

Much work has been performed on the flow over unswept backward-facing steps but, until recently, very little interest has been shown in the swept step case. Although the flowfield is quite complex, the flow over a swept backward-facing step is one of the simplest three-dimensional reattaching separated flows. This type of flow occurs in everyday engineering problems, such as the flow over joints in swept wings of airplanes, flow around buildings and over cliffs, and the flow over rotating bands of artillery projectiles. Also, data on the flowfield over a swept backward-facing step may be useful in the testing of turbulence models for computational fluid dynamics codes because it is a unique three-dimensional flow.

The present study was performed at the Chemical Research Development and Engineering Center, Aberdeen Proving Ground. The flowfield measurements behind a 0.5 inch high, backward-facing step with sweep angles of 0, 15 and 30 degrees, were conducted in the Aerodynamics Research and Concepts and Assistance Branch's subsonic wind tunnel. A single component hot film anemometer was used to measure the velocity parallel and normal to the step face. The component of velocity normal to the surface of the plate was assumed small. Oil flow observations were also made in order to determine similarity of flowfields with the studies of other investigators.

Conclusions

The most significant conclusions determined from this study are presented below.

- (1) The oil flow observations indicate that the flowfields over the three step configurations are similar to those obtained by other investigators. Observed reattachment distances for the three steps

are: 0 degree step, $x'/h = 5.0$; 15 degree step, $x'/h = 4.8$; and 30 degree step, $x'/h = 4.6$. From the oil flow tests, the reattachment length decreases with increasing sweep angle.

(2) The mean velocity components, u and w , were determined (assuming v to be negligible) at various distances up and downstream of the step and at various heights above the step. The 0 degree step results show good agreement with the results of other investigators.

(3) The flow in the recirculation region turns away from the free stream direction until it is approximately normal to the step face. Then, at reattachment and in the beginning of the recovery region the flow realigns itself with the free stream direction.

(4) From the hot film measurements, as the step sweep angle increases, the flow reattachment distance decreases, verifying the oil flow results.

(5) The boundary-layer thickness upstream of the step experiences typical growth for a turbulent flowfield. The experimentally determined δ at the step is in excellent agreement with the result obtained from the Schlichting turbulent boundary-layer thickness equation. Within the recirculation region, δ decreases and remains nearly constant until the flow enters the recovery region. Once downstream of reattachment, δ increases with increasing downstream distance. Also δ tends to increase with increasing sweep angle.

(7) Within the recirculation region the v component stagnation line is approximated by a second order polynomial. As the step sweep angle increases, the magnitude of the slope of the line also increases.

(8) Downstream of the step the w component stagnation line is approximated by a straight line. These results indicate that at reattachment, $u = 0$, the w component continues to have a finite negative value, which is confirmed by the oil flow observation. As step sweep angle increases the magnitude of the slope of the w component stagnation line also increases.

(9) The u -component velocity profile data were correlated using Coles' law of the wall and law of the wake. A least squares technique was used to determine the four constants, C_f , C , Π , δ of Coles' profile equation. Upstream of the step, the results from the four constants suggest the following: for the 0 degree step an adverse pressure gradient is present; a favorable pressure gradient acts on the 15 degree step flowfield; for the 30 degree step, a slight favorable pressure gradient acts on the flow, which represents a nearly equilibrium flow. In the recovery region, the skin friction coefficient, C_f , generally increases with increasing downstream distance and sweep angle. The intercept, C , increases with increasing downstream

distance and decreases with sweep angle. The wake parameter, Π , decreases with increasing downstream distance from reattachment, but even at 10 step heights the value of Π is still a factor of 2 greater than the upstream value. Also, Π decreases with increasing sweep angle indicating that the larger the sweep angle the faster the flow recovers from separation. The boundary-layer thickness determined from the Coles' law analysis is in good agreement with the boundary-layer calculated directly from the experimental data and summarized in conclusion (5).

(10) The semi-logarithmic profiles, at the step for the three configurations, show evidence of the adverse pressure gradient acting on the 0 degree step, a favorable pressure gradient for the 15 degree step and a slight favorable gradient acting on the 30 degree flow. The logarithmic profiles also show that the conditions at separation for the three configurations are not as similar as the y/h versus U/U_e plots indicates. The logarithmic plots downstream of reattachment for the 30 degree step shows that the flow is recovering from the separation with increasing downstream distance.

(11) The velocity profiles (u/u_e versus y/δ) determined from Coles' law agree well with the experimental data. The profiles upstream of the step typically collapse into a single curve. Downstream of reattachment, the profiles typically become fuller as the downstream distance increases.

(12) The applicability of the Baldwin-Lomax algebraic turbulence model to the results of this study was also investigated. The model was modified for the flow over a backward-facing step by accounting for the displacement distance of the shear layer from the wall in the separated or recirculation region. The value of C_{cp} upstream of the step (approximately 1.4) was slightly below the value of 1.6 suggested by Baldwin and Lomax. Downstream of reattachment the value was even lower (approximately 1.1) but increasing with increasing downstream distance. In the recovery region, C_{cp} tended to increase with increasing sweep angle. Within the recirculation region, $C_{cp} C_{wk}$ agreed well with the value suggested by Baldwin and Lomax of 0.40.

(13) The separated profiles were correlated with the Baldwin-Lomax variables. Because of the limited number of data points describing the separated profiles, the profiles were curve fitted with a polynomial, using a least squares technique. This was necessary in order to accurately determine a value for du/dy , which was required for the Baldwin-Lomax method. The correlation achieves good results when the displacement of the shear layer from the wall is taken into account. The u component profiles indicates good similarity for the 0 and 15 degree steps and fair similarity for the 30 degree step. The correlation of the w velocity component for the 15 and 30 degree step is fair. The nondimensional w component, w/w_e ,

achieves values, in the free stream, of approximately 1.25 for the 15 degree step and 1.15 for the 30 degree step.

Recommendations

Recommendations for future research on the flow over swept backward-facing steps are as follows:

- (1) More detailed measurements downstream of the step, especially within the recirculation region. This should include more survey locations, one every 0.1 or 0.2 inches, to better define the reattachment region and more measurements per profile. The measurements for each profile should be confined below 2.0 inches (for a 0.5 inch step height) with measurements every 0.010 inches.
- (2) Experimentally resolve the flow reversal ambiguity in the recirculation region. This could be accomplished by several techniques such as a pulse wire anemometer, split-film anemometer, pressure probe or shielding and rotating a single component hot wire anemometer.
- (3) Several spanwise measurements need to be made in order to confirm the \$independence\$ principle.
- (4) Numerical solutions of the Navier-Stokes equations should be completed for the flow over swept backward-facing steps. Further, investigate the ability of computational methods to predict the flow over a backward-facing step and the comparison with experimental results.

REFERENCES

- Al-Beirutty, M. H.; S. H. Arterberry and F. B. Gessner. (1988).
"A hot-wire measurement technique for complex turbulent flows."
*In Proceedings of the AIAA/ASME/SIAM/APS 1st Fluid
Dynamics Congress in Cincinnati, Ohio, July 25-28, 1988*, Part 3,
1479-1486, Report 88-3600-CP.
- Avva, R. K., S. J. Kline and J. H. Ferziger. (1988). "Computation of
turbulent flow over a backward facing step - zonal approach."
AIAA 26th Aerospace Sciences Meeting in Reno, NV:
AIAA Paper #88-0611.
- Baldwin, B. S. and H. Lomax. (1978). "Thin layer approximation and
algebraic model for separated turbulent flows."
AIAA 16th Aerospace Sciences Meeting, Reno, NV:
AIAA Paper #78-257.
- Bradshaw P. and F. Y. F. Wong. (1972). "The reattachment and
relaxation of a turbulent shear layer." *J. Fluid Mechanics* 52,
Part 1: 113.
- Bragg, M. B. and S. A. Spring. (1987). "An experimental study
of the flow field about an airfoil with glazed ice."
AIAA 25th Aerospace Sciences Meeting, Reno, NV:
AIAA Paper #87-0100.
- Cebeci, T. and A. M. O. Smith. (1974). *Analysis of turbulent boundary
layers.* New York: Academic Press Inc.
- Coles, D. E. (1962). "The turbulent boundary layer in a compressible
fluid." Santa Monica, CA: Rand Corp. Report R-403-PR,
Appendix A.
- Coles, D. E. and E. A Hirst, eds. (1968). "Compiled data." *In Proceedings
of the Computation of Turbulent Boundary Layers-1968
AFOSR-IFP-Stanford Conference.* Stanford University,
CA. Vol 2.
- Danberg, J. E. (1971). "A re-evaluation of zero pressure gradient
compressible turbulent boundary-layer measurements." *In
Proceedings of AGARD Fluid Dynamics Panel Specialists'
Meeting on 'Turbulent Shear Flows' in London, England,*
AGARD CP-93.
- _____. (1973). "A re-evaluation of zero pressure gradient
compressible turbulent boundary-layer measurements." U. S. Army
Ballistic Research Laboratory, Aberdeen Proving Ground, MD:
Report 1642.

- Danberg, J. E. and N. R. Patel. (1989). "An algebraic turbulence model for flow separation caused by forward and backward facing steps." Ballistic Research Laboratory, Aberdeen Proving Ground, MD: to be published.
- Eaton, J. K. and J. P. Johnston. (1981). "A review of research on subsonic turbulent flow reattachment." *AIAA Journal*, Vol. 19, No. 9, 1093-1100.
- Ellzey, J. L. and J. G. Berbee. (1988). "Aspect ratio and Reynolds number effects on the flow behind a rearward facing step." *AIAA 26th Aerospace Sciences Meeting, Reno, NV*: AIAA Paper #88-0612
- Etheridge, D. W. and H. P. Kemp. (1978). "Measurements of turbulent flow downstream of a rearward-facing step." *J. Fluid Mechanics* 86, Part 3; 545.
- Flow Corporation. (no date). *The Hot Wire Anemometer*. Watertown, MA: Flow Corporation. Technical Bulletin 53.
- Hartman, R. M. (1988). "Computational study of subsonic turbulent flow over a swept rearward-facing step." Ph.D. diss., Univ. of Delaware, Dept. of Mech. Engr.
- Hartman, R. M., B. S. Seidel, and J. E. Danberg. (1989). "Computational study of turbulent flow over a swept backward-facing step." Presented at 6th International Conference on Numerical Methods of Laminar and Turbulent Flow, University College of Swansea, Wales U.K., July 11-15.
- Hu, Q. K., Q. Wang, J. Danberg, and B. Seidel. (1984). "The Calculation of incompressible laminar flow over a swept rearward-facing step using the finite element method." University of Delaware, DE: Department of Mech. and Aerosp. Engr.
- Hughes, W. F. and J. A. Brighton. (1967). *Theory and problems of fluid dynamics*. Schaum's Outline Series. New York: McGraw Hill.
- Lomas, C. G. (1986). *Fundamentals of hotwire anemometry*. New York: Press Syndicate of the University of Cambridge.
- Miller, M. C. (1986). "Experimental facilities of the Aerodynamics Research Concepts Assistance Branch." Chemical Research Development and Engineering Center, Aberdeen Proving Ground, MD: Report ARCSL-SP-83007.

- Novak, C. J. and B. R. Ramaprian. (1982). "Measurements in the wake of an 'infinite' swept airfoil." Iowa Institute of Hydraulic Research, The University of Iowa, Iowa City: IHR Report No. 240.
- Olivari, D. (1978). *Hot wire Anemometer*. von Karman Institute for Fluid Dynamics, Belgium: [course notes].
- Potter, M. C. and John F. Foss. (1982). *Fluid mechanics*. Great Lakes Press, East Lansing, MI.
- Sabersky, R. H., A. J. Acosta and E. G. Hauptmann. (1971). *Fluid flow a first course in fluid mechanics*. New York: Macmillan Publishing Co. Inc.
- Schlichting, H. (1979). *Boundary-layer theory*. 7th ed. New York: McGraw-Hill Book Co.
- Selby, G. V. (1982). "Phenomenological study of subsonic turbulent flow over a swept rearward-facing step." Ph.D. diss., Univ. of Delaware, Dept. of Mech. and Aerosp. Engr., Newark.
- Spring, Samuel Alan. (1987). "An experimental mapping of the flow field behind a glaze ice shape on a NACA 0012 airfoil." Master of Science thesis, The Ohio State University, Columbus.
- Thomas, C. E., K. Morgan and C. Taylor. (1981). "A finite element analysis of a backward facing step." *Computers and Fluids* Vol 9, 265-78.
- Thermo-Systems Inc. (no date). "Hot film and hot wire anemometry, theory and application." Saint Paul, MN: Thermo-Systems Inc., Technical Bulletin TB5.
- _____. (no date). "Temperature compensation of thermal sensors." Saint Paul, MN: Thermo-Systems Inc., Technical Bulletin TB16.
- _____. (no date). "Procedure for temperature correction on velocity measurements." Saint Paul, MN: Thermo-Systems Inc., Technical Bulletin TB18.
- White, F. M.. (1974). *Viscous fluid flow*. New York: McGraw-Hill Inc.

Blank

LIST OF SYMBOLS

a 's	constants used in reformulation of Coles' Law
a, c	constants used in polynomial curve-fits of separated profiles in the Baldwin-Lomax analysis
A^+	Van Driest damping function = 26
A, B	constants used in King's law
AR	aspect ratio, (width of wind tunnel model)/ h
b	half width of shear layer
C	intercept of the semi-logarithmic law of the wall
C_{cp}	constant in Baldwin-Lomax turbulence model for attached flows ≈ 1.6
C_f	skin friction coefficient, $2(u_\tau/u_e)^2$
C_{kleb}	Klebanoff intermittency factor = 0.3
C_{wk}	constant in Baldwin-Lomax turbulence model for separated flow = 0.25
E	output voltage from hot film anemometer
$e(\eta)$	polynomial function used for polynomial fit of separated profile in Baldwin-Lomax analysis
$F(y)$	moment of vorticity
F_{max}	maximum of moment of vorticity
$F(\alpha)$	overall velocity ratio based on $\alpha + \theta$
$f(\alpha)$	velocity ratio as a function of α
$f(\alpha + \theta)$	velocity ratio as a function of $\alpha + \theta$
$f(\alpha - \theta)$	velocity ratio as a function of $\alpha - \theta$

$f(\eta)$	polynomial function used for polynomial fit of separated profiles in Baldwin-Lomax analysis
$G(\alpha)$	overall velocity ratio based on $\alpha - \theta$
$g(\eta)$	polynomial function used for polynomial fit of separated profiles in Baldwin-Lomax analysis
h	height of the step
h_y	displacement distance of the shear layer from the wall in separated flows
K	the Clauser constant = 0.0168
L_{sep}	distance along centerline from leading edge to top of step
n	King's law exponent = 0.5
Re_h	Reynolds number based on step height, $U h/\nu$
Re_{sep}	Reynolds number based on separation length, $U L_{sep}/\nu$
T_{cal}	ambient air temperature at time of calibration, ($^{\circ} F$)
T	ambient air temperature at time of velocity profile survey, ($^{\circ} F$)
T_s	temperature of the hot film sensor, ($^{\circ} F$)
U	total velocity
U_d	$\sqrt{(u^2 + v^2 + w^2)_{max}} - \sqrt{(u^2 + v^2 + w^2)_{min}}$
U_e	total edge velocity
U_{eff}	velocity measured by hot film anemometer at some α to the flow
U_{∞}	freestream velocity
u	component of velocity perpendicular to step face
u^+	defined by $u^+ \equiv u/u_{\tau}$
\tilde{u}	velocity scale for polynomial fits of separated profiles in Baldwin-Lomax method

u_e	u-component edge velocity
u_{\max}	maximum u velocity component
u_{\min}	minimum u velocity component, =0 for attached flow, negative for separated flows
u_τ	shear velocity, $\sqrt{\tau_w/\rho_w}$
v	component of velocity perpendicular to wall
w	component of velocity parallel to step face
w_e	w component edge or average velocity
x	coordinate in streamwise direction
x'	coordinate normal to step
y	coordinate normal to wind tunnel test section floor, same as y'
y_{\max}	distance above surface to the maximum of the moment of vorticity
y^+	defined as $y u_\tau/\nu$
y'	coordinate normal to wind tunnel test section floor, same as y coordinate
z	lateral coordinate perpendicular to freestream direction
z'	coordinate parallel to step face
Λ	step sweep angle
Π	Coles' wake parameter
α	total velocity flow direction with respect to the freestream direction
γ	Klebanoff intermittency factor
δ	boundary layer thicknesses
δ_k^*	incompressible displacement thickness
η	length scale for polynomial fit of separated profiles in Baldwin-Lomax method

θ	angular offset for hot film measurements = 15 degrees
κ	the von Karman constant = 0.43
μ_t	eddy viscosity
μ_t^o	outer region eddy viscosity
ν	kinematic viscosity
ρ	fluid density
τ	shear stress
ω	vorticity